Identification and Characterization of Radioactive Particles in the Environment

A thesis submitted to The University of Manchester
for the degree of Doctor of Philosophy (PhD) in the Faculty of Engineering and Physical Sciences

2010

Mustafa Sajih

School of Chemistry

Table of Contents

Abstract 12

Declaration 13

Copyright statement 14

Acknowledgments 15

Thesis structure 16

Chapter 1: Introduction

1. Sources of radioactive particles 19

1.1 Nuclear weapon tests 19

1.2 Accidents with nuclear devices 22

1.3 Nuclear accidents 22

1.4 The nuclear fuel cycle and reprocessing in the UK 23

1.4.1 Reprocessing of spent nuclear fuel 24

1.4.2 Radioactive particles from Sellafield discharges 27

1.4.3 Radioactive particles from Dounreay nuclear site 29

1.5 Depleted Uranium (DU) 31

Natural and depleted uranium 31

Physicochemical properties of DU 32

Military use of DU 33

DU in surface and subsurface soils 35

Environmental and health impacts of DU 36

2. Characterization of radioactive particles 36

References 38

Chapter 2: Identification and characterisation of radioactive particles in salt marsh sediments

Abstract 44

1. **Introduction** 44

2. Methods and analysis 46

2.1 Study site and sample collection 46

2.2 Analysis 47

2.2.1 Autoradiography 47

2.2.2 Heavy liquid density separation 48

2.2.3 Scanning electron microscopy (SEM) – Energy dispersive X-ray analysis (EDX) 49

2.2.4 Alpha spectrometry 49

3. Results and discussion 49

3.1 Size, shape and composition analysis by SEM-EDX 49

3.2 Radionuclide and isotopic composition 51

4. Conclusion 53

References 53

Supporting information 54

Chapter 3: Physicochemical Characterisation of Depleted Uranium (DU) Particles at a UK Firing Test Range

Abstract 59

1. Introduction 59

2. Methods 61

2.1 Study site and sample collection 61

2.2 Autoradiography 61

2.3 Scanning electron microscopy (SEM)/Energy dispersive X-ray analysis (EDX) 62

2.4 X-ray diffraction 62

2.5 Chemical separation and measurement of uranium 62

2.5.1 Alpha spectrometry 63

2.5.2 ICP-MS and ICP-AES 63

3. Results and discussion 63

3.1 Firing impact-derived particles 63

3.1.1 SEM-EDX 63

3.1.2 Elemental composition and X-ray diffraction 66
3.1.3 Isotopic fingerprinting 69
3.2 Corrosion site particles 69
3.2.1 SEM-EDX 69
3.2.2 X-ray diffraction 71
3.2.3 Isotopic fingerprinting 72
4. Conclusion 72
Acknowledgement 73
References 73
Supporting information 75

Chapter 4: Application of Secondary Ion Mass Spectrometry to Analysis of Depleted Uranium Particles from a Test-Firing Range

Abstruct 81
Introduction 81
Methods and analyses 82
Study site and sample collection 82
Particle separation 82
Particle analyses 83
Scanning electron microscopy (SEM)/Energy dispersive X-ray analysis (EDX) 83
Secondary ion mass spectrometry (SIMS) 83
Results and discussion 85
SEM-EDX 85
Particle A (Molten Particle) 85
Particle B (DU fragment) 86
SIMS 87
Molten Particle (Particle A) 87
Elemental mapping 87
Hydrocarbon contamination 87
Quantitative analysis 88
DU Fragment (Particle B) 90
Imaging and quantitative analysis 90
Isotopic composition of U 92
Particle B 92

Measurement using different ions 92
Determination of mean ratio 92
Particle A 93
Summary and Conclusion 93
Acknowledgment 94
References 94
Supporting information 95

Chapter 5: Biogeochemical Controls on the Corrosion of Depleted Uranium Alloy in Subsurface Soils

Abstruct 101
Introduction 102
Experimental section 103
Sampling and characterization 103
Microcosm experiments 103
DU coupon analysis 104
Geochemical methods and modelling 104
DU distribution and particle analysis 104
Microbiological methods 104
Results and Discussion 105
Soil and water characterization 105
Impact of DU on redox processes in field-moist soil 105
Impact of DU on redox processes in waterlogged soil 106
Corrosion of DU under field-moist conditions 107
Corrosion of DU under progressively reducing waterlogged conditions 108
Rate of DU corrosion as a function of redox environment 108
Corrosion products and their solubility 110
Microbial community profile 112
DU corrosion as a function of soil conditions 113
Acknowledgment 114
References 115
Supporting information 118

Chapter 6: Summary, Conclusions and Suggestions for Future Work

Summary and conclusions 120
Suggestion for future work 123

Appendix: Experimental Techniques

A) Particle separation 125
1. Autoradiography 125
2. Heavy liquid density separation 126
B) Electron microscopy and X-ray analysis 127
1. Scanning electron microscopy (SEM)/Energy dispersive X-ray analysis (EDX) 127
2. X-ray diffraction (XRD) 129
C) Atomic and mass spectrometric techniques 130
1. ICP-AES/MS 130
2. Secondary Ion Mass Spectrometry SIMS 132
D) Radiometric techniques 133
Alpha and Gamma spectrometry 134
References 135

Final word count: 29789

Lists of Tables

Chapter 1

Table 1. Composition of spent nuclear fuel 25

Table 2. Contribution (%) to the total discharges within the European community made by reprocessing plants for discharges up to 1984. 26

Table 3. Composition and activities of natural and depleted uranium 32

Table 4. Experimental and analytical techniques used to identify and characterize environmental radioactive particles in this study 37

Chapter 2

Table S1. Observed particle sizes and morphologies 55

Chapter 3

Table 1. Composition of natural uranium and DU 60

Table 2. Mole ratio (stable element:U) in firing impact particles 66

Table S1. $^{235}U/^{238}U$ and $^{234}U/^{238}U$ atom ratios and $^{234}U/^{238}U$ activity ratio of 5 DU firing impact particles 76

Chapter 4

Table 1. Correlation coefficients for different pairs of elements 89

Table 2. $^{235}U/^{238}U$ atom ratio measured from a spot on U ion images 92

Table S1. Critical Values of the Pearson Product-Moment Correlation Coefficient 97

Appendix

Table 1. Parameters of ICP-MS 132

Table 2. Detection limits for the elements analysed by ICP-MS and ICP-AES 132

List of Figures

Chapter 1

Figure 1. A radioactive fallout particle from a tower shot in Nevada. The particle has a dull metallic lustre and shows numerous adhering small particles 21
Figure 2. Schematic of the nuclear fuel cycle in the UK 24
Figure 3. Reprocessing of spent nuclear fuel 26
Figure 4. Sellafield Discharges of Plutonium 28
Figure 5. Example of a Dounreay MTR particle 30
Figure 6. Isotopic composition of natural U and DU 32
Figure 7. Principal locations of DU munitions use in Iraq and Kuwait 34
Figure 8. DU round fired in Kosovo 35
Figure 9. Experimental and analytical techniques used to identify and characterize environmental radioactive particles in this study 37

Chapter 2

Figure 1. Salt marsh sediment profile and Sellafield discharge of ^{241}Pu 45
Figure 2. UK map (left), enlargement for Cumbria (top right), and the salt marsh study site (right) 47
Figure 3. Left: autoradiograph of radioactive particles. The red spots represent radioactive particles in the sample.Right: photostimulable luminescence (PSL) signal for the three red spots 47
Figure 4. Sediment particles on a filter paper 48
Figure 5. Left: heavy liquid density separation with heavy particles in the bottom and sediment floating on top. Right: an optical microscope image of the heavy particles on a nitrocellulose membrane 48
Figure 6. BSE image of a sediment sample shows uranium particles as bright spots. The gray materials are the sediment matrix 50
Figure7. BSE image (left) and secondary electron (SE) image (right) of a particle 50
Figure 8. EDX spectrum of a spot on the bright area of the BSE image 51
Figure 9. An electron image (BSE) and energy dispersive X-ray analysis (EDX) of a particle separated by heavy liquid 51
Figure 10. Alpha spectrum of the dissolved particles 52

Figure 11. Left**:** Alpha spectrum of Pu isotopes and the activity ratio $^{238}Pu/^{239+240}Pu$. Right: $^{238}Pu/^{239+240}Pu$ activity ratio for 1970s Sellafield discharges 52

Figure S1. The Ravenglass esturay showing the location of salt marsh and sampling site 54

Figure S2. BSE image of three separated particles and their EDX spectra 56

Figure S3. Alpha spectrum of U fraction of the three dissolved particles 57

Chapter 3

Fig. 1. SEM-EDX of firing impact particles (first type) 64

Fig. 2. SEM-EDX of firing impact particles (second type) 65

Fig. 3. X-ray diffraction patterns of two DU firing impact particles 68

Fig. 4. SEM-EDX of corrosion particles 70

Fig. 5. X-ray diffraction pattern of the yellow U coating, together with the characteristic reflections of metaschoepite 71

Fig. S1. Schematic of Eskmeals firing range showing sample positions 75

Fig. S2. Autoradiograph of DU sample showing black spots 75

Fig. S3 Diffraction patterns of two yellow DU particles, pure sand pattern and Metaschoepite reflections 76

Fig. S4. $^{235}U/^{238}U$ atom ratio for balck and yellow particles 77

Fig. S5. $^{235}U/^{238}U$ vs. U mass for black and yellow particles 78

Fig.S6. $^{234}U/^{238}U$ activity ratios for 4 yellow particles (DU corrosion particles) 79

Chapter 4

Fig.1 Autoradiograph of DU sample showing hot spots 83

Fig. 2 SEM-EDX of particle A 85

Fig. 3 SEM-EDX of particle B 86

Fig.4 Secondary ion maps show the distribution of elements within particle section, and BSE image of the particle (top left). Field of view 290 µm 87

Fig.5 Secondary ion maps showing the distribution of some elements and hydrocarbons within the particle section. Field of view 64 microns 88

Fig. 6 Secondary ion images of a 72 microns field of view (BSE image shown top left 89

Fig. 7 Secondary ion images of 125 microns field of view (BSE image shown top left) 90

Fig. 8 Element abundance vs. element abundance (counts per pixel) diagrams, 91

showing correlation between different elements.
Fig. 9 Regression of $^{235}UO_2^+$ against $^{238}UO_2^+$ 92
Fig. S1 Correlation plot shows the relationship between Si and CH_3 95
Fig. S2 Element abundance vs. element abundance (counts) plots, showing correlation between different elements 96
Fig. S3 Areas of interest used for quantitative analysis 98
Fig. S4 Relationship between Fe and Cr in Fe and Cr areas 98
Fig.S5 Correlation between Fe and Al in Al, Fe and Cr areas 99
Fig. S6 Correlation between Ti and Al in Al, Fe and Cr areas 99

Chapter 5

Figure 1. DU-amended (×) and control (o) redox indicator time series data for the subsurface field-moist (A,D,G), open waterlogged (B,E,H), and closed waterlogged (C,F,I) microcosms. Nitrate (A−C), acid extractable Fe(II) (D−F), and sulfate (G−I) concentrations are shown over time. Error bars ± 1 s.d. (n = 3) 106
Figure 2. Black and white photographs showing DU coupons retrieved from the field-moist microcosm 108
Figure 3. Time series for DU corrosion in the field-moist, open waterlogged and close waterlogged 108
Figure 4. ESEM images (A,C) and EDAX spectra (B,D) of a corroded DU particle retrieved from field-moist microcosm (A,B) and a soil particle from a closed waterlogged microcosm (C,D) 111
Figure 5. Phylogenetic affiliations of clones in field-moist (A,B) and the closed waterlogged (C,D) soils on day 435. Alpha, Beta, Delta, and Gamma represent proteobacterial divisions 112
Figure S1. A representative phosphor image of field-moist soil showing the distribution of DU particles (black spots) in the sample 118

Appendix

Figure 1. Autoradiograph of a sample containing depleted uranium particles. Black spots represent depleted uranium particles 126
Figure 2. Heavy liquid density separation with heavy particles in the bottom and soil matrix floating on top 127
Figure 3. The different signals produced by interaction of electron beam with solid sample 128

Figure 4. Bragg's Law diffraction. The arrows are the incident and diffracted X-rays, the horizontal lines are lattice planes, d is the lattice spacing and θ is the diffraction angle 129
Figure 5. Steps involved in the analysis of a liquid sample by ICP-AES 131
Figure 6. Ion beam sputtering 133
Figure 7. Band structure of a semiconductor detector 134

University of Manchester

Mustafa Sajih

Doctor of Philosophy (PhD) in Chemistry

Identification and Characterization of Radioactive Particles in the Environment

2010

Abstract

Radioactive particles have been released into the environment from different sources (e.g. nuclear weapon tests, nuclear accidents, nuclear reprocessing plants, and use of depleted uranium (DU) munitions). Nuclear fuel particles have been released from authorised discharges of low-level radioactive effluent into the Irish Sea sediments from the nuclear fuel reprocessing plant at Sellafield, UK. Following the use of depleted uranium munitions in the Gulf wars and the Balkan conflicts, the environmental impact of depleted uranium and its behaviour in the environment have been of great concern.

In this thesis, nuclear fuel particles released from Sellafield and retained in the intertidal Irish Sea salt marsh sediments, and DU particles arising from testing of DU munitions against hard targets and corrosion of DU metal buried in soil at Eskmeals firing range, UK, were investigated using a range of microanalytical, analytical and radiometric techniques. The particles were characterised in terms of size and morphology, elemental and radionuclide compositions, isotopic composition of associated radionuclides and, crystalline structure of uranium forms. The results demonstrate the usefulness of the applied techniques in characterising environmental radioactive particles, and lead to better understanding of the origin, behaviour and fate of these particles in the environment.

The nuclear fuel particles were 1-20 µm in size, composed mainly of uranium and irradiated in the reactor as the transuranium elements (Np, Pu, Am and Cm) can be identified. The isotopic composition of uranium and plutonium suggest that these particles are derived from reprocessing of spent fuel. The results demonstrated the persistence for some decades of irradiated fuel particles in estuarine marine environment.

DU particles from firing impacts were oxidized uranium forms (UO_2 and U_3O_8) and composed mainly of uranium with few molten particles composed of a mixture of uranium and iron. DU particles from corrosion processes were mainly sand grains coated with metaschoepite corrosion product. The results showed the diversity of particles which can be produced through the use of DU munitions and the potential for these to persist in the environment for many years.

Declaration

No portion of this work referred to in the thesis has been submitted in support of any application for another degree or qualification of this or any other university or other institute of learning.

Copyright Statement

Acknowledgements

I would like to thank most sincerely my supervisor, Prof. Francis Livens for his guidance and great help and support throughout my PhD study.

Thank you for all people in Radiochemistry group.

I am very grateful to my sponsor (University of Aleppo, Syria)

Last but not least I would like to thank my wife Nour for her love and support during my study, my daughter Masa for the great time, and my family at home for their support.

Thesis structure

This thesis has been written in a series of standalone but related studies, centred around the identification and characterization of radioactive particles in the environment. One part has already been published in the proceedings of the Actinides 2009 conference, another has been published in the leading journal in the field, a third is in review, while the fourth is close to submission. This therefore lends itself to presentation of the thesis in alternative format. The structure is outlined below.

Chapter one will review the literature on the different sources contributing to environmental radioactivity (e.g. nuclear weapon tests, discharges from nuclear reprocessing plant, use of depleted uranium munitions), and characterization of radioactive particles in the environment.

Chapter two describes characterisation of radioactive particles in salt marsh sediment. The particles are derived from the authorized low-level radioactive effluent discharged from Sellafield nuclear reprocessing plant, and transported to the Esk estuary, where they retain in salt marsh sediment. The particles were characterized in terms of size, shape, elemental and radionuclide compositions. This chapter has been published in the Actinides 2009 proceedings.

Chapter three talks about wide range of techniques used to characterize depleted uranium particles from test-firing and corrosion of depleted uranium penetrators at Eskmeals terrestrial environment. This chapter has been submitted to the journal Science of the Total Environment.

Chapter four describes the application of secondary ion mass spectrometry (SIMS), in investigating depleted uranium particles from firing impacts. This chapter is in the process of being submitted to the Journal of Analytical Atomic Spectrometry.

Chapter five is a collaborative study, which was carried out by a team from the University of Plymouth and University of Manchester. It details experiments that were carried out investigating depleted uranium corrosion under realistic subsurface soil environments. This chapter has been published in the journal Environmental Science and Technology.

Finally, the last chapter will draw the various conclusions from earlier chapters and looks at future work that could be carried out to develop and apply more methods for characterizing radioactive particles in the environment.

Chapter 1

Introduction

Introduction

Since the start of industrial nuclear operations, anthropogenic radionuclides have been released into the environment from various sources (e.g. nuclear weapon tests, nuclear fuel cycle and use of depleted uranium munitions). The main contributor to both marine and terrestrial radioactivity is global fallout from nuclear weapon tests performed in the atmosphere, especially in the 1950s and 1960s (Livingston and Povinec, 2000). The nuclear fuel cycle contributes to releases mainly at the stages of uranium mining and milling and nuclear fuel reprocessing (MacKenzie, 2000). Application and testing of depleted uranium munitions has led to the release of depleted uranium into the environment at numerous sites around the world. A large fraction of the radionuclides released from nuclear events becomes associated with radioactive particles. Such radioactive or 'hot' particles are localized aggregations of radioactive atoms larger than ca. 0.5 µm that give rise to an inhomogeneous distribution of radionuclides significantly different from that in the background matrix (Salbu, 2000; Török et al 2004). They are formed through critical or subcritical destruction of radioactive material (e.g. explosion, fire, corrosion processes), and by clustering, condensation, or interactions of radionuclides with reactive particle surfaces during release and dispersion (Salbu, 2000). Radioactive particles enter the environment from different sources, and the behaviour and impact of these particles in the environment is related to their physicochemical forms and weathering effects. This chapter will review all sources of radioactive particles in the environment, focusing on actinide-containing particles derived from reprocessing of nuclear fuel and use of depleted uranium munitions which were of interest in this thesis.

1. Sources of environmental radioactive particles

1.1. Nuclear weapon tests

The main contribution to artificial environmental radioactivity is the testing of nuclear weapons in the atmosphere, from 1945 to 1980. Each nuclear test resulted in uncontrolled release into the environment of substantial quantities of radioactive materials, which were widely dispersed in the atmosphere and deposited on the Earth's surface (UNSCEAR, 2000).

Focusing on actinides, fallout from more than 2300 atmospheric, surface, underground and underwater nuclear weapon tests is the major global source of radioactive contamination

(UNSCEAR, 1993). Atmospheric nuclear weapons tests conducted from 1945 until 1980 are responsible for the majority of actinide deposition onto the Earth's surface (Pentreath, 1995). During a nuclear explosion a large amount of unfissioned uranium and/or plutonium is dispersed, with a consequent release of radioactivity into the atmosphere. It has been estimated that about 1.1 x 10^{16} Bq of $^{239+240}$Pu have been globally released from atmospheric nuclear testing, mainly from explosions of megaton-range weapons that took place before 1963 (UNSCEAR, 2000). During the late 1950s and 1960s, radioactive particles were observed at different test sites (Crocker et al., 1966).

Marshall Islands (1946-1958): During the period from 30th June 1946 to 18th August 1958, the US conducted 67 atmospheric and ground-surface nuclear tests in the Marshall Islands (UNSCEAR, 2000). Following the nuclear weapon tests at Bikini and Enewetak atolls and the Marshall Islands, hot spots or localized heterogeneities in soils have been identified (Eriksson et al., 2005). Based on microanalytical and X-ray techniques, µm-sized particles, composed mainly of Pu, with a ^{240}Pu/^{239}Pu atom ratio less than 0.065, corresponding to weapons-grade plutonium, have been identified in Runit Island soil (Jernstrom et al., 2006). Particle characteristics (size, shape, and colour) depend on devices and shot conditions (Crocker et al., 1966).

Nevada test site (1951-1962): At the Nevada test site, USA, 84 atmospheric and surface ground weapon tests and more than 900 underground tests were conducted during 1951-1962 (Salbu, 2008). Following these tests, radioactive particles have been isolated from topsoil samples and characterized using microanalytical and X-ray techniques (Faber and Landingham, 1977). The particle size distribution was also reported to be dependent on device and shot conditions. Shots at high altitude resulted in spherical, small, dense particles with high activity, while shots at low altitude and ground level gave larger, spherical (Figure 1), and irregular shaped particles with low density and low activities (Crocker et al., 1966).

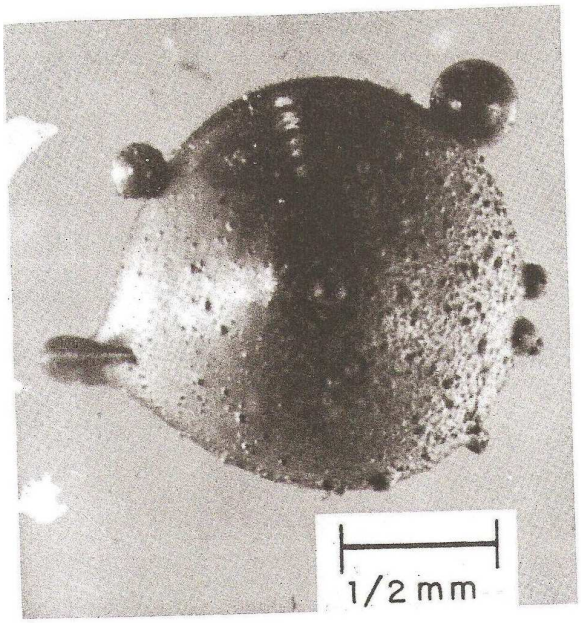

Figure 1. A radioactive fallout particle from a tower shot in Nevada. The particle has a dull metallic lustre and shows numerous adhering small particles (Crocker et al., 1966).

Maralinga, Australia (1953-1963): At the Maralinga and Emu sites, Southern Australia, nine nuclear weapon tests and several hundred smaller-scale weapon trials were conducted by the UK during 1953-1963. The largest and most significant area of contamination, resulted from the 12 hydronuclear experiments conducted at Maralinga from 1960 to 1963, in which 22.2 kg of uranium and 47.3 kg of plutonium were dispersed. Particles up to several hundred μm in size, composed mainly of plutonium, homogenously distributed across the particles surface, were observed (Cooper et al., 1994; Burns et al., 1995).

Semipalatinsk, Kazakhstan (1949-1989): At Semipalatinsk, nuclear weapon tests were performed mainly in the atmosphere. Subsequently, after the signing of the 1963 treaty banning nuclear weapon tests in the atmosphere, in outer space and under water, only underground tests were conducted at Semipalatinsk. Nuclear tests at the site ceased in 1989. A total of 456 nuclear tests were conducted at the site with the total energy released being 17.4 Mt of TNT equivalent (IAEA, 1998). Following such nuclear weapon tests, relatively large radioactive particles (several hundred μm) containing Pu and U were identified at the ground surface. Pu associated with particles or fragments, with activity levels exceeding 50 kBq kg^{-1}, has been reported (Salbu, 2008).

Mururoa and Fangataufa, French Polynesia (1966-1996): Most of the tests were conducted at Mururoa, the larger of the two atolls, although the larger tests were generally conducted at Fangataufa. 41 atmospheric and 137 underground nuclear weapon tests and

15 surface and underground trials using conventional explosives were conducted during 1966-1996. Most of the atmospheric tests were done by hanging the device from a balloon at a considerable elevation above the ground. The majority of underground tests were performed with devices lowered into holes drilled into the rock beneath either the rim or the lagoon of the atolls (IAEA, 2010). Following the nuclear weapon tests and particularly weapon trials, radioactive particles up to several hundred µm in size, with activities typically 5-30 kBq but up to 1MBq, were identified (Bleise et al., 2003).

Novaya Zemlya (1950s-1990): At Novaya Zemlya, about 130 atmospheric, underground and underwater nuclear weapon tests were carried out during 1950-1990. Significant contamination, hot spots and localized heterogeneities were observed within the three major test sites, and could be attributed to specific shot scenarios (Salbu, 2000). In particular, in Chyornaya Guba, where underwater weapons tests took place in 1955, 1957 and 1961, localized heterogeneities of radionuclides in sediments indicate the presence of radioactive particles (Salbu, 2008).

1.2 Accidents with nuclear devices

Palomares, Spain (1966): On 17 January 1966, a B-52 bomber aircraft caught fire at an altitude of 8500 m above the village of Palomares. Two of the bombs detonated conventionally upon impact on land. The explosion and subsequent fire caused the dispersion of particles containing Pu and U over a terrestrial area of about 2.3 km^2 situated close to the Mediterranean (Jimenez-Ramoz, 2006). The particles contained a mixture of enriched uranium and weapon-grade plutonium material (Lind et al., 2007).

Thule, Greenland (1968): In January 1968, a B-52 bomber from the US Strategic Air Command carrying four nuclear weapons, caught fire and crashed on the sea ice on Bylot Sound, about 12 km off the Thule Air Base in northwest Greenland (Moring et al., 2001). As a result, particles containing Pu and U were dispersed in sediments at the point of impact (Eriksson et al., 2005).

1.3 Nuclear accidents

Windscale, Sellafield UK: During the early 1950s, about 20 kg of uranium were released to the atmosphere from one of the two air-cooled, graphite-moderated uranium metal reactors operating at Windscale, UK, from 1951 to 1957 (Salbu, 2000). Due to corrosion of spent fuel elements misplaced in the air duct leading to the discharge stack, and inefficient

filtering, fuel particles up to 700 μm in size were deposited in the region (Salbu et al., 1998). The release of irradiated nuclear fuel particles from Windscale was reviewed by Smith et al. (2007).

Chernobyl accident 1986: In 1986, about 6-8 tonnes of irradiated UO_2 fuel were released into the atmosphere from the Chernobyl reactor due to the initial explosion and the subsequent fire at Unit 4 (Salbu, 2000). About 2 x 10^{18} Bq of condensable radioactive materials were released, the majority of which was deposited in Europe. Large fuel particles with variable radionuclide composition deposited within the 30 km zone, while small-sized particles were identified up to 2000 km from the site (Devell et al., 1986; Kuriny et al., 1993). Following the high temperature accident, different uranium fuel particles were observed, varying in composition, morphology and structure (Salbu et al., 1998).

1.4 The nuclear fuel cycle and reprocessing in the UK

The nuclear fuel cycle (Figure 2) is the sequence of processes which involve the production of energy from uranium in nuclear reactors. Uranium is widely dispersed and usually found in low concentrations. It is mined in a number of countries and needs to be enriched and fabricated in order to be used as fuel for nuclear reactors. Spent fuel can be reprocessed to produce fresh fuel, after being removed from the reactor. The nuclear fuel cycle starts with the mining of uranium and ends with the disposal of nuclear waste. With the reprocessing of used fuel as an option for nuclear energy, the stages form a true cycle (WNA, 2010a).

Nuclear fuel reprocessing will be discussed in detail, as a source of radioactive particles associated with the low-level radioactive effluent discharged into the sea.

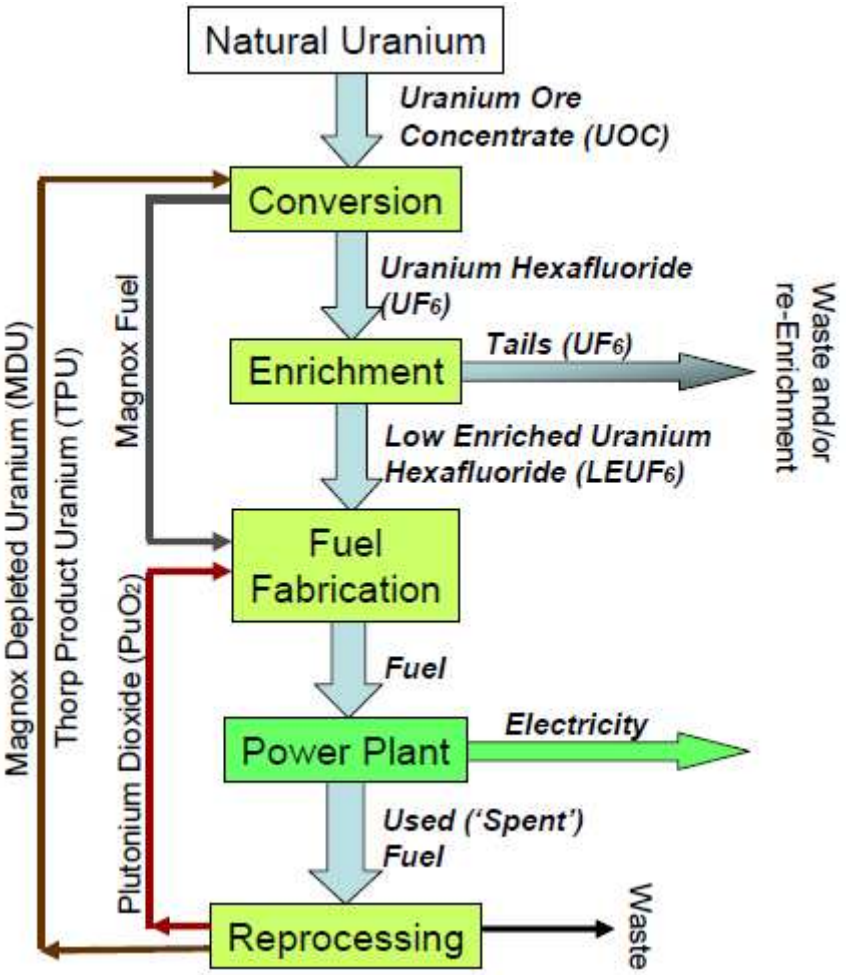

Figure 2. Schematic of the nuclear fuel cycle in the UK (NDA, 2007)

1.4.1 Reprocessing of spent nuclear fuel

An exceptional characteristic of nuclear energy is that used fuel (irradiated nuclear fuel that no longer sustains nuclear reactions) can be reprocessed in order to provide fresh fuel for nuclear reactors. UK, France, Russia and Japan have a policy to reprocess used nuclear fuel. The main reason for reprocessing used fuel has been to recover uranium and plutonium for reuse and thus close the fuel cycle, gaining more energy from the original uranium in the process (WNA, 2010b). A secondary reason is to condition the waste into suitable form for disposal (Wilson, 1995). The composition of spent fuel varies as a function of the type of fuel and reactor, neutron spectrum, flux, burn-up and the cooling time after removal from the reactor (Choppin et al., 2002). Table 1 shows the typical composition of spent nuclear fuel after it has been used in the reactor.

Materials	Mass %	Radioactivity %
U	96	0.0001
Pu	1	2.5
Fission products	3	97.1
Minor actinides (Np, Am, Cm)	0.2	0.4

Table 1. Composition of spent nuclear fuel (Wilson, 1995)

Used fuel assemblies taken from the reactor core are highly radioactive and give off a lot of heat. They are therefore stored in special ponds which are usually located at the reactor site, to allow both their heat and radioactivity to decrease. The water in the ponds acts as a barrier against radiation and disperses the heat from the spent fuel. This storage is intended only as an interim step before the spent fuel is either reprocessed or sent to final disposal (Lo Frano et al., 2010).

All currently operating, large scale reprocessing plants use PUREX (plutonium and uranium recovery by extraction) process employing a mixture of tri-n-butyl phosphate (TBP) in hydrocarbon diluent. This involves dissolving the fuel elements in hot concentrated nitric acid and chemical separation of uranium and plutonium is then undertaken by solvent extraction (Figure 3). The Pu and U are transferred to the organic phase by forming nitrate complexes with TBP, leaving most of the fission products (FPs) in the aqueous phase (Mcfarlane, 2004). TBP is a neutral extractant which requires a negative counter-ion to allow extraction of metallic cations. Certain oxidation states of actinides complex with many ions, but nitrate complexes have proved to be uniquely useful for the extraction of U and Pu (Wilson, 1995).

$$UO_2^{2+} + 2NO_3^- + 2TBP \longrightarrow UO_2(NO_3)_2.2TBP$$

$$Pu^{4+} + 4NO_3^- + 2TBP \longrightarrow Pu(NO_3)_4.2TBP$$

In the subsequent cycle, U/Pu separation is achieved by back-extracting Pu into the aqueous phase by reduction to Pu(III).

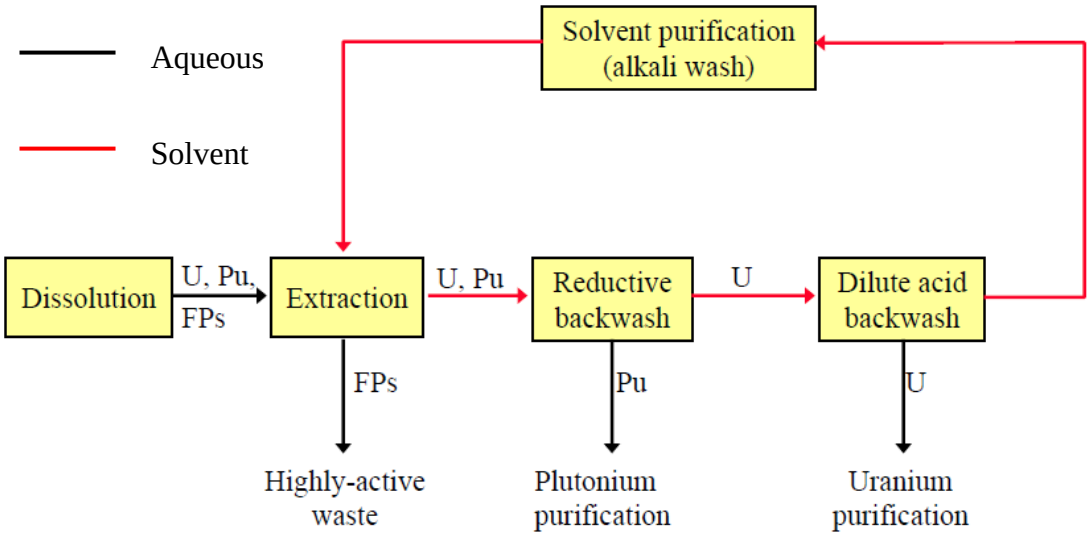

Figure 3. Reprocessing of spent nuclear fuel

The remaining liquid after Pu and U are removed is high-level waste, containing about 3% by mass of the used fuel in the form of fission products and minor actinides (Np, Am, Cm). It is highly radioactive and continues to generate a lot of heat. It is conditioned by calcination and incorporation of the dry material into borosilicate glass, then stored pending disposal. Fuel reprocessing gives rise to low level radioactive effluent which is discharged into the sea or rivers via pipelines. The world's first plutonium reprocessing plant in Hanford (USA) discharged liquid waste via the Columbia River into the Pacific Ocean (Poston et al., 2007). The two largest reprocessing facilities in Europe, Sellafield in northern England and La Hague in northern France, discharge radioactive waste into the Irish Sea and English Channel respectively. Historically, these have represented some of the highest radioactive waste discharges into the sea and over 97 percent of all the radioactive discharges from all nuclear facilities in Europe.

European nuclear reprocessing plants: Effluent from the reprocessing plants at Sellafield and Dounreay, UK, and La Hague, France, are the major sources of radionuclides entering the North Sea, Irish Sea, Norwegian Sea, Barents and Kara Seas. The great majority of artificial radionuclides released to the sea originate from Sellafield (Table 2)

Facility	Sellafield	La Hague	Dounreay	Total (%)	Total Bq
α – activity	92.5	0.52	1.8	97.5	1.4×10^{15}

Table 2. Contribution (%) to the total discharges within the European community made by reprocessing plants for discharges up to 1984 (Salbu et al., 2003).

Many radionuclides released into the Irish Sea from the Sellafield plant become associated with suspended particles (Kershaw et al., 1986) or are discharged in particulate form (Hamilton, 1981). Due to accidental releases via the effluent discharges at Dounreay, Scotland, in the 1960s, a number of radioactive particles are annually collected at beaches close to the site. The particles are relatively large with high activities (1 x 10^6 Bq), comprise U fuel and contain a series of fission products (Thomson, 2007).

No information on identification of particles released from La Hague identified in the environment is available. However, a major fraction of radionuclides in the effluent from La Hague and Sellafield during normal operation is associated with particles and colloids which are relatively stable in sea waters (Salbu et al., 1993).

Russian reprocessing plants: The Mayaka Production Association (Mayaka PA) was established in the late 1940s to produce Pu for the Soviet nuclear weapons programme. The site is located at the head of the Techa River in the southern Urals and comprises military reactors (isotope production) and civilian reactors (power) as well as reprocessing and metallurgical plants. At Mayaka PA, three major incidents have released radionuclides into the environment (Skipperud et al., 2005):

1- Authorized discharges of liquid radioactive wastes to the Techa River (1949-1951).

2- The Kyshtym accident releases due to an explosion in a high level radioactive waste tank (1957).

3- Wind transport of contaminated sediments from Lake Karachay (1967)

Between 1949 and 1951, an estimated of 110 x 10^{15} Bq of beta emitters and 10 x 10^{12} Bq of alpha emitters were released into the Techa River, causing heavy contamination of the river and flood points (Skipperud et al., 2005). Radioactive particles containing U and heavy metals have been identified in sediments and soils (Salbu, 2005).

1.4.2 Radioactive particles from Sellafield discharges

The direct discharge of low-level radioactive effluents into the NW Irish Sea from Sellafield nuclear fuel reprocessing plant has been a significant flux to the marine environment. Discharges of radioactive effluents from Sellafield to the environment have gone on since commencement of operations at the site in 1951. Currently, authorisation to discharge under the Radioactive Substances Act 1993 is granted by the UK Environment Agency (Gray, 1995). After the mid-1960s, the amounts of discharges increased rapidly,

peaked in the 1970s and have been decreasing since the 1980s (Kershaw et al., 1995; Gray, 1995).

Low level liquid effluents arising from a number of sources on the Sellafield site are discharged to the Irish Sea via pipelines which extended about 2.5 km from the high water mark. As discussed earlier, reprocessing involves separating uranium, plutonium and highly radioactive fission products by a series of solvent extraction stages, leaving approximately 99% of the fission products concentrated into the aqueous acid effluent stream for evaporation and storage (Gray, 1995). As plant feed materials have changed during Sellafield's life time, the elemental and isotopic compositions of the discharge have also changed (Gray, 1995). Figure 4 shows Sellafield discharges of plutonium from 1952 to 2005.

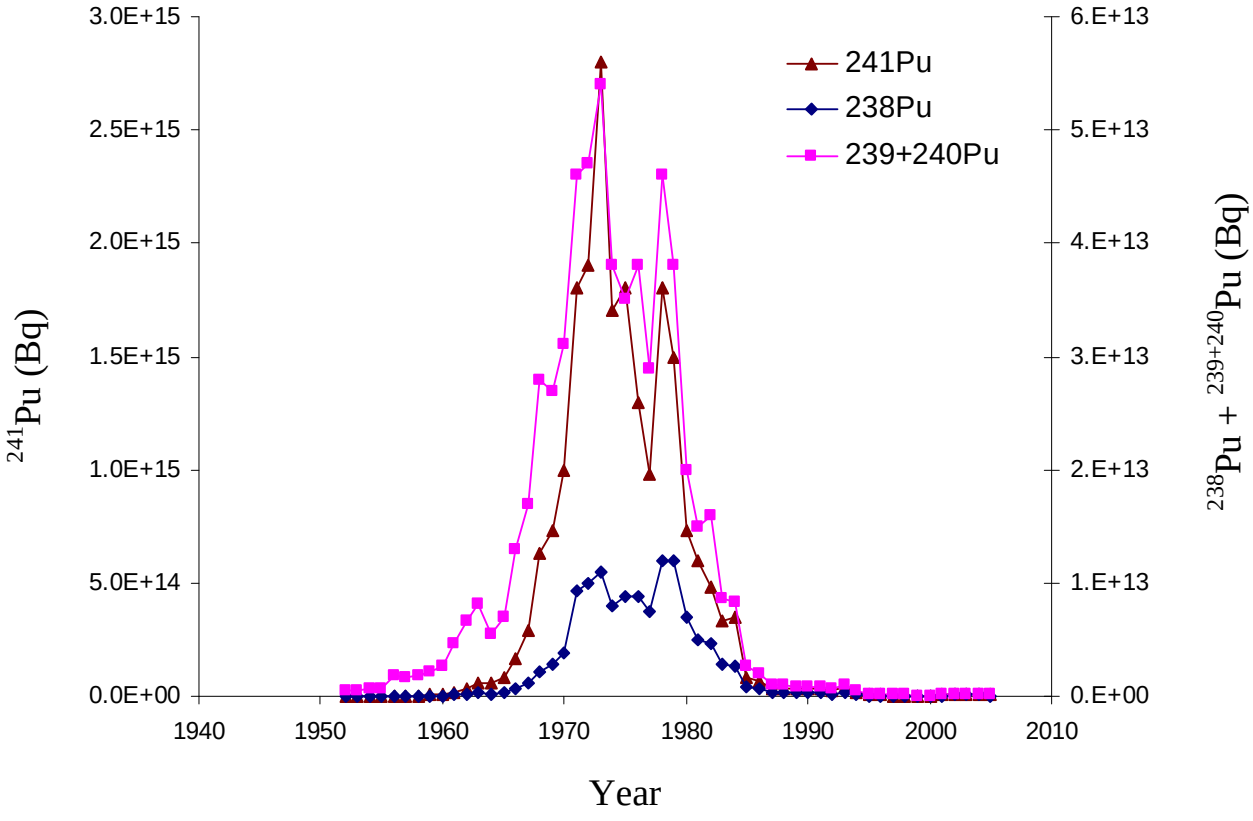

Figure 4. Sellafield Discharges of Plutonium (Gray, 1995; BNFL, 2005).

Because of the need for relatively pure ^{239}Pu for weapons, the fuel rods are removed and the plutonium is separated from them after brief irradiation (low burn-up); the resulting "weapons grade" plutonium is about 93 atom% ^{239}Pu with low ^{238}Pu content, and this was characteristic of early plutonium discharges to the Irish Sea. For power production the fuel in the reactor is irradiated much longer (high burn-up), resulting in a mix that includes

more of the higher isotopes of plutonium and also a higher proportion of ^{238}Pu. Such material is typical of more recent plutonium discharges.

The Sellafield effluent has two sources: pond water, which is discharged continuously, in which spent fuel elements are stored prior to reprocessing, and waste arising from a variety of processes on site, particularly from fuel reprocessing, which are routed through sea tanks and discharged into the sea (Kershaw, 1986). The effluent contains small quantities of U and the α-emitting transuranium elements Np, Pu, Am and Cm (Kershaw et al., 1986). The interaction of these radionuclides with seawater, suspended particulate matter and seabed sediments will be influenced greatly by their chemical and physical forms and associations of the radionuclides in the effluent, together with any changes which take place upon release to the sea (Kershaw, 1986). The eastern Irish Sea basin is generally quite shallow, typically only 30 m deep and, as a result of tidal movement and currents, the fine-grained particles with their associated radionuclides are focused into a belt (ca 15 km long x 3 km wide) of muds and muddy sediments (the 'mud patch') which lies parallel to the coast (Mackenzie et al., 1994; Marsden et al., 2006). Onshore transfer of the particles has resulted in deposition of radionuclides in intertidal, floodplain and beach environments of this area, with highest level of contamination occurring in fine-grained salt marsh and estuarine sediments (MacKenzie et al., 1999). In the Esk estuary (south of Sellafield), a large proportion of the radionuclides which are retained in sediments, is associated with particulate matter (Hamilton and Clarke, 1984). The significant sources of alpha emitting radionuclides in Irish Sea sediments have been classified into three categories. The highest level of activity is associated with hot particles, typically less than 20 μm × 50 μm in size, found in the Esk estuary sediments, originating from spent nuclear fuel debris from Sellafield plant (Hamilton, 1981). The other significant components containing alpha emitters are the minerals hematite and magnetite, and hydrated iron oxides, which have accumulated radionuclides from the sea water (Hamilton, 1998). The salt marsh sediment profiles preserve a record of the Sellafield discharge history (MacKenzie et al., 1994; Morris et al., 2000). The 1970s discharges (when the activity discharged was highest) are reflected in the 10-15 cm section of the intertidal salt marsh sediments in the Esk estuary (Marsden, 2003). In this thesis, nuclear fuel particles derived from 1970s Sellafield discharges and retained in Esk estuary salt marsh sediments were investigated.

1.4.3 Radioactive particles from Dounreay nuclear site

The Dounreay nuclear site, located on the north west of Scotland, released unknown quantities of irradiated nuclear fuel particles during the late 1950s, 1960s and 1970s. The particles were produced during the processing of fuel from the Materials Test Reactor (MTR) and Dounreay Fast Reactor (DFR). MTR particles were produced as a result of fault conditions during milling and cropping operations, prior to reprocessing, whereas DFR particles were most likely produced during combustion incidents in the dissolution cycle during reprocessing (Dennis et al., 2007). In 1983, a routine radiological survey on the Dounreay beach, using handheld beta-gamma probes, discovered a radioactive particle. Analyses showed the particle was a fragment of irradiated MTR fuel. It was composed of aluminium and small amount of uranium as well as fission products (Toole, 2007). Since the 1983 discovery, routine monitoring for particles has been carried out at selected locations distributed over 25 km of coastline, centred on the Dounreay foreshore and seabed sediments and the public beaches. A large number of high activity (MBq) particles have since been found in the intertidal and marine environment in the vicinity of Dounreay, by detecting ^{137}Cs gamma radiation (Crawford et al., 2007; Goss and Liddiard, 2007). In August 2008, Dounreay Site Restoration Ltd (DSRL) started to clean up the seabed where the most hazardous of these particles are to be found. This continued in the summer of 2009, when more than a hundred particles were retrieved from the seabed. DSRL regularly updates a list of all particles detected around the site (DSRL, 2010). Figure 5 below shows a Dounreay particle.

Figure 5. Example of a Dounreay MTR particle.Cs-137 activity ~ 3 x 10^5 Bq, Spesific activity ~2 x 10^9 Bq g^{-1}(Charles and Harrison, 2007).

1.5 Depleted Uranium (DU)

Natural and depleted uranium

Uranium is present in most rocks and soils in concentrations of 2 to 4 ppm and is as common in the Earth's crust as tin, tungsten and molybdenum. It is also found in sea water, at an average concentration of 1.3 ppb. It occurs as the mixed uranium oxide (U_3O_8) in amorphous (pitchblende), or crystalline forms (uraninite) (Craft et al., 2004). There are a number of locations in different parts of the world where it occurs in economically-recoverable concentrations. Natural uranium is comprised of three main isotopes, primordial ^{238}U and ^{235}U, which are parent members of natural radioactive decay series and ^{234}U, which is a decay product of ^{238}U. The isotope ^{235}U is the only naturally-occurring isotope which can sustain a fission chain reaction, releasing large amounts of energy. For most of the world's reactors, the next step in making a useable fuel is to convert the uranium oxide into a gas, uranium hexafluoride (UF_6), which enables it to be enriched. Enrichment increases the proportion of the ^{235}U isotope from its natural level of 0.7% to about 3 - 5%. The uranium that remains after the enrichment process, commonly called depleted uranium (DU), has decreased levels of ^{235}U and ^{234}U, and a slightly increased level of ^{238}U (Table 3). Every tonne of natural uranium produced and enriched for use in a nuclear reactor gives about 130 kg of enriched fuel (ca 3.5% ^{235}U). The balance is depleted uranium tails (^{238}U, typically with 0.2-0.3% ^{235}U and 0.001% ^{234}U) (WNA, 2009). In addition, because some reprocessed uranium is used in the enrichment process, DU may also contain small traces of ^{236}U, transuranium nuclides ($^{239+240}Pu$, ^{241}Am and ^{237}Np) and the fission product ^{99}Tc (Nuccetelli et al., 2005). The presence of traces of ^{236}U and transuranium radionuclides has been conformed in samples from Kosovo (Danesi et al., 2003). All three natural isotopes of uranium have long half-lives and natural uranium is therefore classified by the International Atomic Energy Agency in the lowest hazard class for radioactive materials as a low specific activity material (The Royal Society, 2001). DU, although having all the chemical and biological properties of natural uranium, is about 40% less radioactive than natural uranium.

Isotope	Natural U wt %	DU wt %	Activity (Bq/mg natural U)	Activity (Bq/mg DU)	Half-life (y)
^{238}U	99.28	99.79	12.35	12.41	4.47×10^9
^{235}U	0.72	0.20	0.57	0.16	7.04×10^8
^{234}U	0.0054	0.001	12.49	2.31	2.45×10^5
U			25.41	14.88	

Table 3. Composition and activities of natural and depleted uranium (UNEP, 2003).

The isotopic composition of natural uranium is clearly different from that of depleted uranium, and that can be used to identify and quantify DU in environmental samples, by measuring the isotopic ratios $^{235}U/^{238}U$ and $^{234}U/^{238}U$, which are indicative of the degree of depletion Figure 6.

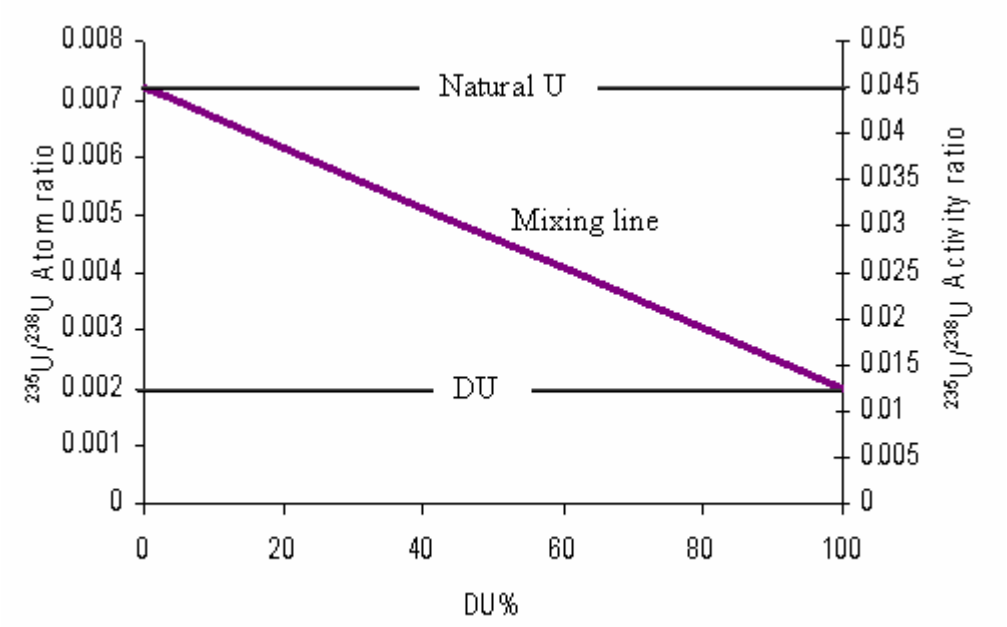

Figure 6. Isotopic composition of natural U and DU

Physicochemical properties of DU

DU in the metallic form has a high density of 19.07 g /cm^3, i.e., 1.7 times the density of lead and its hardness, as well as self-sharpening properties, make it superior to classical tungsten armour-piercing munitions (Bem and Bou-Rabee, 2004). When they strike a target, tungsten penetrators blunt while DU sharpens itself as it moves through the armour. DU metal is pyrophoric (so ignites easily when it fragments), and burns at high temperature (600-700 ^oC) to form a series of oxides such as UO_2, UO_3 and U_3O_8 (Harley et al., 1999). When a DU round hits a hard target such as armour-plate, some DU aerosolises and ignites, generating a cloud of oxidized DU dust and aerosol particles. As a result, DU

particles will be dispersed in the vicinity of target area (The Royal Society, 2001). Any remaining particles of metallic uranium will oxidize over time due to weathering (UNEP 2003). On average 10-35% (with a maximum of 70%) of a DU bullet becomes airborne or aerosolised on impact and the particles can spread up to 400 m (Nellis, 2006).

Metallic natural uranium and DU, and many of their alloys, are unstable in contact with air or water and will readily corrode in the natural environment (i.e. they are thermodynamically unstable), giving rise to the formation of corrosion products (typically oxides and hydroxides) on the metal surface (Dstl, 2006).

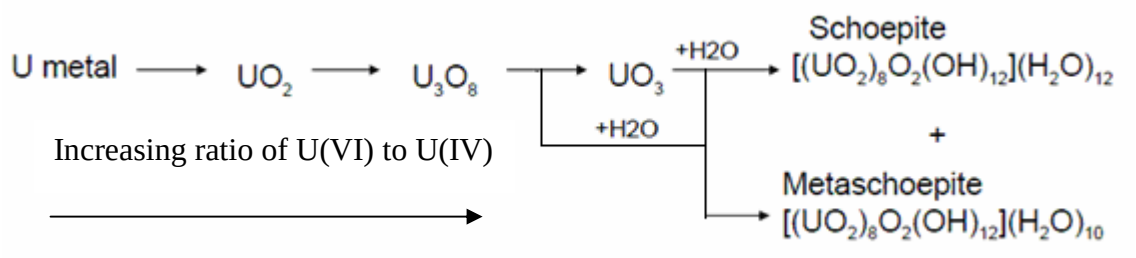

The rate at which they corrode is dependent on particular environment. Reaction rates are affected by many factors such as metal/alloy composition, and environmental factors such as temperature, pH, humidity, microbial community, gas composition and pressure (Dstl, 2006; Handley et al., 2008).

Military use of DU

Gulf war (1991)

During the first Gulf War (Desert Storm), the first conflict where DU munitions were known to be used, about 300 tons of DU was deposited in Kuwait and southern Iraq (Figure 7). Most DU (~250 tonnes) was fired from A-10 aircraft as 30 mm rounds (300 g DU each), and ~50 tonnes DU was fired from tanks as 120 mm rounds (5 kg each) (Fitter and Hippel, 2000; Bleise, 2003). A large fraction of DU bullets (~ 90%) fired from aircraft missed their intended targets (Ben and Bou-Rabee, 2004). The majority of these projectiles is still buried at various levels in the ground.

Figure 7. Principal locations of DU munitions use in Iraq and Kuwait (Marshall, 2005).

Bosnia and Herzegovina (1995)

About 10,800 DU rounds (approximately 3 tonnes of DU) were fired during NATO air strikes in Bosnia-Herzegovina in 1994 and 1995, mainly around Sarajevo (Bleise et al., 2003). The area was exposed to DU dust, which dispersed in the surface soil (0-5 cm), but the contamination was quite localized giving widely variable concentrations of 0.01-100 g DU/ kg of soil (UNEP, 2003).

Kosovo (1999)

Beginning on 24 March 1999, NATO aircraft bombarded Yugoslavia for 78 days. In particular, US A-10 aircraft used at least 30,000 rounds, corresponding to about 10 tonnes of DU, against Serbian tanks in Kosovo. A total of 112 sites in and close to the border of Kosovo were hit with DU munitions (Bleise et al., 2003). The majority of these rounds missed their targets and remain buried in the ground at depths that make them very difficult to recover (McLaughlin et al., 2003).

The aircraft-fired DU rounds employed have a length of 173 mm and a diameter of 30 mm and contain a conical DU penetrator, 95 mm in length and with a base diameter of 16mm, weighing 300 g. The penetrator is fixed in an aluminium jacket 60 mm long and 30 mm in width (Figure 8). When the penetrator hits an armoured vehicle, the penetrator continues through the armouring, but the jacket usually remains outside.

Figure 8. DU round fired in Kosovo (UNEP, 2001)

DU in surface and subsurface soils

DU munitions deposited during military activities consist mainly of whole penetrators and large fragments, since 70–90% of penetrators fired from aircraft miss their targets (Mellini and Riccobono, 2005); and a penetrator that hits its target will normally lose 10–35% and up to 70 % of its mass (Papastefanou, 2002). Most dust particles formed are smaller than 5 micrometers in size and, when released into the atmosphere, spread according to wind direction. By sedimentation, DU particles are deposited on the ground and other surfaces. Pieces or fragments of metallic DU can also be formed and scattered around (The Royal Society, 2002; UNEP, 2003). Over time, these will be gradually transported down into the upper soil layer, mostly through physical turnover (UNEP, 2003).

Since about 70% of DU penetrators miss their target, a significant amount of DU will be buried in the ground. Most penetrators hitting soft ground will probably penetrate intact more than 50 cm into the ground and remain there for a long period of time, depending on the weathering/ geochemical conditions (The Royal Society, 2002). Uranium metal is unstable in the natural environment, so corrosion products (e.g. schoepite, metaschoepite) will form on the metal surface. The maximum solubility of oxidized uranium phases forming surface layers on penetrators (e.g. schoepite) at near-neutral pH is about 10 ppm (UNEP, 2003). As the uranium metal oxidizes, the soils and rocks will initially contain elevated concentrations of corroding uranium rather than solid uranium metal. With time, the corroding uranium will dissolve and uranium will move downward through the soil as

mobile UO_2^{2+}.Through the dissolution of corrosion products, UO_2^{2+} can be transported to deeper ground layers and may reach the ground water (Mellini and Riccobono, 2005).

Environmental and health impacts of DU

The use and testing of DU munitions has led to the release of DU into the environment at several locations around the world. There are two types of environmental impact of DU: (1) Firing impact, arising when a DU penetrator hits a hard target and DU aerosol particles and fragments are deposited in the vicinity; (2) Corrosion impact: when DU penetrators miss their target and embed in the ground, corrosion products will be formed and distributed in the surrounding soils. Concerns arise from both as DU is chemically toxic and weakly radioactive. Its use on the battlefield can lead to it being spread over a wide area, with potentially hazardous consequences for both military and civilian populations and for the environment generally (The Royal Society, 2001; Bailey et al., 2002). The three main routes of human exposure to DU on the battlefield are inhalation, ingestion and wounding. The greatest exposure to radiation resulting from inhaled DU particles will be to the lungs and associated lymph nodes, and an increased risk of lung cancer is considered to be the main radiation risk (Bailey et al., 2002). Any health effects will depend critically on the particle size and chemical nature of the inhaled aerosol.

With time, chemical weathering will cause corrosion of metallic DU in the ground, dispersion in the soil and, after slow oxidation, transformation into soluble chemical forms. Finally after migration to the surface and underground water it will eventually be incorporated into the food chain. Therefore, people can be exposed to the released DU in a number of ways. These include external exposure to the radiation emitted from uranium, the inhalation of DU particles mainly during the war period and the ingestion of contaminated water or food after the end of war (Papastefanou, 2002; DoD, 1998).

1.2 Characterization of radioactive particles

In the majority of the above mentioned release scenarios, the radioactive material is dispersed into the environment as discrete particles. Therefore, it is very important to study the behaviour of these radioactive particles in the environment in terms of mobility, weathering and corrosion rates. To understand environmental behaviour, detailed information is required on particle characteristics such as size, morphology, and elemental composition which influence the particle weathering, as well as crystal structure and oxidation states of elements contained in the particle, which influence corrosion and mobility (Salbu et al.,1998). The isotopic composition of uranium and plutonium contained

in the particles reflect the properties and history of the source material and provide detailed information on origin of radioactive particles (Jambers et al., 1995). Overall understanding of the environmental behavior of radioactive particles and related physicochemical processes are key factors in the assessment of their environmental impact and the fate of U and Pu present in the environment in the form of hot particles. Therefore, radioactive particles incorporated in the low-level effluent discharged from Sellafield into the Irish Sea and retained in salt marsh sediments, and depleted uranium particles produced through test-firing of DU pentrators against hard targets and corrosion of unfired DU metal in soils, were investigated in this study. A wide range of characterization techniques will be used to obtain information on these particles (Table 1). The experimental techniques used in this study are explained in Appendix A.

Method	**Information**
Autoradiography	Localization of radioactive particles in soil in order to isolate them for further analysis.
Density separation	Separation of radioactive particles (dense particles) from soil matrix
SEM-EDX	Size and morphology of the particles and surface elemental composition.
XRD	Crystal structure of uranium phases in the particles
Alpha spectrometry	Measuring the activity ratios $^{234}U/^{238}U$ and $^{238}Pu/^{239+240}Pu$ to get information on particle origin
ICP-MS	Measuring the atom ratio $^{235}U/^{238}U$ to quantify DU in environmental samples.
ICP-AES	Quantifying elemental composition to get information on associated elements and environmental behavior.
SIMS	Surface chemistry of the particle and measuring the isotopic composition of uranium to obtain information on the origin of starting and associated elements and their correlations.

Table 4. Experimental and analytical techniques used to identify and characterize environmental radioactive particles in this study.

In this thesis, the techniques listed above will be applied to identification and characterization of environmental radioactive particles to obtain information which will help in understanding environmental behaviour, determining origins, predicting fate, and assessing environmental impact.

References

Bailey, M. R., V. Beral, et al. (2002). "The health effects of depleted uranium munitions: A summary." Journal of Radiological Protection **22**(2): 131-139.

Bem, H. and F. Bou-Rabee (2004). "Environmental and health consequences of depleted uranium use in the 1991 Gulf War." Environment International **30**(1): 123-134.

Bleise, A., P. R. Danesi, et al. (2003). "Properties, use and health effects of depleted uranium (DU): A general overview." Journal of Environmental Radioactivity **64**(2-3): 93-112.

BNFL (2005). "Annual reports on Radioactive Discharges and Monitoring of the environment published annually." Warrington: BNFL.

Burns, P. A., M. B. Cooper, et al. (1995). "Characteristics of plutonium and americium contamination at the former U.K. atomic weapons test ranges at Maralinga and Emu." Applied Radiation and Isotopes **46**(11): 1099-1107.

Charles, M. W. and J. D. Harrison (2007). "Hot particle dosimetry and radiobiology--past and present." Journal of radiological protection : official journal of the Society for Radiological Protection **27**(3 A): A97-109.

Choppin, G., Liljenzin, J, Rydberg, J (2002). "Radiochemistry and Nuclear Chemistry." 3rd edition.

Cooper, M. B., P. A. Burns, et al. (1994). "Characterization of plutonium contamination at the former nuclear weapons testing range at Maralinga in South Australia." Journal of Radioanalytical and Nuclear Chemistry **177**(1): 161-184.

Craft, E. S., A. W. Abu-Qare, et al. (2004). "Depleted and natural uranium: Chemistry and toxicological effects." Journal of Toxicology and Environmental Health - Part B: Critical Reviews **7**(4): 297-317.

Crawford, R., J. Toole, et al. (2007). "Studies at Dounreay on the repopulation of offshore sediments by hot particles." Journal of radiological protection : official journal of the Society for Radiological Protection **27**(3 A): A61-76.

Crocker, G. R., J. D. O'Connor, et al. (1966). "Physical and radiochemical properties of fallout particles." Health Physics **12**(8): 1099-1104.

Danesi, P. R., A. Bleise, et al. (2003). "Isotopic composition and origin of uranium and plutonium in selected soil samples collected in Kosovo." Journal of Environmental Radioactivity **64**(2-3): 121-131.

Dennis, F., G. Morgan, et al. (2007). "Dounreay hot particles: the story so far." Journal of radiological protection : official journal of the Society for Radiological Protection **27**(3 A): A3-11.

Devell, L., H. Tovedal, et al. (1986). "Initial observations of fallout from the reactor accident at Chernobyl." Nature **321**(6067): 192-193.

DoD (1998). "Depleted uranium in the Gulf." http://www.gulflink.osd.mil/du.

DSRL (2010). "Dounreay Site Restoration Ltd, Particle clean-up" http://www.dounreay.com/particle-cleanup.

Dstl (2006). "MOD DU Programme - the corrosion of depleted uranium in the Kirkcudbright and Eskmeals terrestrial environments."

Eriksson, M., J. Osan, et al. (2005). "Source term identification of environmental radioactive Pu/U particles by their characterization with non-destructive spectrochemical analytical techniques." Spectrochimica Acta - Part B Atomic Spectroscopy **60**(4): 455-469.

Faber, K. T. and R. L. Landingham (1977). "The separation, identification and characterization of radioactive particles in topsoil." Powder Technology **16**(2): 209-216.

Fetter, S. and F. N. von Hippel (2000). "The hazard posed by depleted uranium munitions." Science & Global Security: The Technical Basis for Arms Control, Disarmament, and Nonproliferation Initiatives **8**(2): 125 - 161.

Goss, O. E. and M. Liddiard (2007). "Management of particles detected on the Dounreay site." Journal of radiological protection : official journal of the Society for Radiological Protection **27**(3 A): A89-96.

Gray, J., S. R. Jones, et al. (1995). "Discharges to the environment from the Sellafield site, 1951-1992." Journal of Radiological Protection **15**(2): 99-131.

Hamilton, E. I. (1981). "Alpha-particle radioactivity of hot particles from the Esk estuary." Nature **290**(5808): 690-693.

Hamilton, E. I. and K. R. Clarke (1984). "The recent sedimentation history of the Esk estuary, Cumbria, U.K.: The application of radiochronology." Science of the Total Environment **35**(3): 325-386.

Handley-Sidhu, S., P. J. Worsfold, et al. (2008). "Corrosion and Fate of Depleted Uranium Penetrators under Progressively Anaerobic Conditions in Estuarine Sediment." Environmental Science & Technology **43**(2): 350-355.

Harley, N., E. C. Foulkes, et al. (1999). "A Review of Scientific Literature as it Pertains to Gulf War Illnesses; Volume 7; Depleted Uranium. RAND Document Number MR-1017/7-OSD." http://www.rand.org/publications/MR/MR1018.7.

IAEA (1998). "Radiological Conditions at the Semipalatinsk Test Site, Kazakhstan: Preliminary Assessment and Recommendations for Further Research." Radiological Assessment Report (Vienna: IAEA)

IAEA (2010). "The Situation at Mururoa And Fangataufa Atolls." http://www-ns.iaea.org/appraisals/mura-fang.htm.

Jambers, W., L. De Bock, et al. (1995). "Recent advances in the analysis of individual environmental particles: A review." The Analyst **120**(3): 681-692.

Jernstrom, J., M. Eriksson, et al. (2006). "Characterization and source term assessments of radioactive particles from Marshall Islands using non-destructive analytical techniques." Spectrochimica Acta - Part B Atomic Spectroscopy **61**(8): 971-979.

Kershaw, P. J., J. H. Brealey, et al. (1986). "Alpha-emitting, hot particles in Irish Sea sediments." Science of the Total Environment **53**(1-2): 77-87.

Kershaw, P. J., D. S. Woodhead, et al. (1995). "Plutonium from european reprocessing operations - Its behaviour in the marine environment." Applied Radiation and Isotopes **46**(11): 1121-1134.

Kuriny, V. D., Y. A. Ivanov, et al. (1993). "Particle-associated Chernobyl fall-out in the local and intermediate zones." Annals of Nuclear Energy **20**(6): 415-420.

Livingston, H. D. and P. P. Povinec (2000). "Anthropogenic marine radioactivity." Ocean and Coastal Management **43**(8-9): 689-712.

Lo Frano, R., G. Pugliese, et al.(2010). "Thermal analysis of a spent fuel cask in different transport conditions." Energy **in press**.

MacKenzie, A. B. (2000). "Environmental radioactivity: Experience from the 20th century - Trends and issues for the 21st century." Science of the Total Environment **249**(1-3): 313-329.

MacKenzie, A. B., G. T. Cook, et al. (1999). "Radionuclide distributions and particle size associations in Irish Sea surface sediments: Implications for actinide dispersion." Journal of Environmental Radioactivity **44**(2-3): 275-296.

MacKenzie, A. B., R. D. Scott, et al. (1994). "Sediment radionuclide profiles: Implications for mechanisms of Sellafield waste dispersal in the Irish Sea." Journal of Environmental Radioactivity **23**(1): 39-69.

Marsden, O. J. (2003). "Determination of actinide distributions in intertidal sediments from West Cumbria, UK." Ph.D Thesis, University of Manchester, UK.

Marsden, O. J., L. Abrahamsen, et al. (2006). "Transport and accumulation of actinide elements in the near-shore environment: field and modelling studies." Sedimentology **53**(1): 237-248.

Marshall, A. C. (2005). "An analysis of uranium dispersal and health effects using Gulf war case study." Sandia Natinal Laboratories.

Mcfarlane, H. F. (2004). "Nuclear Fuel Reprocessing" Encyclopedia of Energy, Elsevier (2004). **4**: 351-364.

McLaughlin, J. P., L. León Vintró, et al. (2003). "Actinide analysis of a depleted uranium penetrator from a 1999 target site in southern Serbia." Journal of Environmental Radioactivity **64**(2-3): 155-165.

Mellini, M. and F. Riccobono (2005). "Chemical and mineralogical transformations caused by weathering in anti-tank DU penetrators ("the silver bullets") discharged during the Kosovo war." Chemosphere **60**(9): 1246-1252.

Moring, M., T. K. Ikaheimonen, et al. (2001). "Uranium and plutonium containing particles in a sea sediment sample from Thule, Greenland." Journal of Radioanalytical and Nuclear Chemistry **248**(3): 623-627.

Morris, K., J. C. Butterworth, et al. (2000). "Evidence for the remobilization of Sellafield waste radionuclides in an intertidal salt marsh, West Cumbria, U.K." Estuarine, Coastal and Shelf Science **51**(5): 613-625.

NDA (2007). "Uranium and Plutonium: Macro-Economic Study, final report." Nuclear Decommissioning Authority. http://www.nda.gov.uk/documents/upload/Uranium-and-Plutonium-Macro-Economic-Study-June-2007.pdf

Nellis (2006). "Environmental Assessment for Increased Depleted Uranium Use on Target 63-10, Nevada Test and Training Range."
http://www.nellis.af.mil/shared/media/document/AFD-060922-008.pdf

Nuccetelli, C., M. Grandolfo, et al. (2005). "Depleted uranium: Possible health effects and experimental issues." Microchemical Journal **79**(1-2): 331-335.

Papastefanou, C. (2002). "Depleted uranium in military conflicts and the impact on the environment." Health Physics **83**(2): 280-282.

Pentreath, R. J. (1995). "The analysis of Pu in environmental samples: A brief historical perspective." Applied Radiation and Isotopes **46**(11): 1279-1285.

Poston, T. M., R. E. Peterson, et al. (2007). "Past radioactive particle contamination in the Columbia river at the Hanford site, USA." Journal of radiological protection : official journal of the Society for Radiological Protection **27**(3 A): A45-50.

Salbu, B. (2000). "Source-related characteristics of radioactive particles: A review." Radiation Protection Dosimetry **92**(1-3): 49-54.

Salbu, B. (2008). Radioactive Particles Released from Different Nuclear Sources: With Focus on Nuclear Weapons Tests. Nuclear Risks in Central Asia**:** 7-17.

Salbu, B., T. Krekling, et al. (1998). "Characterisation of radioactive particles in the environment." Analyst **123**(5): 843-849.

Salbu, B., L. Skipperud, et al. (2003). "Radionuclide speciation in effluent from La Hague reprocessing plant in France." Health Physics **85**(3): 311-322.

Salbu, B. and O. C. Lind. (2005). "Radioactive particles released from various nuclear sources." Radioprotection 2005, Vol. 40, Suppl. 1, pages S27-S32.

Skipperud, L., B. Salbu, et al. (2005). "Plutonium contamination in soils and sediments at Mayak PA, Russia." Health Physics **89**(3): 255-266.

The Royal Society (2001). "The health hazards of depleted uranium munitions." PartI. http://royalsociety.org/The-health-hazards-of-depleted-uranium-munitions-Part-1-Full-Report/

The Royal Society (2002). "The health hazards of depleted uranium munitions." PartII. http://royalsociety.org/The-health-hazards-of-depleted-uranium-part-II/

Thomson, C. (2007). "A particular problem." Nuclear Engineering International **52**(631): 24-29.

Toole, J. (2007). "History of monitoring beaches around Dounreay, and some future work." Journal of radiological protection : official journal of the Society for Radiological Protection **27**(3 A): A13-21.

Torok, S., J. Osan, et al. (2004). "Characterization and speciation of depleted uranium in individual soil particles using microanalytical methods." Spectrochimica Acta - Part B Atomic Spectroscopy **59**(5): 689-699.

UNEP (2001). "Depleted uranium in Kosovo, Post-conflict environmental assessment." United Nations Environment Programme: Geneva.
http://postconflict.unep.ch/publications/uranium.pdf

UNEP (2003). "Depleted Uranium in Bosnia and Herzegovina. Post-Conflict Environmental Assessment Report." IAEA.
http://postconflict.unep.ch/publications/BiH_DU_report.pdf

UNSCEAR (1993). "Sources and Effects of Ionizing Radiation." United Nations Scientific Committee on the Effects of Atomic Radiation **P 922**.
http://www.unscear.org/unscear/en/publications/1993.html

UNSCEAR (2000). "Sources and Effects of Ionizing Radiation." United Nations Scientific Committee on the Effects of Atomic Radiation **Vol 1**.
http://www.unscear.org/unscear/en/publications/2000_1.html

Wilson, P. (1995). "The Nuclear Fuel Cycle: From Ore to Waste." Oxford Science Publications.

WNA (2009). "Uranium and Depleted Uranium" World Nuclear Association http://worldnuclear.org/info/inf14.html.

WNA (2010a). "The Nuclear Fuel Cycle " World Nuclear Association http://www.world-nuclear.org/info/inf03.html.

WNA (2010b). "Processing of Used Nuclear Fuel" World Nuclear Association http://www.world-nuclear.org/info/inf69.html.

Chapter 2

Identification and characterisation of radioactive particles in salt marsh sediments

The material in the following section has been published in the Actinides 2009 conference proceedings. IOP Conference Series: Materials Science and Engineering, Volume 9, 2010

doi: 10.1088/1757-899X/9/1/012042

Actinides 2009
12–17 July 2009, San Francisco, USA

The candidate's contribution was collection of samples, isolation of particles, radiochemical separation, electron microscopy, alpha spectrometry, interpreting the results, and writing the paper.

Identification and characterisation of radioactive particles in salt marsh sediments

Mustafa Sajih and Francis R. Livens
Centre for Radiochemistry Research, School of Chemistry, University of Manchester, M13 9PL, Manchester, UK.

Abstract. Radionuclides from authorized low level radioactive effluent discharges from the nuclear fuel reprocessing plant at Sellafield, UK, are present in the Irish Sea sediments. The distribution of radionuclides in salt marsh sediment profiles can be related to the discharge history from Sellafield. Radioactive particles, from the intertidal salt marsh sediments in the Esk estuary (10 km from Sellafield), have been isolated and investigated. Autoradiography and heavy liquid density separation were used to find and isolate these particles. Scanning electron microscopy, combined with energy dispersive X-ray analysis (SEM-EDX), was used to obtain information on the morphology and elemental composition of the particles, and alpha spectrometry for radionuclide composition. Particles are typically 1 - 20 μm size. Elemental analysis suggests that they are composed mainly of uranium. Alpha spectrometry shows that they have been irradiated, and transuranium nuclides (Pu, Am, Cm) can be identified in them.

1. Introduction

Low-level radioactive effluents have been discharged under authorization since 1952, into the Irish Sea from the UK nuclear fuel reprocessing plant at Sellafield, UK. The Sellafield effluent has two sources: pond water, which is discharged continuously, in which spent fuel elements are stored prior to reprocessing, and waste arising from a variety of processes on site, particularly from fuel reprocessing, which are routed through sea tanks and discharged into the sea. The effluent contains small quantities of U and the α-emitting transuranium elements Np, Pu, Am and Cm [1]. The interaction of these radionuclides with seawater, suspended particulate matter and seabed sediments will be influenced greatly by

the chemical and physical forms and associations of the radionuclides in the effluent, together with any changes which take place upon release to the sea [1]. The environmental behaviour of radionuclides associated with radioactive particles may differ considerably from that of radionuclides adsorbed reversibly onto solid surfaces, for example of sediment grains, or associated with organic matter. Thus the occurrence and persistence of radioactive particles in the Irish Sea could have important implications for the radiological assessment of the releases and ultimate fate of the radionuclides [1]. The eastern Irish Sea basin is generally quite shallow, typically only 30 m deep and, as a result of tidal movement and currents, the fine-grained particles with their associated radionuclides are focused into a belt (ca 15 km long x 3 km wide) of muds and muddy sediments (the 'mud patch') which lies parallel to the coast [2, 3]. With time, some of the particulates have been redistributed by tidal processes or storm events and deposited in the intertidal areas of local estuaries. The finest sediments settle in the areas of low tidal and wave energy, and are typically found in estuarine salt marshes (where vegetation is an efficient trap for fine suspended particles), for example those of the river Esk. Continuation of these processes will result in an increase in radionuclide inventories in salt marsh sediments [2]. The significant sources of alpha emitting radionuclides in Irish Sea sediments have been classified into three categories [4]. The highest level of activity is associated with hot particles, typically less than 20 μm × 50 μm in size, found in the Esk estuary sediments, originating from spent nuclear fuel debris from Sellafield plant, but these particles have not been fully characterized [5]. The other significant components containing alpha emitters are the minerals hematite and magnetite and hydrated iron oxides [4]. It was observed that the salt marsh sediment profile preserve a record of the Sellafield discharge history. The1970s discharges (when the discharges were maximum) are reflected in the 10-15 cm sections of the intertidal salt marsh sediments in the Esk estuary (Figure 1).

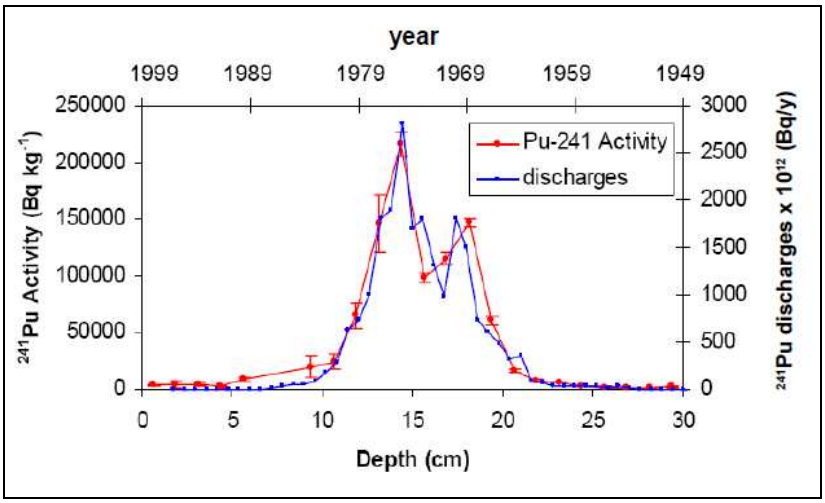

Figure 1. Salt marsh sediment profile and Sellafield discharge of ^{241}Pu from [6].

In this study, radioactive particles from the intertidal salt marsh sediments have been identified and characterized. Particle characteristics produce information on the origin as well as the environmental pathways related to the history of the particle. Characteristics of environmental radioactive particles, i.e. atom/activity ratios, are related to the origin, whereas properties such as size distribution, shape, crystalline structures, and oxidation states of matrix elements depend on the specific conditions of release [7]. Isotopic ratios, as well as elemental distribution in a particle, act as a fingerprint for distinguishing particles from different sources. Analysis of actinide-containing microparticles traditionally consists of search and localization, followed by determination of the phase, general elemental, and isotopic composition, as well as the size and shape of the microparticles. This allows prediction of their fate, i.e., mobility and chemical stability, as well as bioavailability under various conditions [8]. Complex examinations of this kind typically use a combination of different microanalytical methods, such as electron microscopy and X-ray analysis [9].

2. Methods and analysis

2.1. Study site and sample collection

The study area is illustrated in Figure 2. It shows the Esk estuary salt marsh, where sediment sample was collected on 19 March 2008 at low water (detailed site map and sample collection site are presented in supporting information, Figure S1). The sediment core sample (30 cm depth, approximate age range 1950 to present) was sampled by digging and divided into 6 sections (5 cm thick). The 10-15 cm section was analysed in this study, since it is expected to contain radioactive particles deposited from 1970s Sellafield discharges. The other sediment core sections will be investigated later. A block of the 10-15 cm wet sediment section was cut off and hand-ground to small pieces, left to dry and gently ground using a mortar and pestle to obtain a uniform soil sample (particle size < 200 μm).

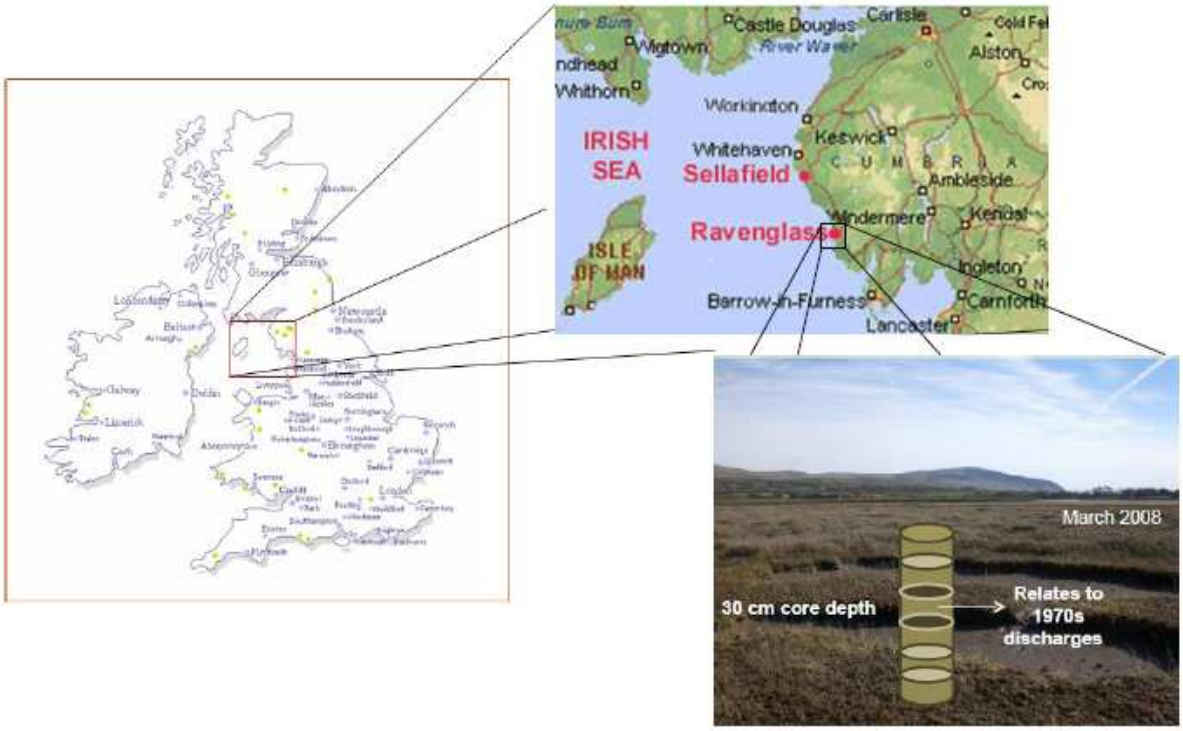

Figure 2. UK map (left), enlargement for Cumbria (top right), and the salt marsh study site (right).

2.2. Analysis

2.2.1. *Autoradiography.* Storage phosphor autoradiography was used to localize radioactive particles in the sediment samples, by placing the phosphor screen (25 x 20 cm) on the sample (dry sediment placed on small filter papers placed on a flat paper) for suitable time and then scanning the screen with laser light using a Typhoon phosphor imager to obtain an image (autoradiograph) of the sample, which maps out the distribution of radioactive particles in the sample (Figure 3).

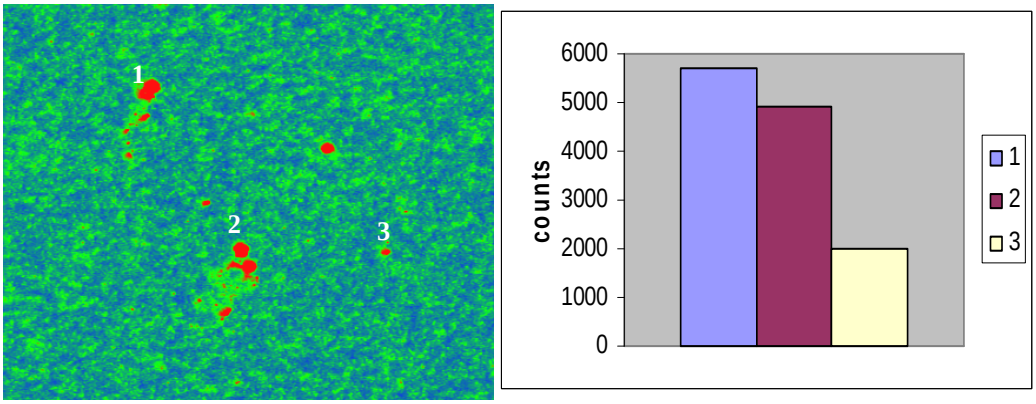

Figure 3. Left: autoradiograph of radioactive particles. The red spots represent radioactive particles in the sample.Right: photostimulable luminescence (PSL) signal for the three red spots.

The other advantage of the technique is that it gives indication of particle activity. The three numbered red spots which have different intensites give different PSL signals which are proportional to the particle activities. These radioactive particles are very difficult to distinguish from fine sediment grains (Figure 4). To isolate the radioactive particles from

the sediment matrix, heavy liquid density separation was used. Uranium oxide particles with a density of about 10 g/cm^3 are much denser than the sediment matrix (~ 2.5 g / cm^3). Separation can be achieved using a heavy liquid with density greater than 2.5 g / cm^3.

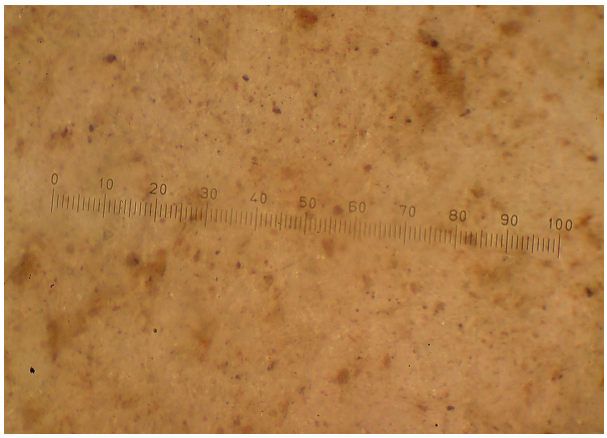

Figure 4. Sediment particles on a filter paper. (one division on the scale = 20 µm).

2.2.2. *Heavy liquid density separation.* In this study, LST fast float heavy liquid (concentrated solution of lithium hetropolytungstate, density 2.83 g/cm^3) was used. Heavy liquid separations are generally done in a separating funnel (Figure 5). The material is transferred from a filter paper into the separating funnel and the heavy liquid is added. The funnel is then shaken to disperse the particles and left to permit light particles to float and heavy particles to sink (when density differences or particle sizes are small, heavy liquid separation can take many hours). When the particles have been separated, the separating funnel is opened and the heavier particles are transferred (in ~1ml heavy liquid) into a 10 ml plastic vial, then washed with deionized water and filtered using a nitrocellulose membrane. The particles are left to dry for further analysis (Figure 5).

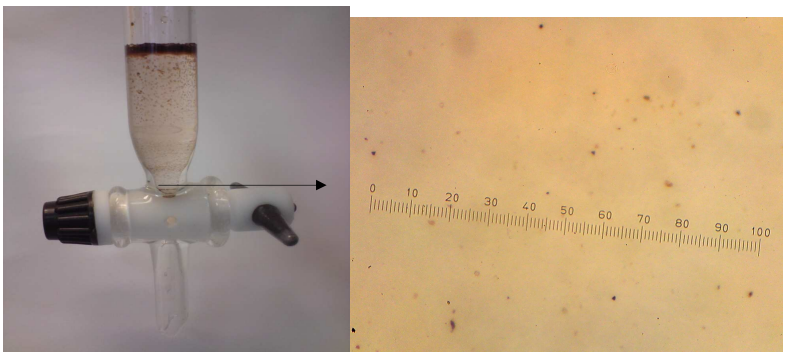

Figure 5. Left: heavy liquid density separation with heavy particles in the bottom and sediment floating on top. Right: an optical microscope image of the heavy particles on a nitrocellulose membrane (one division on the scale = 20 µm).

2.2.3. *Scanning electron microscopy (SEM) – Energy dispersive X-ray analysis (EDX).*

Electron microscopy and X-ray analysis are very useful in characterizing microparticles, providing information on morphology (topographic images and size) and surface elemental composition. The interaction of electrons with matter in electron microscopy can produce different signals which can be used to characterize the sample; secondary electrons to provide information on morphology of the particles, backscattered electrons for detection of high atomic number elements as bright regions and emitted X-rays to provide information on elemental composition. SEM-EDX has been used to obtain information on the morphology and elemental composition of radioactive particles. The samples were prepared by fixing the sample (particles on nitrocellulose filter paper above) on sticky carbon pads stuck on aluminum stubs (12 mm dia) suitable for SEM-EDX analysis. The instrument used throughout this study was a FEI XL 30 ESEM.

2.2.4. *Alpha spectrometry*. Alpha spectrometry was used to identify the radionuclide and isotopic composition of the radioactive particles. The separated particles were dissolved in concentrated nitric acid. The mixture was brought to the boil on a hot plate, then left to cool to ensure full sample digestion. The sample solution was made up with deionized water, filtered through a 0.22 μm PVDF membrane filters, evaporated to dryness and redissolved in 10 ml of 0.1 M HNO_3. An aliquot of the 10 ml sample solution was evaporated to dryness and dissolved in 15 ml electrolyte solution (4% ammonium oxalate in 0.3 m HCl), and electrodeposited onto a stainless steal planchette, with electrodeposition conditions (0.5 A, 20 V, 2 hrs). The remaining aliquot (5 ml) of the sample solution was used for Pu separation using anion exchange resin (Bio-Rad AG1-X8) to determine Pu isotopic composition [10]. Alpha sources were counted using a PIPS type Si detector (Canberra, Belgium, model A 450 – 18 AM), counting efficiency 20-25%. Counting time was variable depending on sample activity. Genie 2000 3.1 software was used to analyze alpha spectra.

3. Results and Discussion

3.1. Size, shape and composition analysis by SEM-EDX

Initially, some samples were analyzed before density separation, preparing SEM samples from the sediment which had been shown by autoradiography to contain radioactive particles. Backscattered electron imaging (BSE) was used to find high Z (uranium) particles as bright spots (Figure 6).

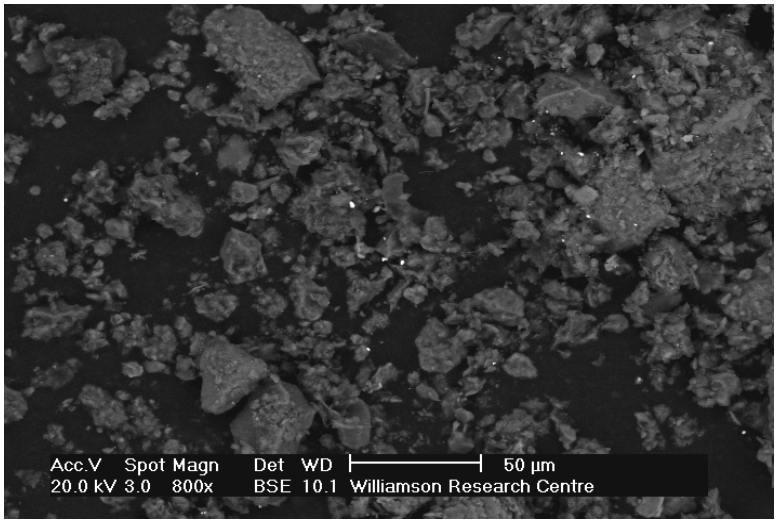

Figure 6. BSE image of a sediment sample shows uranium particles as bright spots. The gray materials are the sediment matrix.

The distribution of radioactive particles in the sample is not homogeneous. The bright particles were characterized by size, shape and elemental composition, and they were found typically to lie in the size range 1-20 µm (Table S1, supporting information). An example of a particle is shown in Figure 7 below.

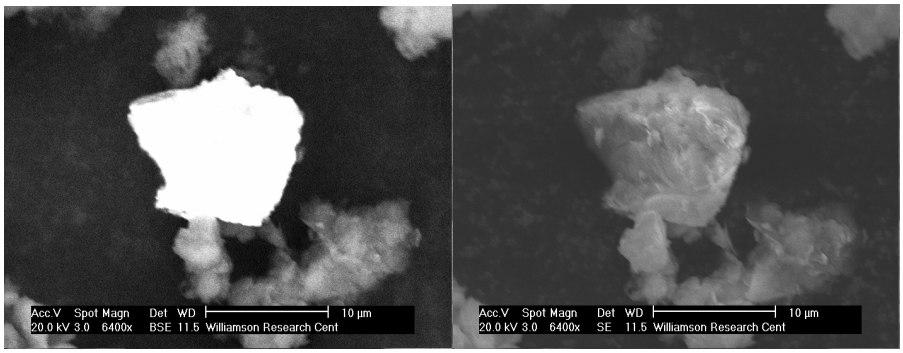

Figure 7. BSE image (left) and secondary electron (SE) image (right) of a particle.

The BSE image shows the particle as bright patch, while the SE image shows the shape and morphology of the particle. It is difficult to distinguish the particle from the sediment matrix in the SE image, so BSE imaging is very useful. The X-ray analysis for the above particle was acquired from both spot and area analysis on the bright area on BSE image, giving characteristic spectra (Figure 8).

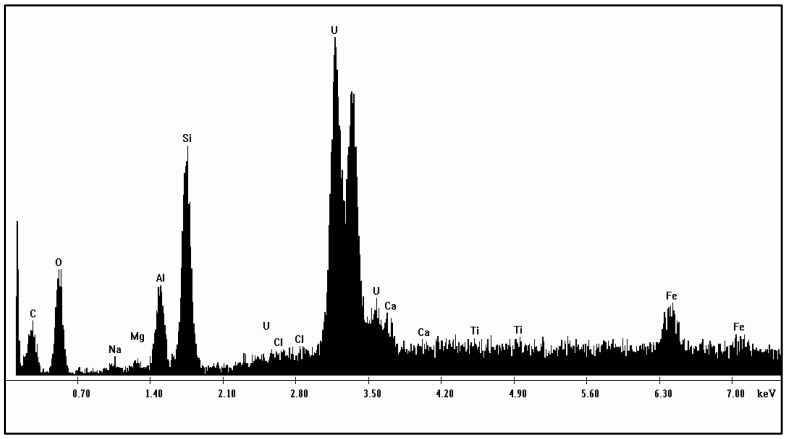

Figure 8. EDX spectrum of a spot on the bright area of the BSE image.

The EDX spectrum shows that the particle is composed mainly of U with some other elements (C, O, Al, Si and Fe), typical of the sediment matrix also present. However, after heavy liquid density separation the matrix was largely eliminated, leaving clean U particles (Figure 9).

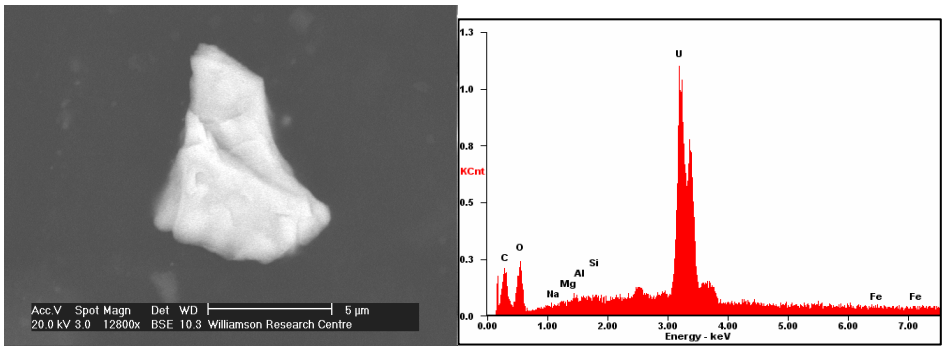

Figure 9. An electron image (BSE) and energy dispersive X-ray analysis (EDX) of a particle separated by heavy liquid.

The spectrum above shows that the particle is mainly uranium. The particle may contain other elements (e.g. Pu as these particles were irradiated), but these are not detectable by EDX. To determine the presence of any other radionuclides, α-spectrometry was applied.

3.2. Radionuclide and isotopic composition

The radionuclide composition of the dissolved heavy particles analyzed by alpha spectrometry is shown in (Figure 10).

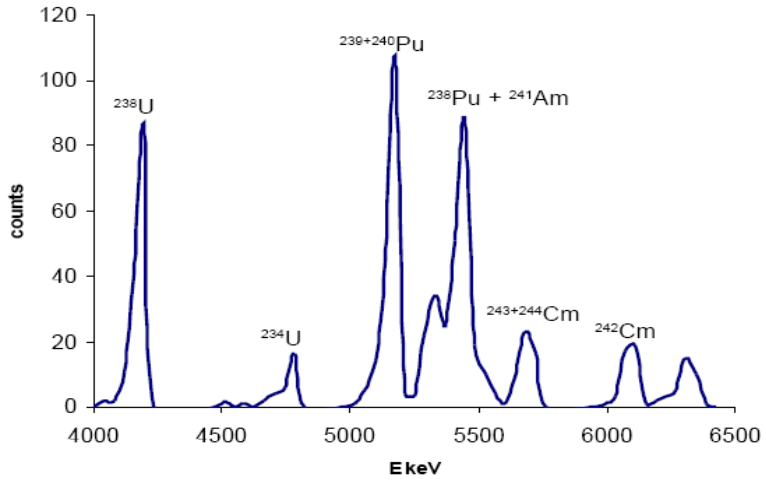

Figure 10. Alpha spectrum of the dissolved particles. Counting time = 2.28 days.

The alpha spectrum shows that a range of α-emitting transuranium radionuclides was identified in the particles, suggesting that these particles have been irradiated. Pu was separated from an aliquot to determine the Pu activity ratio $^{238}Pu/^{239+240}Pu$ which was consistent with that from the Sellafield discharges (Figure 11).

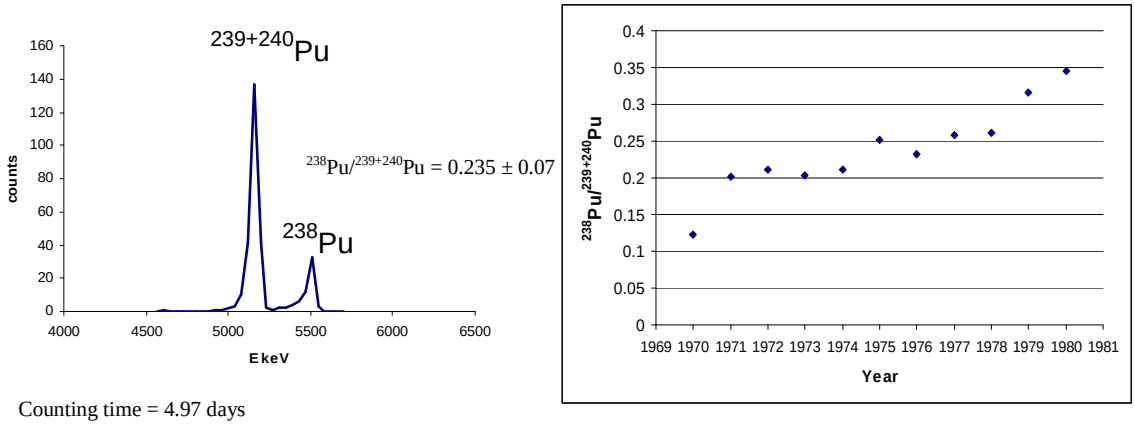

Counting time = 4.97 days

Figure 11. Left**:** Alpha spectrum of Pu isotopes and the activity ratio $^{238}Pu/^{239+240}Pu$. Right: $^{238}Pu/^{239+240}Pu$ activity ratio for 1970s Sellafield discharges [11].

A major source of error in an alpha spectrometry result is the uncertainty arising from the counting process. This arises from the random nature of radioactive decay and, provided the peak integrals are large (some hundreds of counts), the distribution of counts is described by the Poisson distribution such that, for a peak integral of I counts, the standard deviation is $\sigma = (I)^{1/2}/I$. At 2 σ uncertainty the activity ratio ($^{238}Pu/^{239+240}Pu$ = 0.235 ± 0.07) may lie between 0.165 and 0.305, which is still consistent with that from Sellafield (Figure 11 right).

Three particles analyzed by SEM-EDX (supporting in formation, Figure S1), were dissolved in nitric acid, and then analyzed by ICP-MS to determine the atom ratio $^{235}U/^{238}U$, which showed a depletion in ^{235}U ($^{235}U/^{238}U$ = 0.002149 ± 0.000108), suggesting that U was derived from spent Magnox fuel. The activity ratio $^{234}U/^{238}U$ measured by alpha spectrometry after chemical separation of U, showed depletion in ^{234}U as well ($^{234}U/^{238}U$ = 0.26 ± 0.0351) (supporting information, Figure S2), suggesting that ^{234}U gets burned up gradually during irradiation, by absorbing neutrons.

4. Conclusion

Radioactive particles, typically 1-20 µm size, from estuarine salt marsh have been identified. Elemental analysis suggests that these particles are composed mainly of uranium, although alpha spectrometry shows that they have been irradiated, and transuranium nuclides (Pu, Am and Cm) can be identified in them. These results demonstrate conclusively the persistence for some decades, of irradiated fuel particles in the marine and estuarine environments.

References

[1] Kershaw P J, Brealey J H, Woodhead D S, and Lovett M B 1986 *Sci. Total. Environ*. **53** 77.
[2] MacKenzie A B, Scott R D, Allan R L, Ben Shaban Y A, Cook G T and Pulford I D 1994 *J. Environ. Radioact*. **23** 39.
[3] Marsden O J, Abrahamsen L, Bryan N D, Day P J, Fifield K, Gent C, Goodall P S, Morris K and Livens F R 2006 *Sedimentology*. **53** 237.
[4] Hamilton E I 1998 *Marine. Poll. Bull*. **36** 8.
[5] Hamilton E I 1981 *Nature* **290** 690.
[6] Marsden O J 2003 *Determination of Actinide Distributions in Intertidal Sediments from West Cumbria, UK*.(Ph.D thesis, University of Manchester, Manchester, UK).
[7] Salbu B, Lind O C and Skipperud L 2004 *J. Environ. Rdioact*. **74** 233.
[8] Vlasova I E, Kalmykov S N, Sapozhnikov Yu A, Simakin S G, Anokhin A, Yu Aliev R A and Tsarev D A 2006 *Radiochemistry*. **48** 613.
[9] Salbu B 2008 *Proc. of the NATO Advanced Research Workshop on Radiological Risks in Central Asia* (Almaty, Kazakhstan 20-22 June 2006) pp 7-17.
[10] Morris K and Livens F R 1996 *Rdiochem. Acta*. **74** 195.
[11] Gray J, Jones S R and Smith A D 1995 *J. Radiol. Prot*. **2** 99.

Sample collection site

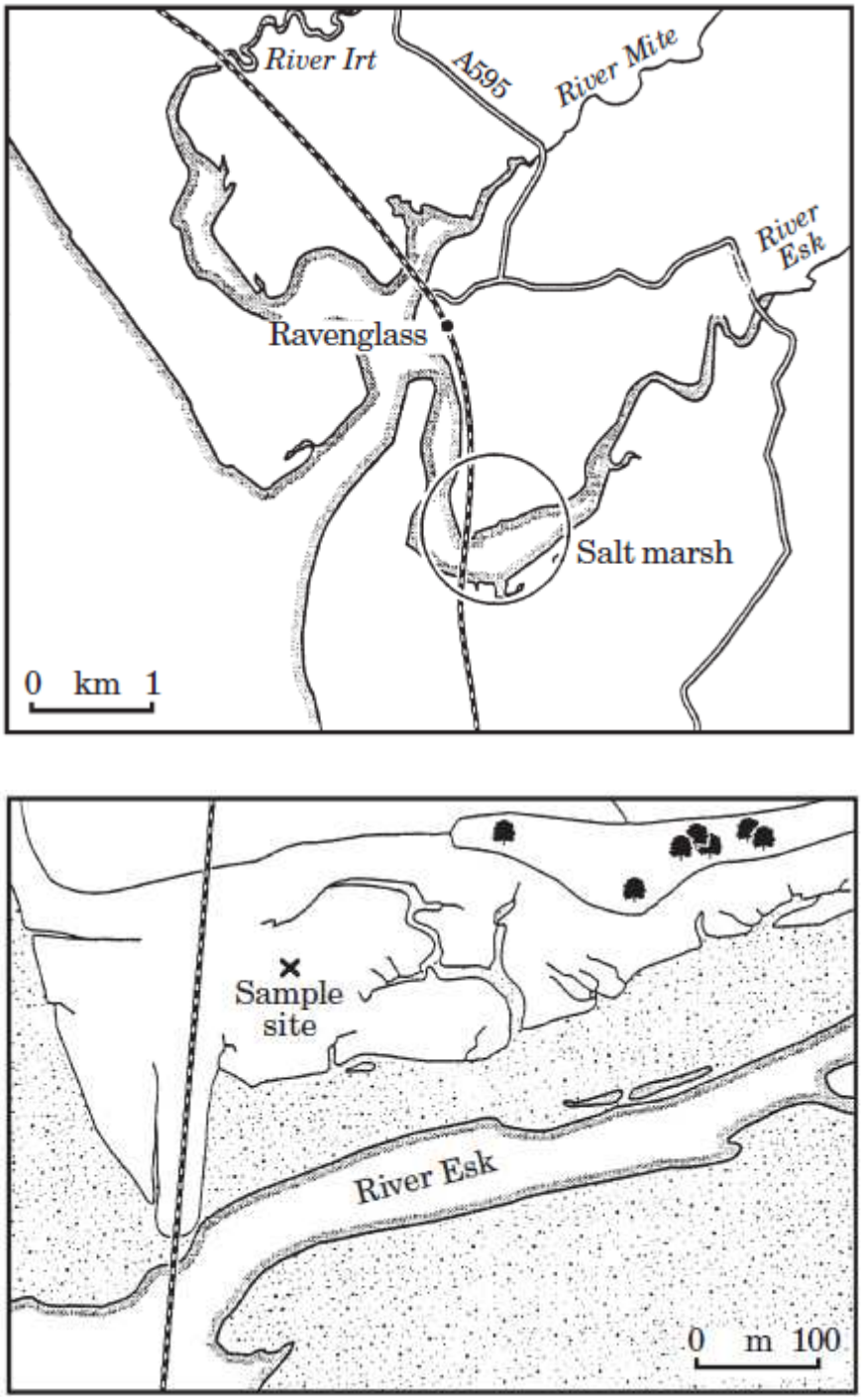

Figure S1. top: The Ravenglass esturay showing the location of salt marsh. Bottom: The salt marsh showing the location of sampling site (UK Natinal Grid Reference 088 947). Adapted from (Morris et al., 2000, doi:10.1006/ecss.2000.0705).

Additional information on typical particle characteristics

Table S1. Observed particle sizes and morphologies*

Particle No	Size µm	Morphology
1	12	Irregular flattened
2	8	Angular
3	3	Volume
4	2	Blurry
5	3	Sharp
6	3	Surface
7	2	Uniform
8	3	Blobs
9	2	Triangular
10	20	Crust

*Separation of particles was on a mass of 1 g and distribution of particles was highly variable across the samples analysed, implying heterogenity.

Analysis of three nuclear fuel particles

The particles were sepatared by heavy liquid density separation and then analysed using SEM-EDX (Figure S1).

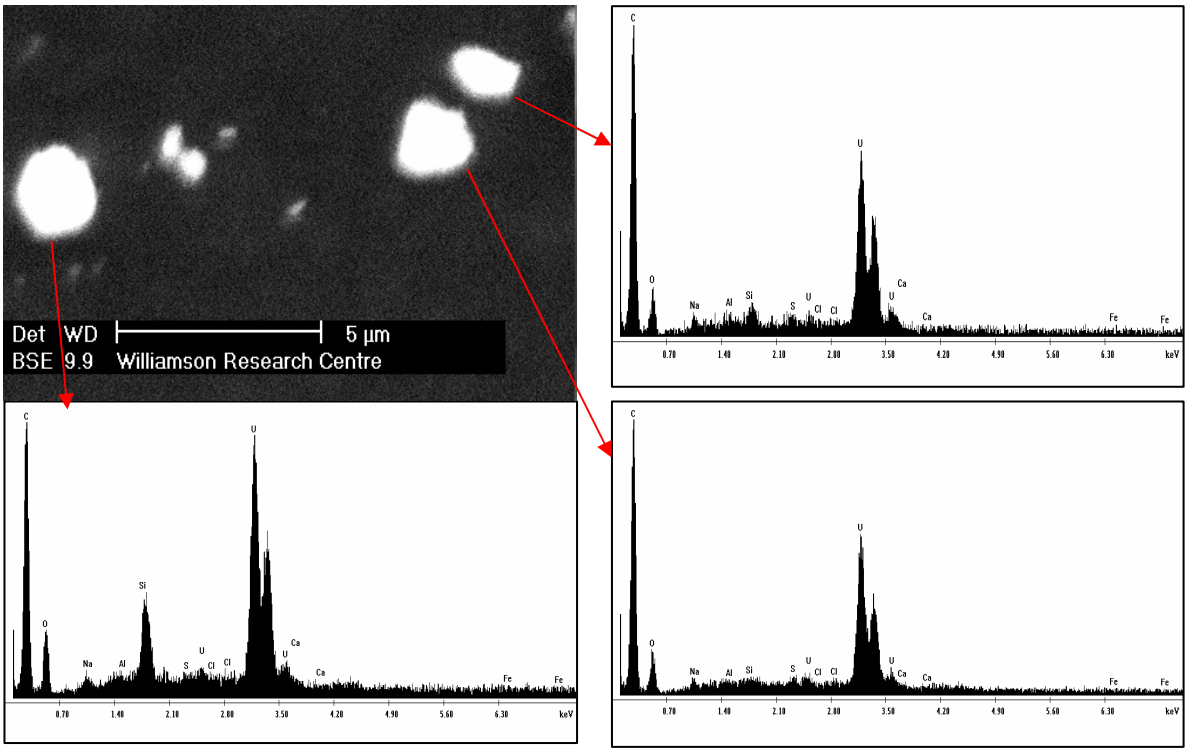

Figure S2. BSE image of three separated particles and their EDX spectra.

The particles were then dissolved in nitric acid and analysed using ICP-MS to obtain the atom ratio $^{235}U/^{238}U = 0.002149 \pm 0.000108$.

Uranium was separated from an aliguot of the dissolved particles and alpha spectrometry was used to measure the activity ratio $^{234}U/^{238}U$ (Figure S2).

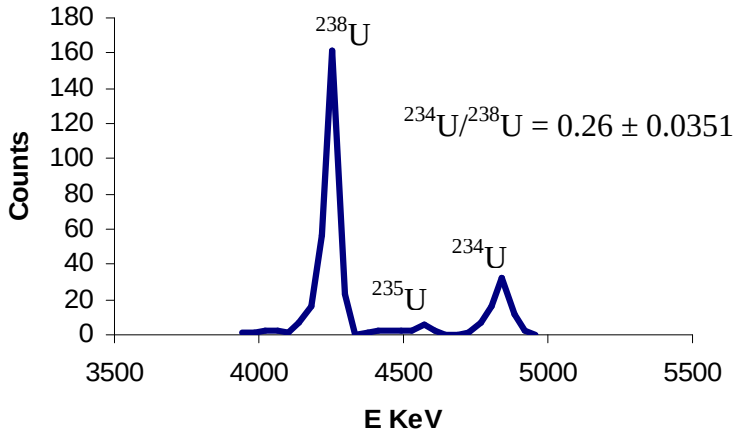

Figure S3. Alpha spectrum of U fraction of the three dissolved particles. Counting time = 11.843 days.

Chapter 3

Physicochemical Characterisation of Depleted Uranium (DU) Particles at a UK Firing Test Range

The material in the following section has been published in the Journal Science of the Total Environment.

Science of the Total Environment 408 (2010) 5990–5996

doi:10.1016/j.scitotenv.2010.07.075

The candidate's contribution was particles isolation, electron microscopy, radiochemical separation, alpha spectrometry, X-ray diffraction, data interpretation, and writing the paper.

The samples were collected by Miranda Keith-Roach (University of Plymouth) and Rebeca Alvarez (University of Manchester)

Physicochemical Characterisation of Depleted Uranium (DU) Particles at a UK Firing Test Range

Mustafa Sajih [a], Francis R. Livens [a,b], Rebeca Alvarez [a,b] and Mathew Morgan [a]

[a] Centre for Radiochemistry Research, School of Chemistry, University of Manchester, Manchester, M13 9PL, UK.
[b] School of Atmospheric and Environmental Sciences, University of Manchester, Manchester, M13 9PL, UK.

Abstract

Depleted uranium (DU) particles were isolated from soils at Eskmeals, UK, where DU munitions have been tested against hard targets, and unfired DU buried in soils for corrosion studies. Using electron microscopy and X-ray analyses, three classes of particles were identified: (1) DU aerosols and fragments, typically 1-20 µm diameter, composed mainly of uranium as UO_2 and U_3O_8, (2) solidified molten particles, typically 200-500 µm diameter, composed of U, mixed with Fe from target materials. (3) Deposits and coatings, often of metaschoepite on sand grains up to 500 µm diameter. The first two particle types derive from firing impacts, the last from corrosion of buried uranium metal. Alpha and mass spectrometry allowed quantitative elemental and isotopic characterisation of DU-containing particulate environmental samples.

Keywords: Firing impact**,** Metaschoepite, Depleted uranium, DU corrosion

1. Introduction

Depleted uranium (DU), a by-product of the U enrichment process, has been used in military munitions because of its high density and penetrating power. However, testing and use of such munitions has led to release of DU into the environment at several locations around the world.

Natural uranium consists of three isotopes: ^{234}U, ^{235}U and ^{238}U. In nuclear fuel production, natural uranium is isotopically enriched, increasing the concentration of the fissile isotope ^{235}U, usually to 3-5 atom%. The residue from this enrichment process is called ‘depleted

uranium' and has a decreased proportion of both ^{234}U and ^{235}U, and hence a slightly increased proportion of ^{238}U as shown in Table 1 (UNEP, 2003; Oliver et al., 2007).

Parameter	DU	Natural U
Atom % ^{238}U ($t_{1/2}$ 4.47 x 10^9 yr)	99.79	99.28
Atom % ^{235}U ($t_{1/2}$ 7.04 x 10^8 yr)	0.20	0.72
Atom % ^{234}U ($t_{1/2}$ 2.45 x 10^5 yr)	0.001	0.0054
$^{235}U/^{238}U$ activity ratio	0.013	0.046
$^{235}U/^{238}U$ atom ratio	0.002	0.0072
$^{234}U/^{238}U$ activity ratio	0.18	0.8 -1.2[a]
$^{234}U/^{238}U$ atom ratio	0.000010	0.000056

Table 1. Composition of natural uranium and DU. [a] the ratio is given as a range because of the possibility of preferential leaching of ^{234}U.

Depleted uranium therefore has an isotopic fingerprint clearly different from that of natural uranium and this can be used to identify and quantify DU contamination in environmental samples.

Depleted uranium alloys (99.25% U/ 0.75% Ti) were used extensively during the Gulf War 1991, Bosnia 1995, Kosovo 1999 and Iraq 2003. The Gulf War resulted in the deposition of approximately 320 tonnes of DU in the terrestrial environment (Bleise et al, 2003). When a DU round hits a hard target such as armour plate, some DU aerosolizes and ignites at high temperature during the impact, because U metal is pyrophoric. Oxidized uranium aerosols and fragments will thus be produced and deposited around the area surrounding the target (Papastefanou, 2002; Craft et al., 2004). DU particles ranging from sub-microns to several hundred microns, and comprising the uranium oxides UO_2 and U_3O_8 were observed in Kosovo and Kuwait (Salbu et al, 2003; Salbu et al, 2004). 70 - 90 % of aircraft DU projectiles miss their targets and embed in the ground at a depth of more than 2 m in clay soil and 6-7 m in soft soil (UNEP, 2003). Because of the thermodynamic instability of

metallic uranium and its alloys in the natural environment, they will readily corrode and new U-rich mineral phases may form at the reactive surface, while some uranium may be lost in solution as very mobile UO_2^{2+} and reach the ground water (Mellini and Riccobono, 2005). In the UK, the Ministry of Defence (MOD) has conducted test-firing of DU munitions against hard targets, and experimental work on corrosion of unfired DU alloy in soils at Eskmeals firing range, to study the overall environmental impact of DU (Dstl, 2006; Oliver et al., 2007). In order to understand the environmental behaviour of DU particles, information on particle characteristics such as size, morphology, elemental composition, crystalline structure, and isotopic composition of U is useful. In this study, a combination of scanning electron microscopy with X-ray analysis (SEM-EDX), inductively coupled plasma-mass spectrometry (ICP-MS), alpha spectrometry and single particle X-ray diffraction (XRD) were used to characterise DU particles from Eskmeals.

2. Methods

2.1 Study site and sample collection

At Eskmeals, UK (national grid reference, SD 078 929), testing of DU munitions began in the 1960s and continued until 1995, with the most intensive period during the 1980s. The test programme involved firing DU projectiles at hard target arrays enclosed within a butt, designated VJ Butt. This testing exposed the area to DU contamination from aerosols and DU fragments produced on impact (Oliver et al., 2007). Subsequently, the MOD commenced a programme on DU corrosion with burial of a number of unfired DU coupons in a "DU garden" and retrieval at intervals to quantify corrosion processes and analyse corrosion products (Dstl, 2006). Soil samples were collected from two DU affected sites. At both sites, the soil is a raw dune sand.

Site 1 (firing site) comprises topsoil collected in front of the target area ~ 40 m from the impact point. This sample is expected to contain exclusively DU aerosols and fragments produced on impact of DU rounds with armour.

Site 2 (corrosion site) comprises subsoil collected from the DU corrosion experimental area where DU coupons were buried and retrieved. This sample is ca 100 m from the impact point and is expected to contain both impact particles and corrosion products of DU. Eskmeals firing range and the sample collection positions are shown in supporting information (Fig.S1).

2.2 Autoradiography

Storage phosphor autoradiography was used to localize DU particles by spreading the sample on filter papers (approx 1 mg sample/cm^2) and then exposing a storage phosphor

screen (25 by 20 cm) to the sample overnight, then reading the screen using a phosphor Imager (GE Healthcare). An example autoradiograph is shown in supporting information (Fig. S2).

The black spots in the obtained image represent DU particles (aerosols and fragments) in the sample. DU fragments were visible to the eye, so they were picked up individually, whereas DU aerosols were difficult to distinguish from surrounding soil, so they were detected by sticking the soil, which contains them, on a carbon sticky pad mounted on aluminium stub for SEM analysis.

2.3 Scanning electron microscopy (SEM)/Energy dispersive X-ray analysis (EDX)

SEM was used to obtain information on the morphology and size of the particles using secondary electron (SE) and backscattered electron (BSE) imaging. The latter was particularly useful for identifying DU particles. For each particle identified by SEM, the X-ray elemental composition (EDX spectrum) was obtained.

2.4 X-ray diffraction (XRD)

X-ray diffraction was used to identify uranium-containing crystalline phases present in DU particles. For particle analysis, an Xcalibur-2 diffractometer from Oxford Diffraction, equipped with a charge-coupled device (CCD) detector was used to obtain powder diffraction patterns from individual DU particles using MoKα radiation (λ = 0.071 nm). The particle was mounted on the tip of a thin glass fibre and rotated to sample all particle orientations. The XRD patterns were interpreted using the inorganic crystal structure database (ICSD).

2.5 Chemical separation and measurement of uranium

DU particles from site 2 were cut away from the carbon pads (leaving a small amount of pad to avoid damaging the particles), whereas DU particles from site 1 were smaller, and were therefore isolated using heavy liquid density separation. Single particles were then dissolved in analytical grade concentrated nitric acid (69% HNO_3, 2 ml per particle) in 5 ml beakers. The mixture was covered with a watch glass and brought to the boil on a hotplate, then left to cool to ensure full sample digestion. The sample solution was made up with 3 ml de-ionized water, filtered through a 0.22 μm PVDF membrane filter, evaporated to dryness and redissolved in 10 ml of 0.1 M HNO_3.

2.5.1 Alpha spectrometry

Alpha spectrometry was used to measure the $^{234}U/^{238}U$ activity ratio. An aliquot (2 ml) of the 10 ml DU sample solution was evaporated to dryness and dissolved in 30 ml of 2.5 M HNO_3. A small column (3.5 ml bed volume) of TRU resin (EiChrom Industrial, Darien, Illinois, USA) was conditioned with 30 ml 2.5 M HNO_3. The sample solution was passed through the preconditioned column, 25 ml de-ionized water was passed to remove the nitric acid from the resin bed, then uranium was eluted using 20 ml 10% m/v $(NH_4)_2$ CO_3. 1 ml 10% (m/v) $KHSO_4$ was added and the beaker warmed to dryness. The residue was treated successively with 10 ml conc HNO_3, then 3 ml conc HCl. The white chloride residue was dissolved in 15 ml electrolyte solution (4% ammonium oxalate in 0.3 M HCl) and uranium electroplated onto a stainless steel planchette (0.5 A, 20 V, 2 hrs). A minute before the power was turned off, 1 ml of concentrated ammonia solution was pipetted into the cell. The planchette was removed from the cell, washed with deionised water and acetone and air-dried for alpha counting.

2.5.2 ICP-MS and *ICP-AES*

Inductively coupled plasma-mass spectrometry (ICP-MS) was used to measure $^{235}U/^{238}U$ and $^{234}U/^{238}U$ atom ratios. A 2 ml aliquot of DU sample solution was made up to 10 ml with 0.1 M HNO_3 for each sample. An additional 6 ml aliquot of DU sample solution was made up to 10 ml with 0.1 M HNO_3 and analysed by inductively coupled plasma-atomic emission spectrometry (ICP-AES) to quantify U and selected stable elements (Fe, Ti, W, Cr and B).

3. Results and Discussion

3.1 Firing impact- derived particles

3.1.1 SEM/EDX

DU particles from site (1) will comprise aerosols and fragments formed from the impact of DU rounds on a hard target. Two types of firing impact particles were found; small aerosol particles composed mainly of uranium, and bigger particles composed of a mixture of uranium and iron with variable U/Fe ratio. The first type of particle was more abundant than the other (supporting information, Fig. S2).

SEM was used in BSE mode to identify particles with high atomic number elements (primarily U) as bright areas (Fig. 1).

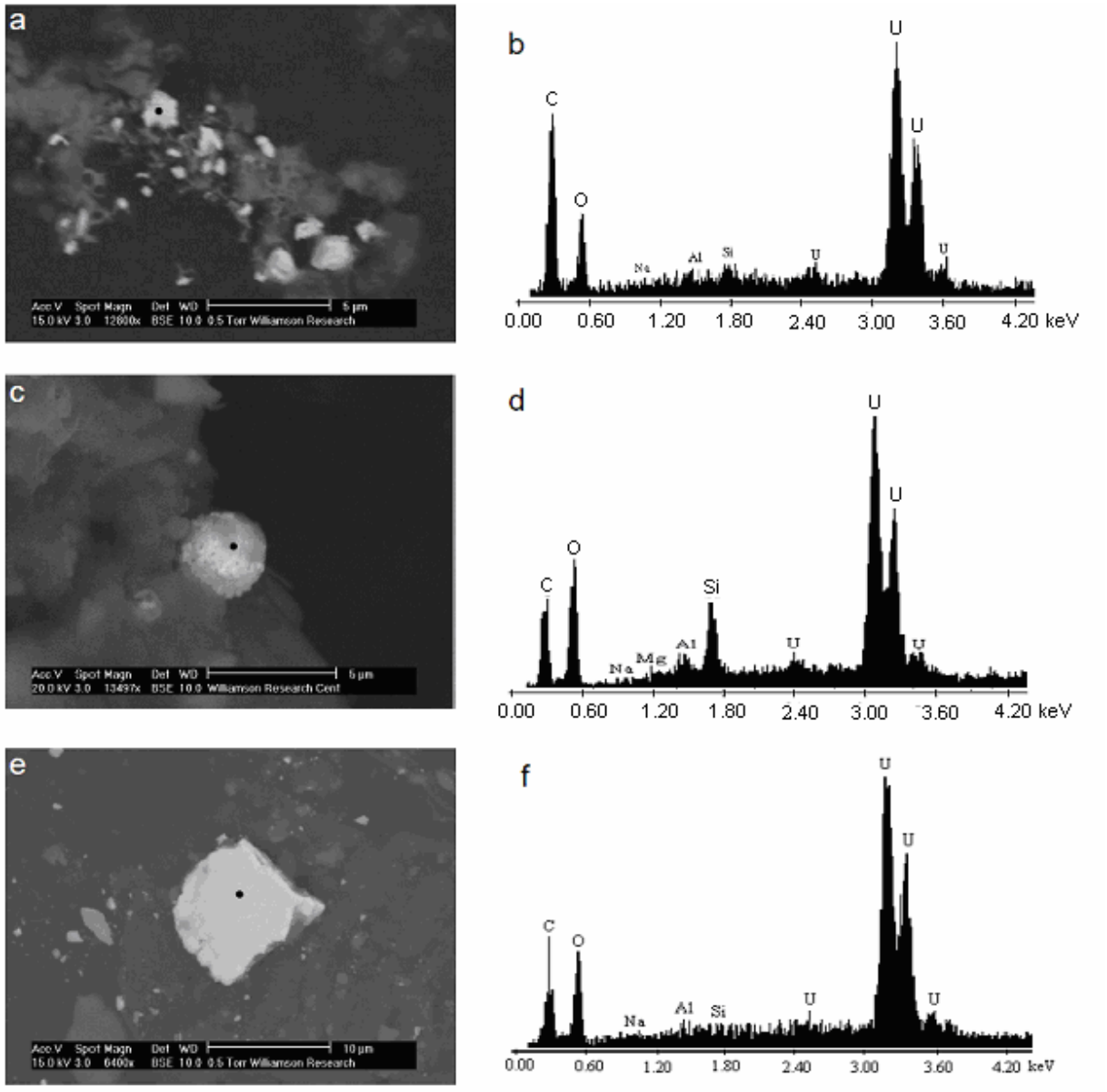

Fig. 1. (a) BSE image of DU aerosols (bright particles) in a soil matrix. (c) BSE image of a spherical particle (bright ball). (e) BSE image of an aerosol fragment.Black spots on images a, c and e are the EDX targets shown in b, d and f respectively. Scale bars are 5, 5 and 10 µm for images a, c and e respectively.

The electron micrographs above illustrate the variability in particle size and shape found, although X-ray analysis consistently showed that they were composed largely of uranium. The aerosol particle sizes range from around 1 µm up to about 20 µm, and the distrubution of particles in the sample was heterogeneous, so there was no clear information about the abundance of particles in soil or the proportions of different particle morphologies. The DU particle in Fig.1c is an example of a characteristic spherical morphology, perhaps suggesting that this particle type represents condensation of molten uranium. The aerosol particles found in this study were very similar to DU aerosols produced in the DU

Capstone study, which involved firing DU penetrators aginst conventional armour (Krupka et al., 2009), and to the DU aerosols produced in Kosovo (Danesi et al., 2003).

Another group of larger particles also has a different, characteristic morphology, suggesting they may be solidified molten droplets containing a mixture of depleted uranium and iron, the latter probably derived from the target material (Fig. 2). On occasion (e.g. Fig. 2e), the composition is consistent with this particle type, but a different morphology is observed.

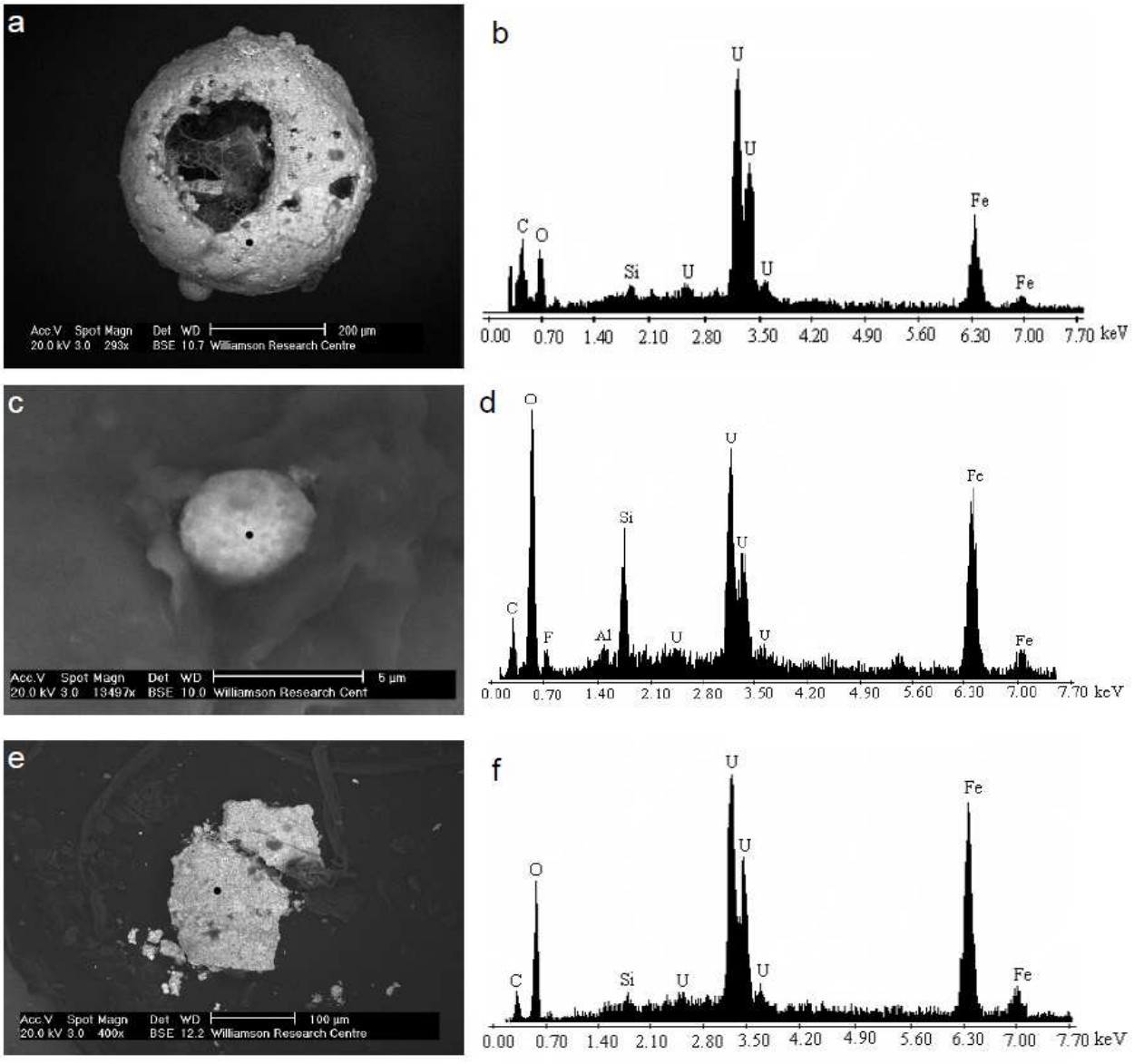

Fig.2. (a) BSE image of a hollow spherical molten particle. (c) BSE image of a small U-Fe alloyed droplet. (e) BSE image of melted fragments. (f) Black spots on images a, c and e are the EDX targets shown in b, d and f respectively. Scale bars are 200, 5 and 100 µm for images a, c and e respectively.

The various molten particles showed heterogeneity in particle size and shape, but X-ray analysis showed that they were composed mainly of alloyed uranium and iron, although the ratio Fe/U varied considerably among particles. The BSE image of the hollow spherical particle is relatively uniform, which means that U is homogeneously distributed on the surface of the particle. X-ray analysis showed a predominant Fe/U composition, though with some localised variability in Fe:U ratio. Similar alloyed Fe-U particles were identified following test firing of DU rounds against spaced armour targets at a firing range in the US (Patrick and Cornette, 1978). This type of particle has rarely been identified in post-conflict environments (Lind et al., 2009), because most DU rounds have been fired from aircraft, and relatively few of these projectiles hit the target (Bleise et al., 2003), whereas in test firing, DU rounds were fired from a gun close to the hard target, which ensures interaction between DU and target materials.

3.1.2 Elemental Composition and X-ray diffraction.

ICP-AES was used to identify and quantify a range of stable elements (Fe, Ti, W, Cr and B) in five representative DU firing impact particles. The concentrations of these elements, as mole ratio of element/U, are listed in Table 2.

Sample	Fe/U	Ti/U	W/U	Cr /U	B/U
DU1	11.934	0.040	0.015	0.111	ND
DU2	18.591	0.059	0.063	0.468	0.760
DU3	1.467	0.008	0.013	0.015	0.036
DU4	1.308	0.063	0.031	0.008	0.107
DU5	0.190	0.049	0.062	ND	18.70

ND: not detected

Table 2. Mole ratio (stable element:U) in firing impact particles

The stable elements could be derived from one or more of the target materials, the DU alloys or the firing range site. These DU particles have a very variable Fe/U mole ratio, with an excess of Fe over U in most particles, which reflects the violent interaction between DU penetrators and target at impact. The Cr/U ratio seems to be correlated with Fe/U ratio, suggesting that Fe and Cr derive from the same origin (target materials). The Ti/U ratio ranges between 0.04 and 0.063 in most particles, and this may reflect the fact

that DU penetrator contains 0.75% Ti. Boron and tungsten could be derived from the soil of the firing range, however the B/U ratio in DU5 suggest that B could be derived from other source, probably target material.

Single particle X-ray diffraction patterns were obtained for several DU firing impact particles. 2/3 of the diffraction patterns matched the principal reflections of UO_2 (Uraninite), and 1/3 of the diffraction patterns matched the principal reflections of U_3O_8 (Fig.3).

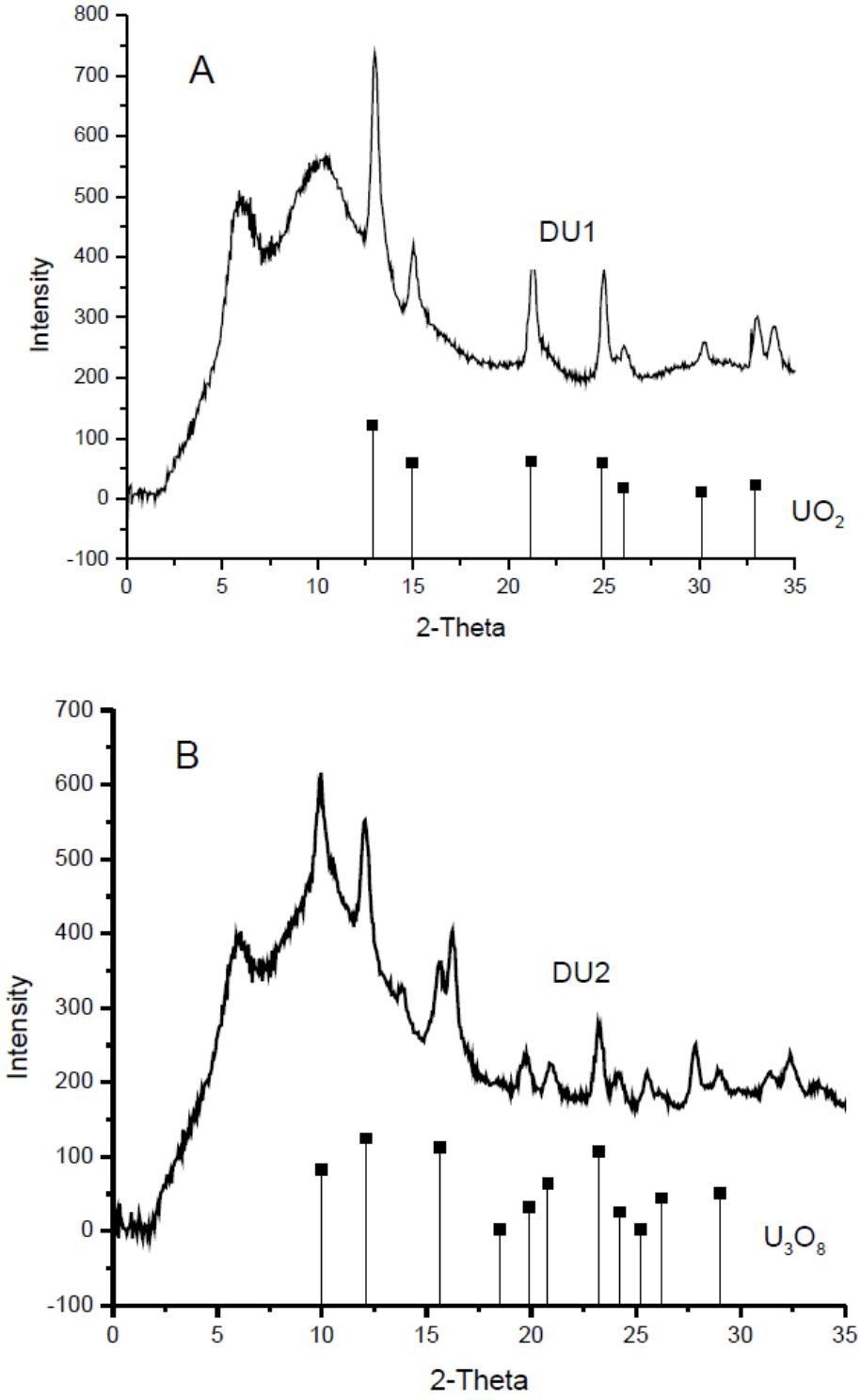

Fig.3. X-ray diffraction patterns of two DU firing impact particles. (A) Diffraction pattern matches with the characteristic reflections of UO_2 (uraninite). (B) Diffraction pattern matches with the characteristic reflections of U_3O_8.

These data are consistent with other studies (Salbu et al., 2003; Salbu et al., 2004), which found that about 50% of DU firing impact particles from Kosovo and Kuwait was present mostly as UO_2, and the remainder as a mixture of UO_2 and U_3O_8 or as U_3O_8.

Török et al (2004) showed that U in DU-containing soil particles from Kosovo, was predominantly U(IV), consistent with the presence of UO_2. UO_2, with variable amounts of U_3O_8, was observed in DU particles released into the environment by combustion of scrap DU metal at a factory in Colonie, USA (Lloyd et al., 2009). The most commonly reported phases in environmental samples containing fired and ignited DU are UO_2 and U_3O_8 respectively, a conclusion supported by this study.

3.1.3 Isotopic fingerprinting

ICP-MS and alpha spectrometry were used to obtain the atom ratios $^{235}U/^{238}U$ and $^{234}U/^{238}U$ and the activity ratio $^{234}U/^{238}U$, respectively, for 5 DU firing impact particles as a measure of depletion. All the isotopic ratios confirmed that U in these particles was predominantly DU (> 93%) (Supporting information, Table S1). From the activity and atom ratios, the uranium inventory in Eskmeals soil had isotopic signatures indicative of 93% - 98% DU (Oliver et al., 2007; Oliver et al., 2008), consistent with that of this study. In the wider context, uranium isotopic ratios of DU particles examined in this study are comparable to those reported from Kosovo (Torok et al., 2004).

3.2 Corrosion site particles

3.2.1 SEM/EDX

At site 2 (corrosion site), two types of particles were found. The first type is visible to the eye, yellow in colour, and composed mainly of U. The other type is also visible to the eye but is black in colour, speckled with uranium, and has a more complex elemental composition (Fig. 4). These two types of particles were concentrated close to the corroding DU coupons, suggesting that uranium is present as corrosion products distributed on the surface of the surrounding sand grains.

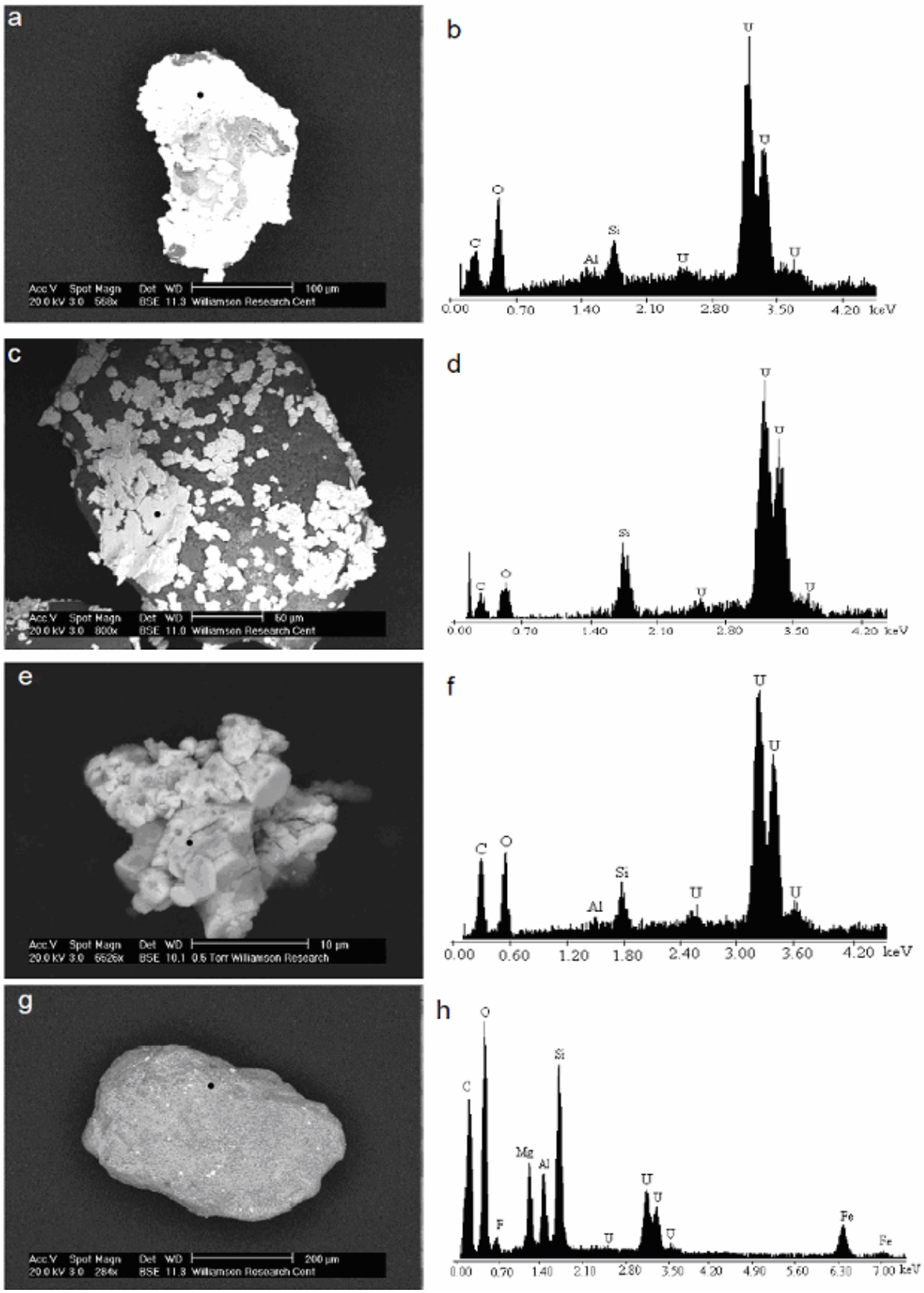

Fig. 4. (a) BSE image of a yellow DU particle, coated with U corrosion products (bright areas). (c) BSE image of another yellow DU particle, partly coated with DU (bright areas on the surface of the sand grain). (e) BSE image of an aggregate of yellow corroding DU. (g) BSE image of a black particle speckled with DU (bright spots on the surface). Black

spots on images a, c, e and g are the EDX targets shown in b, d, f and h respectively. Scale bars are 100, 50, 10 and 200 µm for images a, c, e and g respectively.

Yellow DU corrosion products have also been observed in corroded DU penetrators, which had been fired and hit the ground in Kosovo (Mellini and Riccobono, 2005), and in DU particles originating from a fire in a DU ammunition storage facility in Kuwait (Lind et al., 2009).

3.2.2 X-ray diffraction

X-ray diffraction patterns were obtained for two yellow DU particles and a pure quartz particle, the last used as a reference for background subtraction (supporting information, Fig.S3). Subtraction of background from the measured patterns helps to expose weak diffraction lines from the specimen, which might otherwise not be possible to distinguish from the background signal. The diffraction pattern, after subtraction of the quartz pattern, is illustrated in Fig. 5, and shows the presence of several reflections characteristic of metaschoepite.

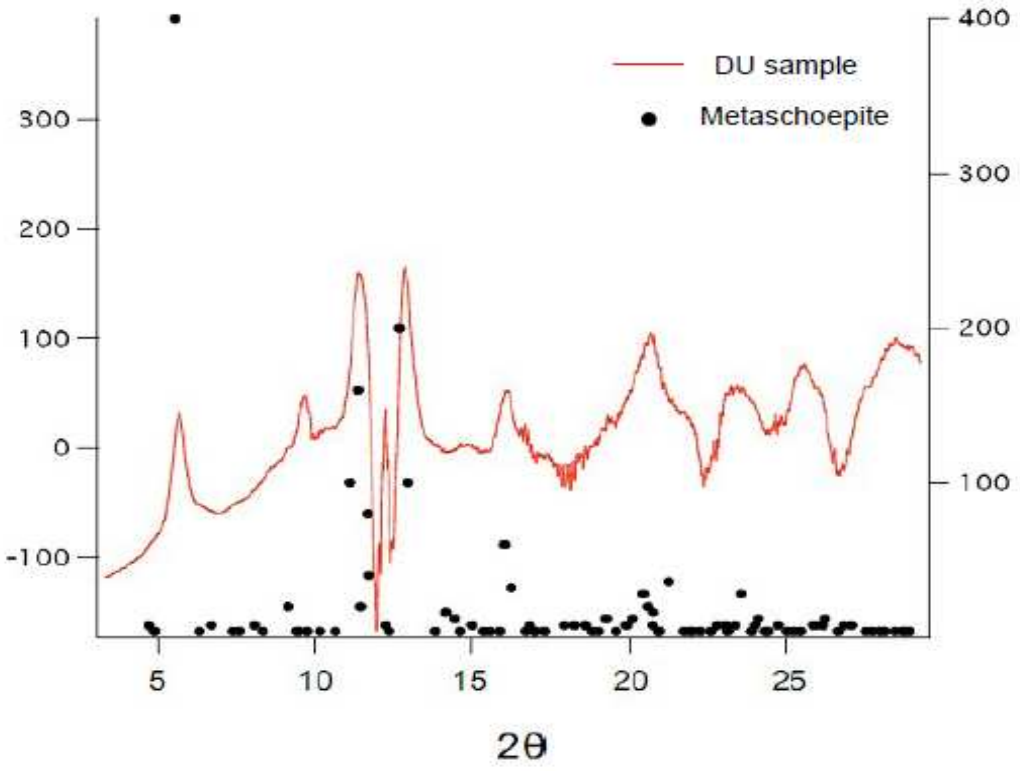

Fig. 5. X-ray diffraction pattern of the yellow U coating, together with the characteristic reflections of metaschoepite. The feature around 12^{o} 2θ is an artefact arising from subtraction of the quartz reference pattern, which has a very strong reflection at this position.

Specifically, the peaks in the diffraction pattern of the yellow deposit at 6^o, 11^o and 13^o 2θ match reflections in the metaschoepite $[(UO_2)_8O_2(OH)_{12}](H_2O)_{10}$ pattern. This is consistent with the finding of Handley-Sidhu et al. (2009), who identified metaschoepite in laboratory microcosm experiments, and also with Buck et al. (2004), who identified schoepite and metaschoepite as the primary corrosion products of DU in a site in the US.

3.2.3 Isotopic Fingerprinting

ICP-MS was used to measure the $^{235}U/^{238}U$ atom ratio for 9 black particles and 9 yellow particles. The black particles have a variable $^{235}U/^{238}U$ ratio, between depleted and natural compositions, although most are strongly depleted. By contrast, the yellow particles are essentially pure DU (supporting information, Fig. S4). This probably reflects the different uranium masses in the two particle types. For black particles, the atom ratio $^{235}U/^{238}U$ decreases as the total mass of U in the particle increases, which is consistent with mixing variable proportions of natural and DU, with most particles containing ~ 20% natural U, though one contains ~ 95%. For yellow particles, the atom ratio $^{235}U/^{238}U$ is always consistent with the DU ratio; this means that U in yellow particles is essentially all DU (supporting information, Fig. S5). Alpha spectrometry was used to obtain the activity ratio $^{234}U/^{238}U$ for 4 of these yellow DU particles. The activity ratio $^{234}U/^{238}U$ showed a signature of predominately DU (supporting information, Fig. S6), consistent with the indication from the ICP-MS results, that most of the particles are fully depleted.

4. Conclusions

Autoradiography and SEM/EDX are useful for localization of DU particles and obtaining information on morphology, size and elemental composition. X-ray diffraction allows determination of the crystal structure of single DU particles, and showed that the aerosols were uranium oxides UO_2 and U_3O_8, and the yellow particles were metaschoepite. Using the atom ratio $^{235}U/^{238}U$, obtained by ICP-MS, and the activity ratio $^{234}U/^{238}U$, obtained by alpha spectrometry, it was possible to quantify DU particulate contamination in environmental samples.

Depleted uranium particles produced by firing impacts are different from particles produced by DU corrosion. DU aerosols and fragments and molten particles found near the target area (firing impact site), have sizes, morphologies and compositions consistent with origin from firing impact. However, the yellow particles from the corrosion site are all believed to form through DU corrosion. These results demonstrate the diversity of particles

which can form through use of DU munitions, and the potential for these to persist in the environment.

Acknowledgment

We thank the UK Defence Science & Technology Laboratory for arranging access to the sampling sites and the Natural Environment Research Council for support.

References

Bleise A, Danesi PR, Burkart W. Properties, use and health effects of depleted uranium (DU): a general overview. J. Environ. Radioact 2003; 64:93 -112.

Buck BJ, Brock AL, Johnson W, H.Ulery AL. Corrosion of depleted uranium in an arid environment: Soil-geomorphology, SEM/EDS, XRD, and electron microprobe analyses. Soil Sediment Contam 2004; 13:545-561.

Craft ES, Abu-Qare AW, Flaherty MM, Garofolo MC, Rincavage HL, Abou-Donia MB. Depleted and natural uranium: Chemistry and toxicological effects. Journal of Toxicology and Environmental Health - Part B 2004; 7:297-317.

Danesi PR, Markowicz A, Chinea-Cano E, Burkart W, Salbu B, Donohue D, Ruedenauer F, Hedberg M, Vogt S, Zahradnik P, Ciurapinski A. Depleted uranium particles in selected Kosovo samples. J. Environ. Radioact 2003. 64:143-154.

Dstl- Defence Science and Technology Laboratory, UK. MOD DU Programme - the corrosion of depleted uranium in the Kirkcudbright and Eskmeals terrestrial environments; 2006.

Handley-Sidhu S, Worsfold PJ, Livens FR, Vaughan DJ, Lloyd JR, Boothman C, Sajih M, Alvarez R, Keith-Roach MJ. Biogeochemical controls on the corrosion of depleted uranium alloy in subsurface soils. Environ. Sci. Technol 2009; 43:6177-6182.

Krupka KM, Parkhurst MA, Gold K, Arey BW, Jenson ED, Guilmette RA. Physicochemical characterization of Capstone depleted uranium aerosols III: Morphologic and chemical oxide analyses. Health Phys 2009; 96:276-291.

Lind OC, Salbu B, Skipperud L, Janssens K, Jaroszewicz J, De Nolf W. Solid state speciation and potential bioavailability of depleted uranium particles from Kosovo and Kuwait. J. Environ. Radioact 2009;100:301-307.

Lloyd NS, Mosselmans JFW, Parrish RR, Chenery SRN, Hainsworth SV, Kemp SJ. The morphologies and compositions of depleted uranium particles from an environmental case-study. Mineralogical Magazine 2009; 73:495-510.

Mellini M, Riccobono F. Chemical and mineralogical transformations caused by weathering in anti-tank DU penetrators ("the silver bullets") discharged during the Kosovo war. Chemosphere 2005; 60:1246-1252.

Oliver IW, Graham MC, MacKenzie AB, Ellam R, M.Farmer JG. Assessing depleted uranium (DU) contamination of soil, plants and earthworms at UK weapons testing sites. J. Environ. Monitor 2007; 9:740-748.

Oliver IW, Graham MC, MacKenzie AB, Ellam R, M.Farmer JG. Distribution and partitioning of depleted uranium (DU) in soils at weapons test ranges - Investigations combining the BCR extraction scheme and isotopic analysis. Chemosphere 2008; 72:932-939.

Papastefanou C. Depleted uranium in military conflict and the impact on the environment. Health Physics 2002; 83:280-282.

Patrick MA, Cornette JC. Morphological Characteristics of Particulate Material Formed from High Velocity Impact of Deleted Uranium Projectiles with Armor Targets. United States Air Force Armament Laboratory, Environics Office 1978; 1-21.

Salbu B, Janssens K, Lind OC, Proost K, Danesi PR. Oxidation states of uranium in DU particles from Kosovo. J. Environ. Radioact 2003; 64:167-173.

Salbu B, Janssens K, Lind OC, Proost K, Gijsels L, Danesi PR. Oxidation states of uranium in depleted uranium particles from Kuwait. J. Environ. Radioact 2004; 78:125-135.

Török S, Osan J, Vincze L, Kurunczi S, Tamborini G, Betti M. Characterization and speciation of depleted uranium in individual soil particles using microanalytical methods. Spectrochim. Acta, Part B 2004; 59:689-699.

UNEP - United Nation Environmental Programme. Depleted Uranium in Bosnia and Herzegovina . Post-Conflict Environmental Assessment Report 2003. http://postconflict.unep.ch/publications/BiH_DU_report.pdf.

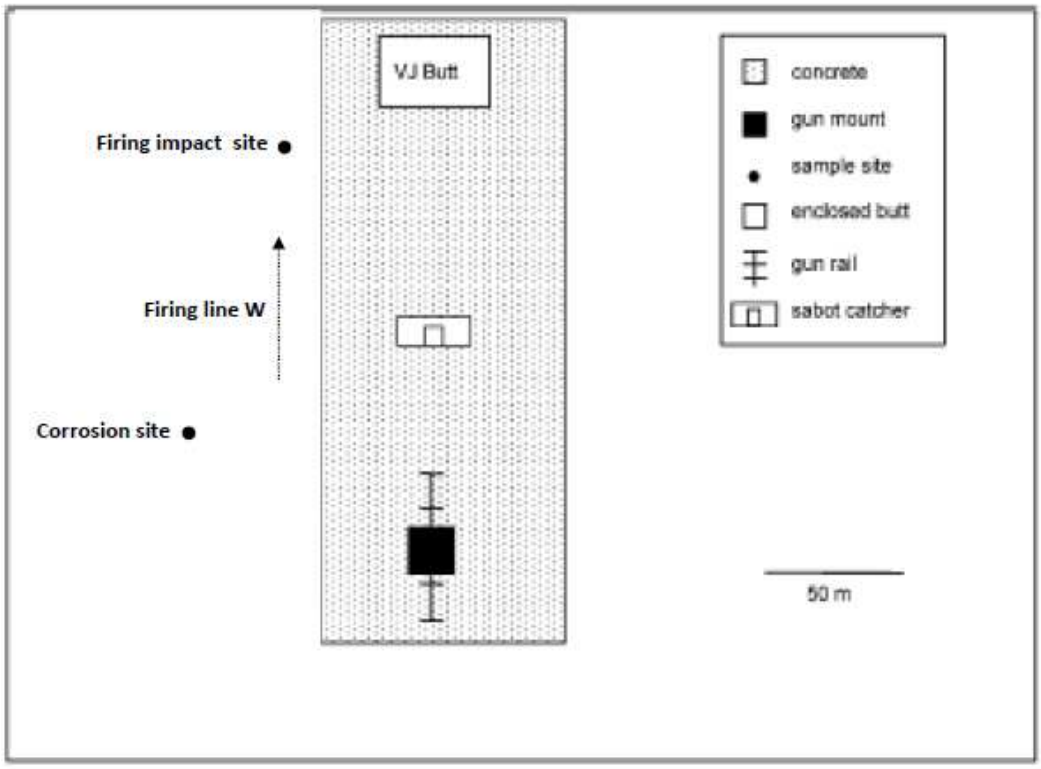

Fig. S1. Schematic of Eskmeals firing range showing sample positions (adapted from Oliver et al., 2007).

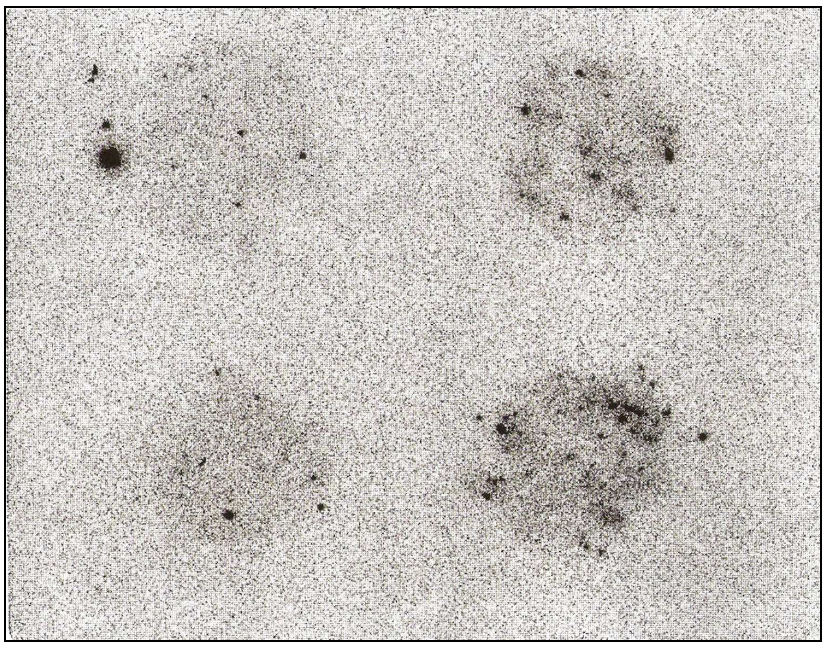

Fig. S2. Autoradiograph of DU sample showing uranium particles as black spots. The small size hot spots represent aerosol particles while the big spot (top left) represents a DU fragment.

.

Sample	$^{235}U/^{238}U$ atom ratio	$^{234}U/^{238}U$ atom ratio	$^{234}U/^{238}U$ activity ratio
DU1	0.00189 ± 0.0000113	6.69E-06 ± 2.05E-07	0.128 ± 0.005
DU2	0.00190 ± 0.0000114	6.94E-06 ± 7.41E-07	0.133 ± 0.024
DU3	0.00234 ± 0.0000487	1.29E-05 ± 9.42E-07	0.263 ± 0.020
DU4	0.00186 ± 0.0000115	7.28E-06 ± 9.01E-07	0.118 ± 0.018
DU5	0.00185 ± 0.0000090	6.32E-06 ± 1.30E-06	0.160 ± 0.017
DU – Natural U	0.002 - 0.0072	1E-05 - 5.6E-05	0.18 – 1.2

Table S1. $^{235}U/^{238}U$ and $^{234}U/^{238}U$ atom ratios and $^{234}U/^{238}U$ activity ratio of 5 DU firing impact particles.

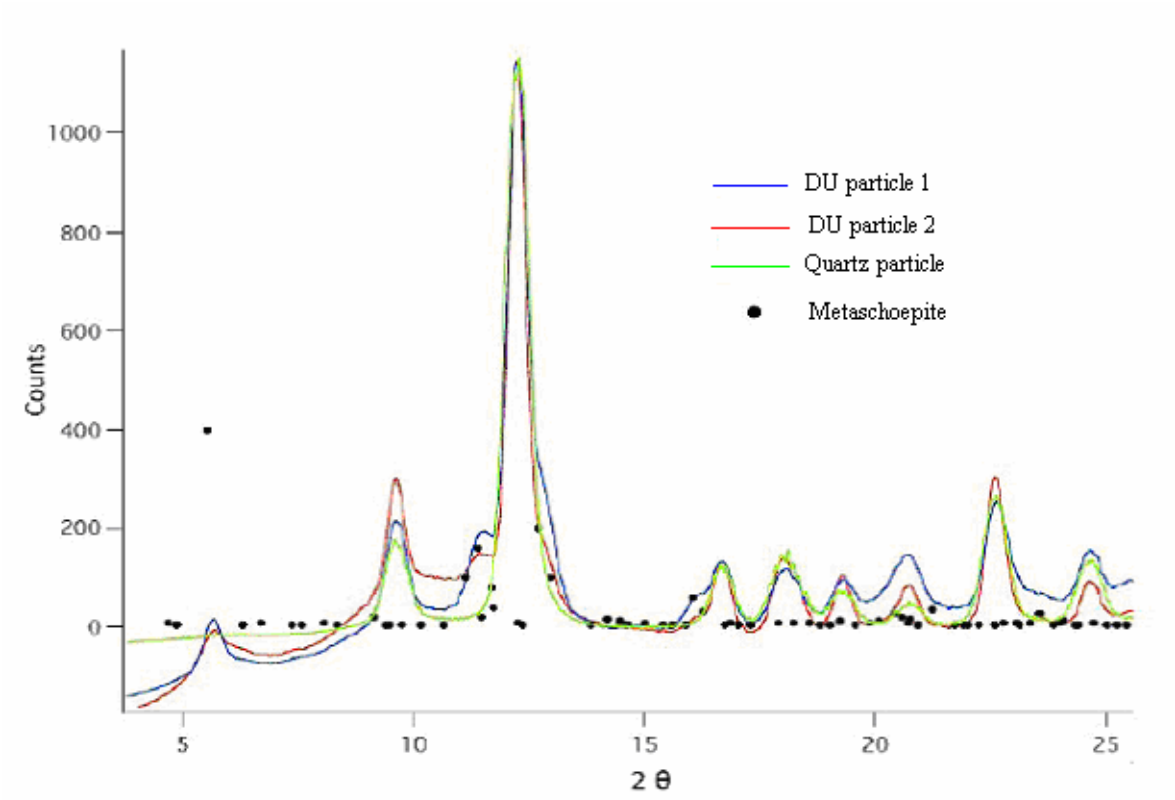

Fig.S3. Diffraction patterns of two yellow DU particles, pure sand pattern and Metaschoepite reflections.

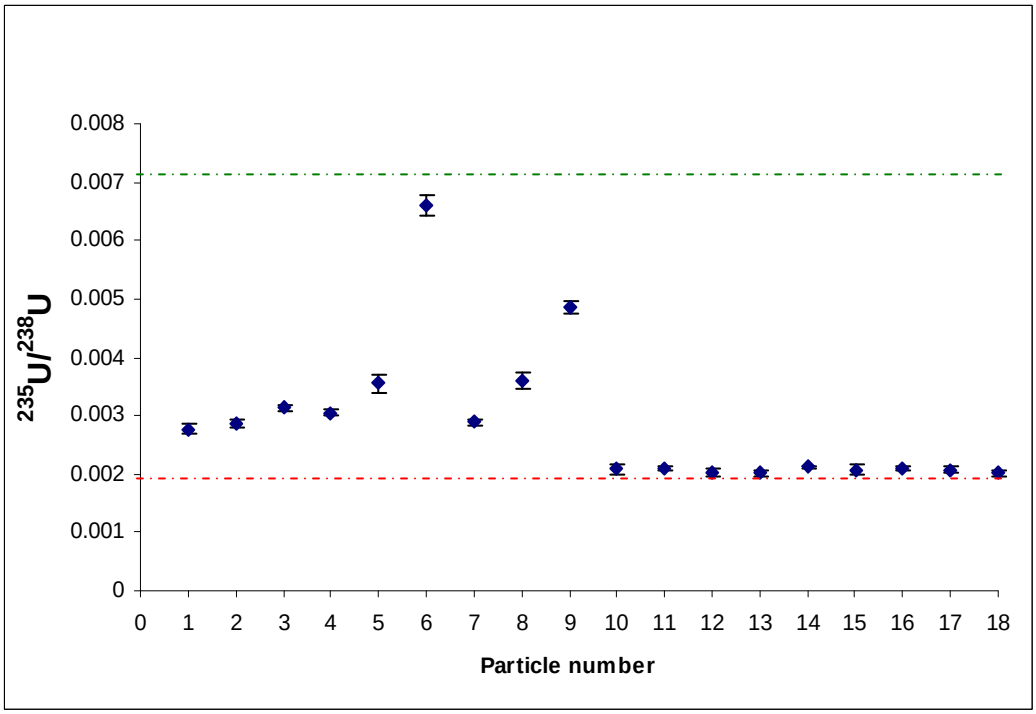

Fig. S4. $^{235}U/\ ^{238}U$ atom ratio representative of analyses taken on hot spots on black DU particles (1-9) such as the one shown in (Figure 4, g) and on the DU particles shown in (Figure 4, a, c, e) which were visibly yellow (10-18). The natural ratio is 0.0072 (green line) and the DU ratio is 0.002 (red line).

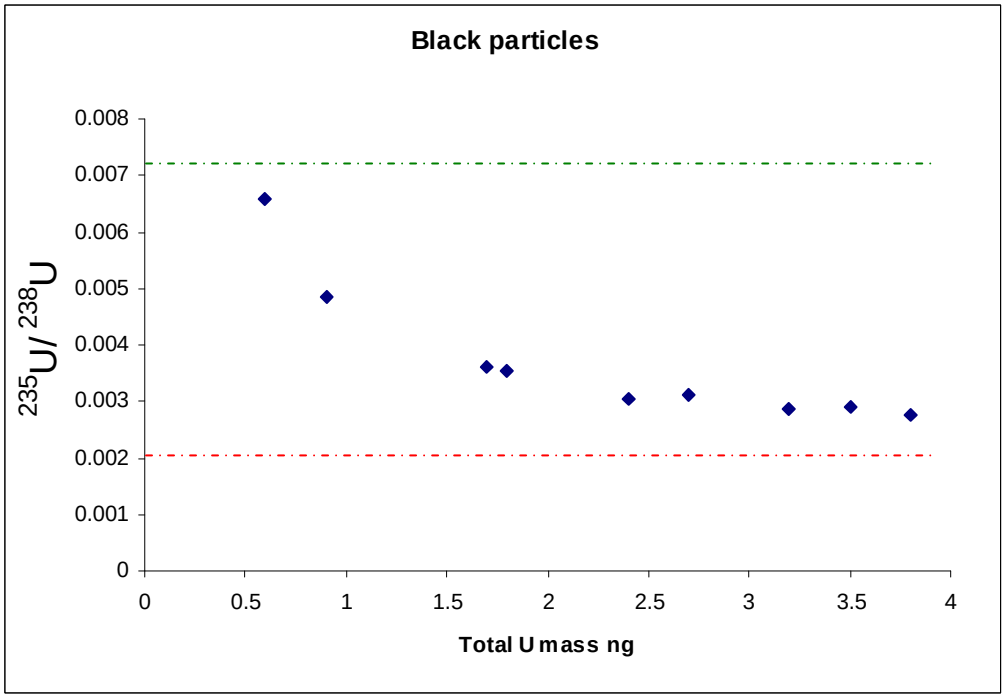

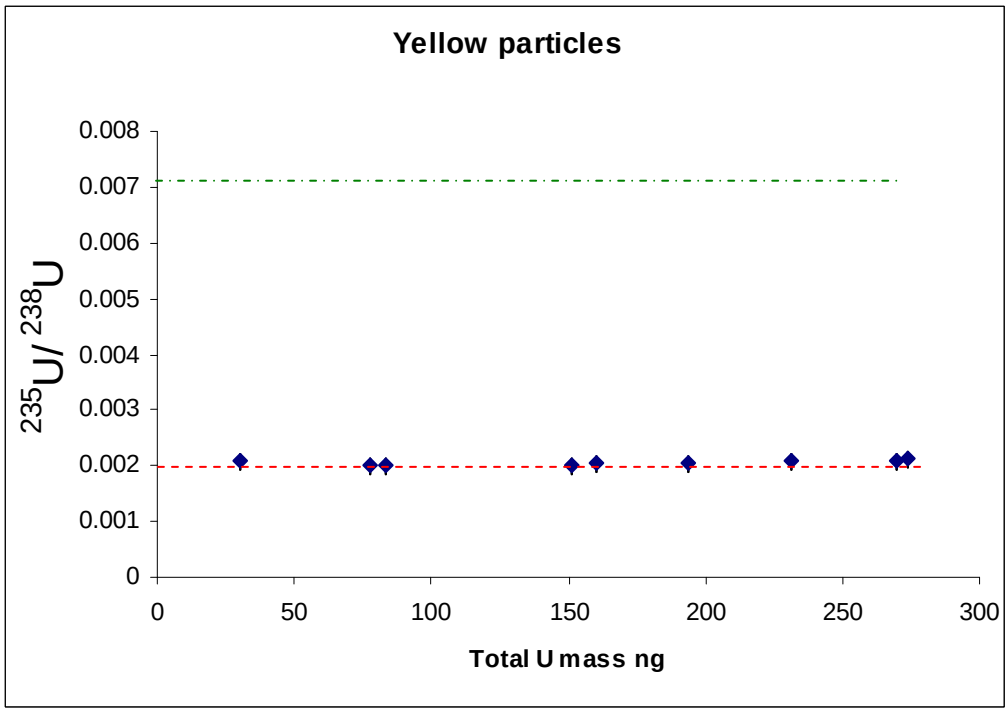

Fig. S5. $^{235}U/^{238}U$ vs. U mass for black and yellow particles. Green line represent natural U ratio and red lines represent DU ratio.

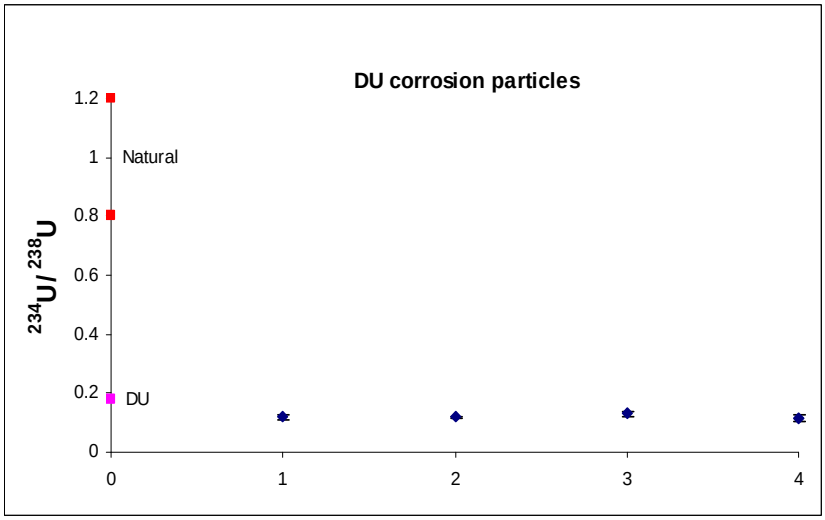

Fig. S6. $^{234}U/^{238}U$ activity ratios for 4 yellow particles (DU corrosion particles). The typical DU ratio is (0.18) and the natural ratio range is (0.8 – 1.2) as indicated on the graphs above.

Chapter 4

Application of Secondary Ion Mass Spectrometry to Analysis of Depleted Uranium Particles from a Test-Firing Range.

The material of the following section is in the process of being submitted to Journal of Analytical Atomic Spectrometry

The candidate's contribution was particles isolation, electron microscopy, data interpretation and writing up the paper..

SIMS analysis was carried out by Ian Lyon and Torsten Henkel (University of Manchester)

Application of Secondary Ion Mass Spectrometry to Analysis of Depleted Uranium Particles from a Test-Firing Range

Mustafa Sajih[1], Torsten Henkel[2], Ian C. Lyon[2] and Francis R. Livens[1,2]

[1] Centre for Radiochemistry Research, School of Chemistry, University of Manchester, Manchester, M13 9PL, UK.
[2] School of Earth, Atmospheric and Environmental Sciences, University of Manchester, Manchester, M13 9PL, UK.

Abstract

Time of flight secondary ion mass spectrometry (TOF-SIMS), was used to examine depleted uranium (DU) particles derived from test-firing of DU penetrators against hard targets. Imaging thin sectioned particles with TOF-SIMS revealed the internal chemistry, and showed the distribution of both major elements (Fe, U, Cr), and a wide range of trace elements (e.g. Ti, K, Ca, Al, Mg). Quantitative analysis showed correlation between the following groups of elements: Fe, Cr, Mn, Ni derived from target material; trace elements derived from soil, and U and Ti, derived from DU (0.75%Ti) alloy. The isotopic composition of U was consistent with DU.

Introduction

Secondary ion mass spectrometry (SIMS) is widely used for surface analysis and has been applied mainly to characterisation of materials in semiconductor technology, metallurgy, geology and biology. It is also a powerful tool in particle analyses. [1,2]

SIMS in general is used for surface analysis. Samples are bombarded with primary ions (10-30 keV), generating secondary ions in a sputtering process from the surface layers. Secondary ions are then separated according to their mass to charge ratios by typical magnetic sector, quadrupole, double focusing, or time of flight mass analyzers.

Time-of-flight secondary ion mass spectrometry (TOF-SIMS), analyzes secondary ions according to their different flight times in the tube when they reach the detector.[3] The choice of primary ion beam in TOF-SIMS depends on the type of analysis. For depth profiling, a high dosage dynamic primary ion beam would be the choice. On the other hand, a low dosage (static) primary beam is better suited to mapping the distribution of elements on a sample surface. [4]

Static TOF-SIMS is unique since it yields surface chemical information about a wide range of elements with high mass resolution. Moreover, using focused ion beams, it is possible to

obtain mass spectra from submicron-sized areas. Therefore, by rastering the ion beam across the surface and collecting a mass spectrum at every point, it is possible to determine chemical distributions with high spatial resolution. [5]

SIMS has previously been used to characterize particles stemming from nuclear activities. The main purpose has been to determine the isotopic composition of U and Pu, as a fingerprint of the materials present in the particles.[6, 7, 8, 9] SIMS has also been used to analyze environmental radioactive particles originating from different sources (e.g nuclear weapon tests,[10] the Chernobyl reactor, [7] or depleted uranium [11]).

Following the use of depleted uranium (DU) munitions in the Gulf war and Balkan conflicts, the environmental impact of depleted uranium and its behaviour in the environment have been of great concern.[12] When a DU round hits a hard target such as amour plate, some DU aerosolizes and ignites at high temperature during the impact, because uranium metal is pyrophoric. Heating and aerosol formation from the target material will also create small, reactive particles and fragments. DU-containing particles will therefore be produced and dispersed into the terrestrial environment. In this study TOF-SIMS was used to explore the elemental and isotopic compositions of depleted uranium particles derived from test-firing of DU penetrators against hard targets, by exploiting the imaging capability and high mass and spatial resolution of TOF-SIMS.

Methods and Analyses

Study site and sample collection

At Eskmeals, UK (national grid reference, SD 078 929), testing of DU munitions began in the 1960s and continued until 1995, with the most intensive period during the 1980s. The test programme involved firing DU projectiles (99.25%U/0.75%Ti) at hard target arrays enclosed within a butt. This testing exposed the area to DU aerosols and fragments produced on impact. [13] A topsoil sample was collected from in front of the target area ~ 40 m from the impact point.

Particle separation

Storage phosphor autoradiography was used to localize DU particles by spreading the sample on filter papers (approx 1 mg sample/cm^2), exposing a storage phosphor screen (25 by 20 cm) to the sample overnight, then reading the screen using a phosphor Imager (GE Healthcare). An example autoradiograph is shown in Fig.1.

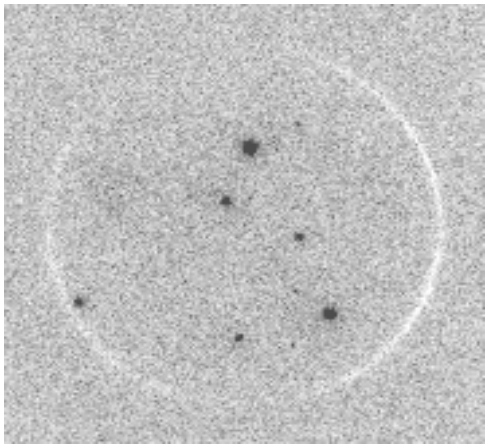

Fig.1 Autoradiograph of DU sample showing hot spots

The black spots represent DU particles (aerosols and fragments) in the sample. Many DU fragments were visible to the eye, so they were picked up individually. The picked particles were embedded in epoxy resin (Araldite, RE1DPF) and dry-polished to produce a flat thin section of the sample. Two types of particle arising from hard target impact can be identified, [14] globular, believed to reflect solidified molten material, and irregular, believed to reflect fragmentation. One example of each type was selected for study.

Particle analyses

Scanning electron microscopy (SEM)/Energy dispersive X-ray analysis (EDX)

The sample was carbon coated to avoid charging effects when analyzed by SEM. Backscattered electron (BSE) imaging was used to identify the different phases of the thin section sample. X-ray analysis was used to explore the elemental composition (EDX spectrum), for each phase in sample surface. Once the surface elemental mapping of the thin section sample was complete, the carbon coating was removed by polishing, prior to SIMS analysis.

Secondary ion mass spectrometry (SIMS)

The thin section sample was coated with ~20 nm of Au to ensure uniform electrical potential at the sample surface. Prior to analysis, 5 nA direct current (DC) Au ion beam was applied to the whole particle surface (up to 300μm x 300μm), firstly to sputter through this coating, and secondly to ensure that the analyzed area was in sputter equilibrium. For

this study a new time-of-flight secondary ion mass spectrometry (TOF-SIMS) instrument was used. It was equipped with a 25 keV Au_n^+ liquid metal ion gun (LMIG) constructed by Ionoptika Ltd. (Southampton, UK; IOG 25Au). The primary ion species were selected by mass using a Wien filter. The secondary ions were detected using a time-of-flight mass spectrometer (R-500 from Kore Technology, Ely, UK), consisting of a two-stage reflectron and micro-channel plate (MCP) detector with secondary ion post-acceleration of 2.4 kV.

SIMS measurements involved rastering a pulsed primary ion beam (pulsed at 5 kHz with pulse lengths of 40ns) over selected areas (60 - 125 μm field of view), and recording each scan separately, results in submicron spatial resolution. These scans (images of the of secondary ions generated from the surface), contained 256 x 256 pixels, with 30 primary ion shots per pixel and each pixel containing a complete mass spectrum,. High mass resolution ($m/\delta m \sim 3000$) was achieved by using delayed extraction.[15]

Results and discussion

SEM-EDX

Particle A (Molten Particle)

Fig. 2 shows an elemental map of the particle thin section, which is composed mainly of two phases, one Fe-rich (dark grey) and one U-rich (light grey).

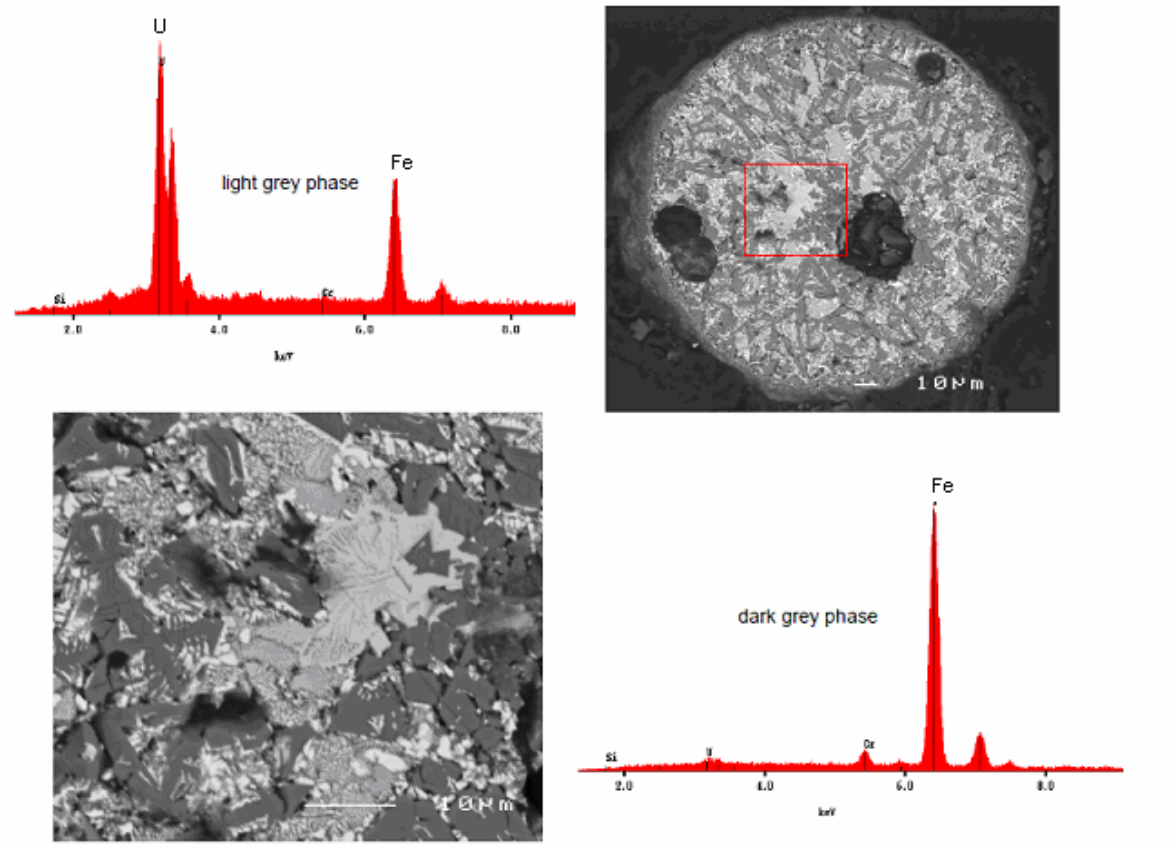

Fig.2 BSE image of a thin section of a round DU particle (top right), and an enlargement of the square area on the particle section (bottom left). EDX spectra of the dark grey phase (bottom right) and light grey phase (top left). The three voids in the particle are present in the original sample. Bars in BSE images are 10 µm.

X-ray analysis of the light grey phase showed predominant U-Fe composition, though with some localized variability in U:Fe ratio, and excess of U over Fe in brighter spots. The texture is consistent with the particle's proposed origin from the crystallisation of molten material.

Particle B (DU fragment)

The thin section of the particle shows both a different morphology and different phases from particle A (Fig. 3).

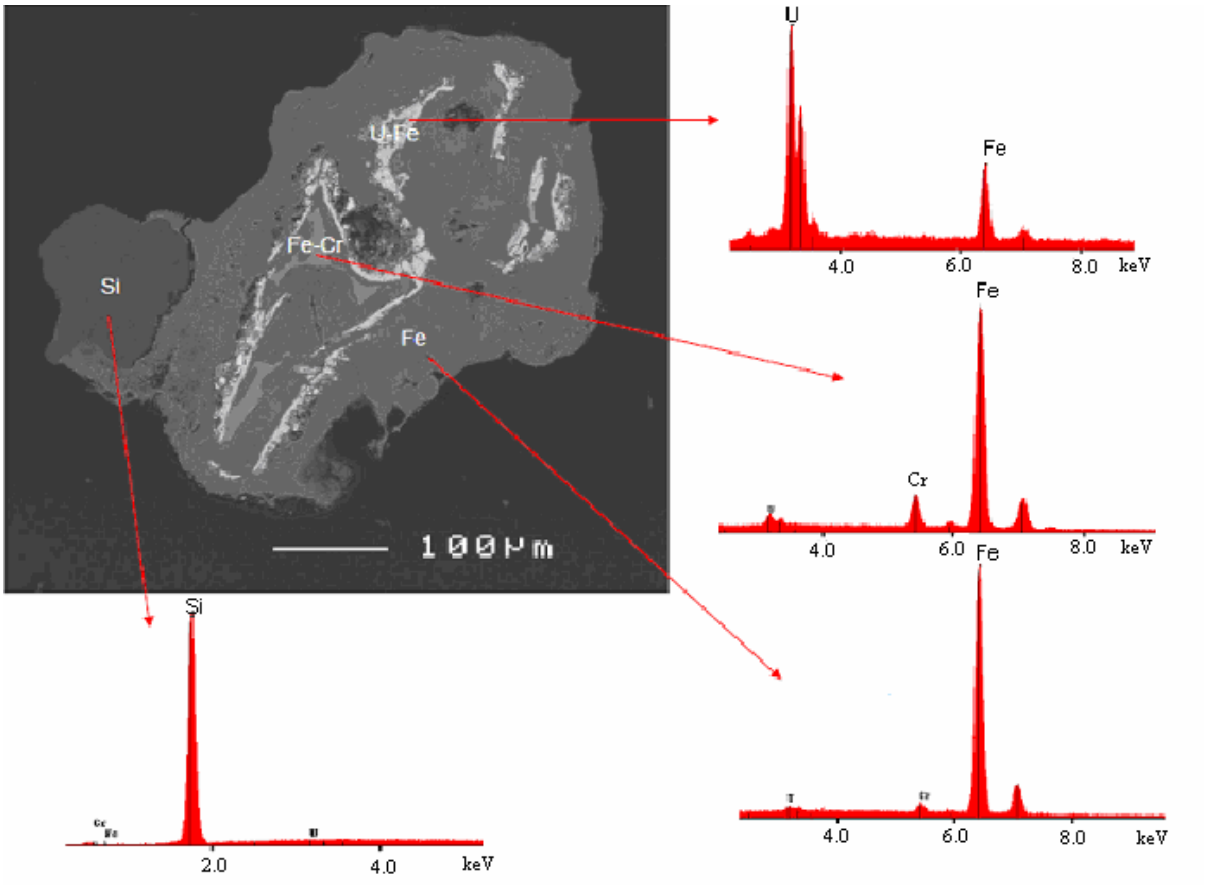

Fig.3 BSE image of a thin section of a DU fragment (Particle B), and the EDX spectra of different phases within the particle.

The BSE image shows regions of four different compositions, and X-ray analysis shows that these phases comprise U-Fe, Fe, Fe-Cr and Si. The different phases presumably reflect the mixing of materials from different origins. U will be derived from the DU penetrator, Fe and Cr are probably derived from hard target material, while the Si-rich region may reflect incorporation of a sand grain.

Using SEM-EDX, it was possible to map the distribution of major elements within thin section particles and obtain semi quantitative elemental composition. A more detailed elemental distribution of major and trace elements, from SIMS analysis of the two thin sectioned particles will be presented below.

SIMS

Molten Particle (Particle A)

Elemental mapping

A set of major and trace elements, chosen to be representative of penetrator, target and background materials, was mapped by collecting positive ion images (Fig. 4).

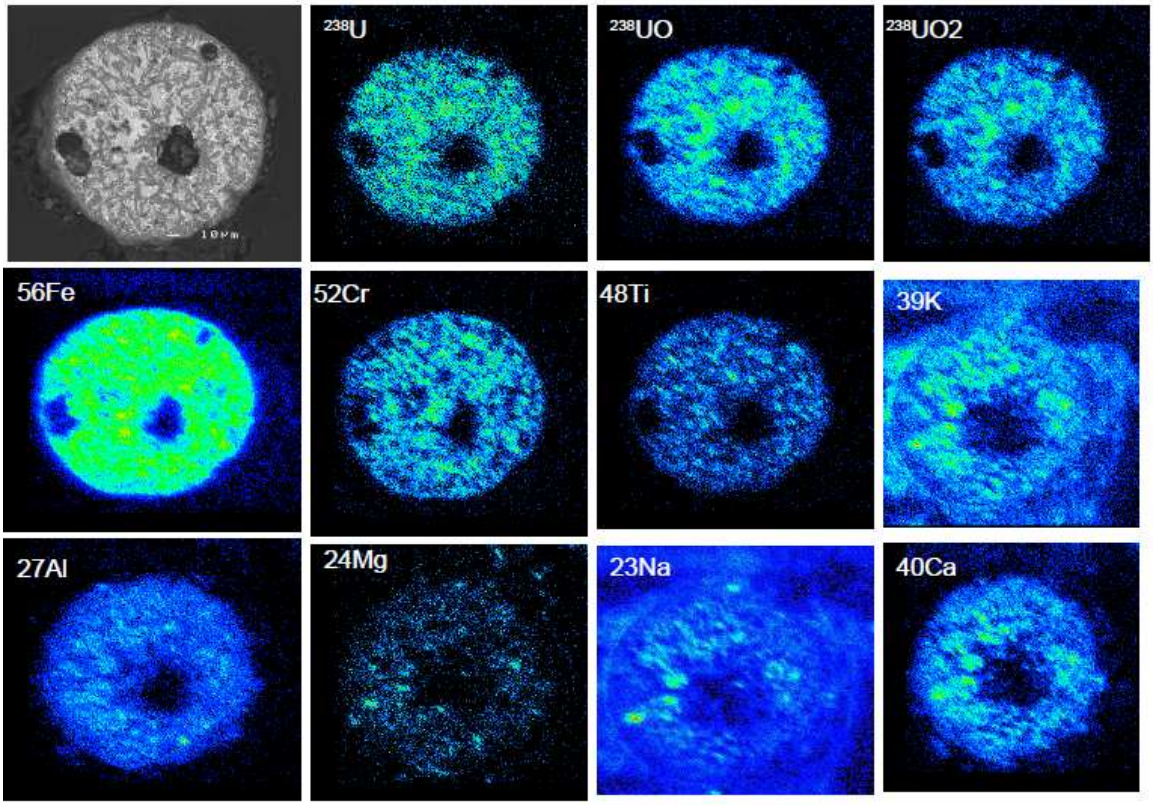

Fig.4 Secondary ion maps show the distribution of elements within particle section, and BSE image of the particle (top left). Field of view 290 µm.

The ion images show an almost homogeneous distribution of the major elements (Fe, U and Cr), and heterogeneous distribution of the other trace elements within the particle section.

Hydrocarbon contamination

The presence of hydrocarbons gave significant mass interference problems since the hydrocarbon-derived ions span almost the entire mass spectrum. Since TOF-SIMS analyzes only the uppermost surface layers, contamination is possible. Usually the sample surface is cleaned using a direct current (DC) beam or primary ion beam to remove adsorbed contaminants before analysis. However, a cleaned sample surface can regain atoms and molecules like hydrogen and hydrocarbons from the residual gas or from the embedding resin which contains C, H and O. With its low duty cycle, the primary ion

source may not be able to prevent this adsorption sufficiently, especially when a large area is scanned [16]. To minimize this interference, a 64 x 64 µm area from the particle section above, as free as possible from hydrocarbons, was analyzed (Fig. 5).

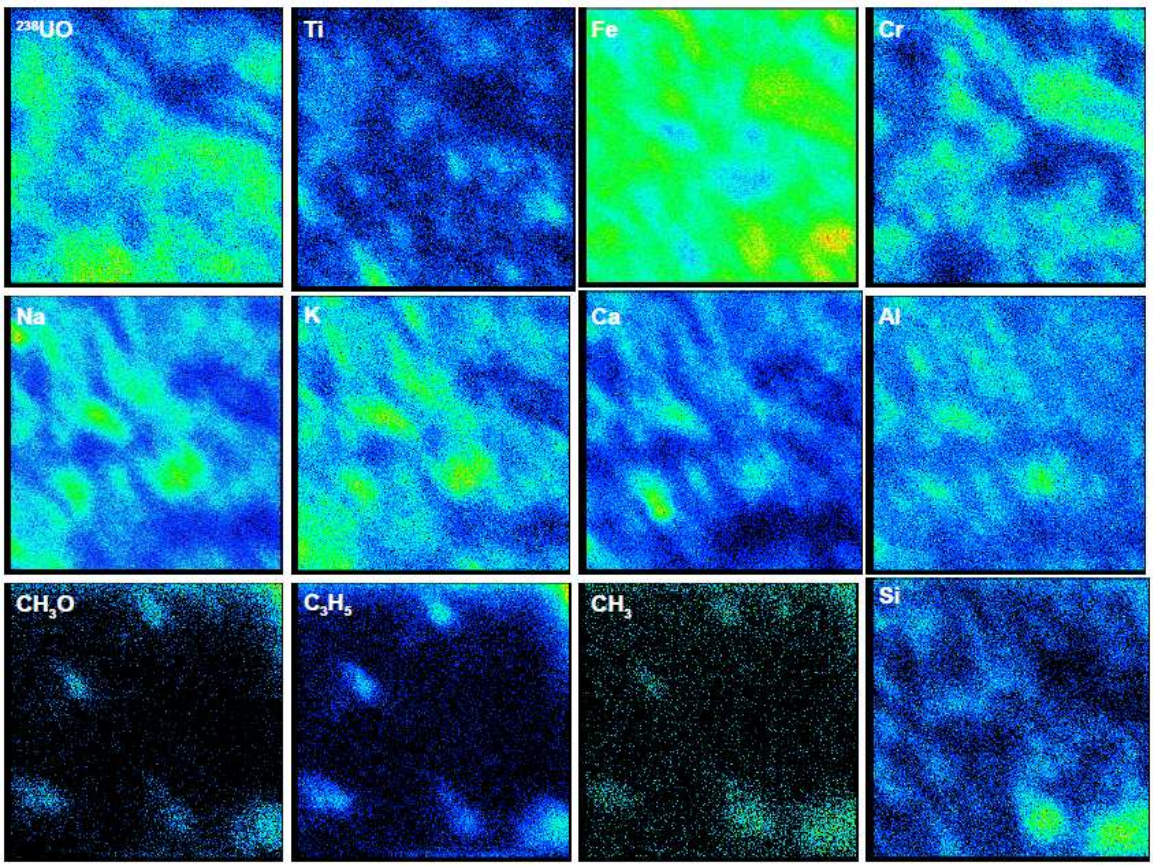

Fig.5 Secondary ion maps showing the distribution of some elements and hydrocarbons within the particle section. Field of view 64 microns from the area between the edge and the hole in the middle of the top right image in Fig 2.

Qualitatively, the ion images suggest that Fe and Cr correlate, and K, Na, Ca, Al correlate as well, but U does not seem to correlate with any element except, to some degree, with Ti. The hydrocarbon images in the bottom row suggest that the hydrocarbon-rich spots coincide with the Si ion map, suggesting that hydrocarbons originate in the particle and derived from the same origin along with Si. Statistically, there is a reasonably strong correlation (R = 0.87) between Si and CH_3 (Supporting information, Fig. S1).

Quantitative analysis

To obtain detailed information on element abundances and correlations in a particle section, quantitative analysis can be performed, based on the number of counts. Fig. 6 shows another 72 x 72 µm area of the particle, selected to minimize hydrocarbon contamination. This area was analyzed by measuring element counts from an array of 36 small circular regions of interest (~ 10 µm dia), almost covering the whole area.

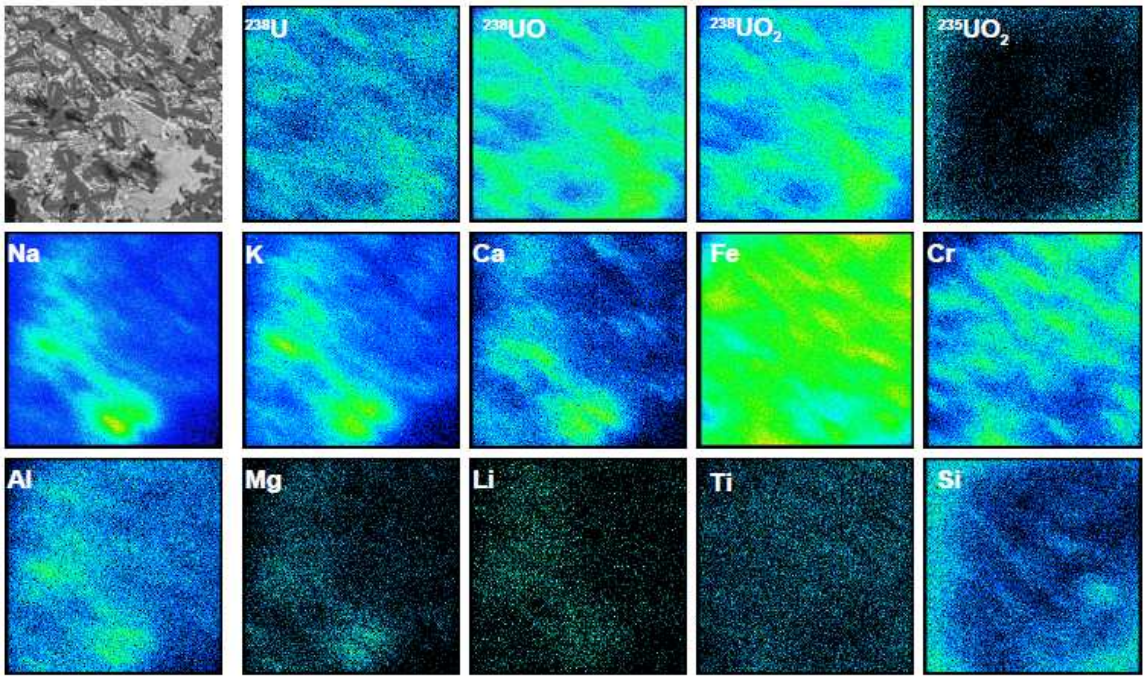

Fig. 6 Secondary ion images of a 72 microns field of view (BSE image shown top left). Field of view is the area defined by the red square in Fig 2.

The TOF-SIMS maps are generally consistent with the semiquantitative EDX data obtained from SEM imaging. The ion images show a lot of structure, which can be attributed to the different elements being derived from different sources. The simplest way to describe the relationship between different elements is the correlation coefficient R (Table 1). Correlation plots are shown in supporting information (Fig. S2).

Elements	Na-K	Ca-Mg	Al-Mg	Fe-Mn	Fe-Cr	Ni-Cr	U-Ti
R	0.97	0.95	0.91	0.86	0.78	0.86	0.45

Table 1. Significant correlation coefficients for different pairs of elements.

Significance of the correlation will depend on the number of data points and their deviations from the regression line. This can be tested using the critical values of statistical significance of correlation coefficients (Table S1, supporting information). Testing R values for 36 data points, all correlations in Table 1 are significant at 95% confidence (p = 0.05).

On the basis of these correlations, the different elements in the particle can be grouped. The first group contains K, Ca, Al, Na, Mg, which may well indicate background material (a coastal sand). The second group contains Fe, Ni, Mn and Cr, probably derived from

target material [17] .As would be expected, U correlates with Ti because the DU projectile is composed of 0.75% Ti by weight.

DU Fragment (Particle B)

Imaging and quantitative analysis

A 125 x 125 µm area of the particle section, selected to be fairly free of hydrocarbons, was analyzed (Fig. 7).

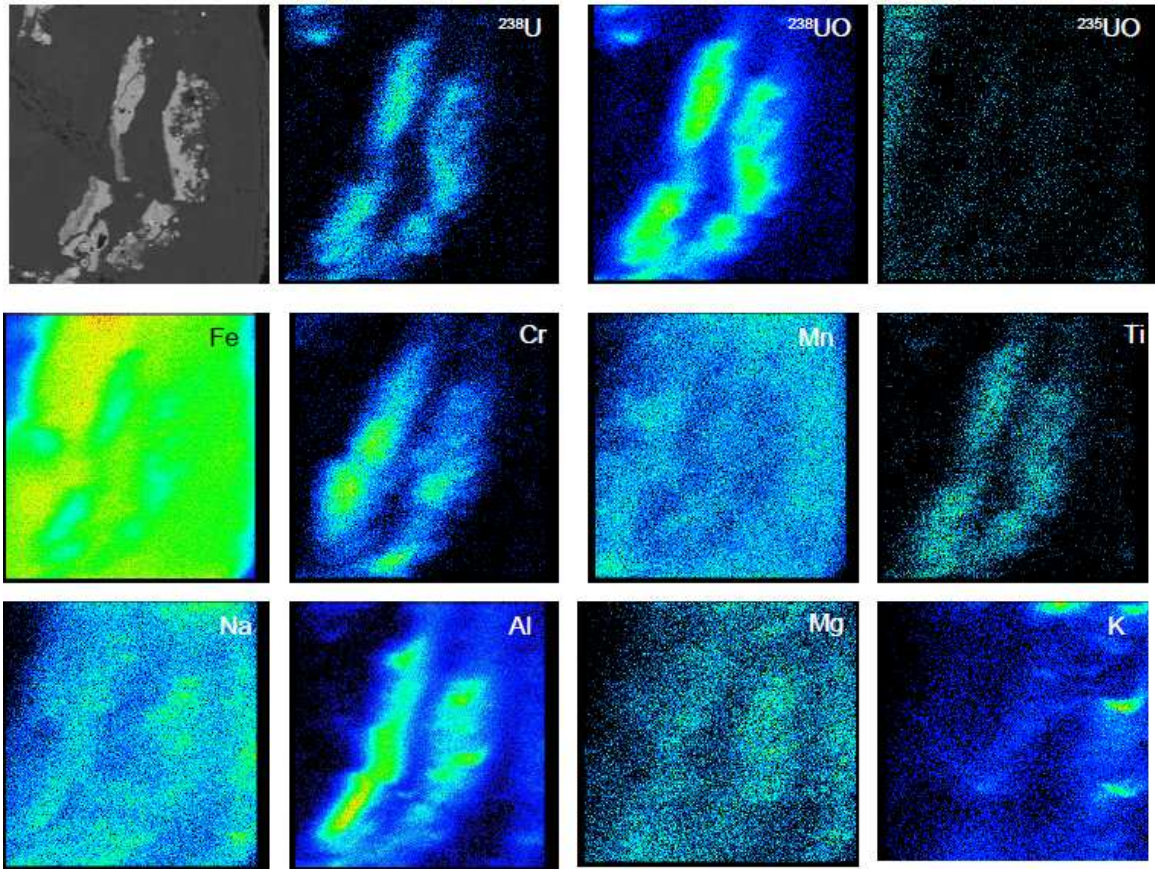

Fig. 7 Secondary ion images of 125 microns field of view (BSE image shown top left).

The ion images suggest that U correlates with Ti, that Fe and Mn are correlated, and that K, Na, and Mg are also correlated. There is no clear visual relationship between Cr, Al and other elements. Chemical features in digital images lead to pixel populations in coherent clusters and can, therefore, be treated by multivariate statistical means to extract analytical information. Kohonen networks for assigning structures in secondary ion distributions to chemical phases can be used to classify the specific chemical features in the sample [18]. A statistical analysis of the observed images was carried out by defining 19 small regions of interest on the Al, U, Cr, Fe ion images, where these elements are present in significant abundances (supporting information, Fig. S3). The counts for the different elements, normalized to the number of pixels in each region, were measured and scatter diagrams

were plotted to determine the pixel density and represent the relationship of the elements in the original sample (Fig. 8).

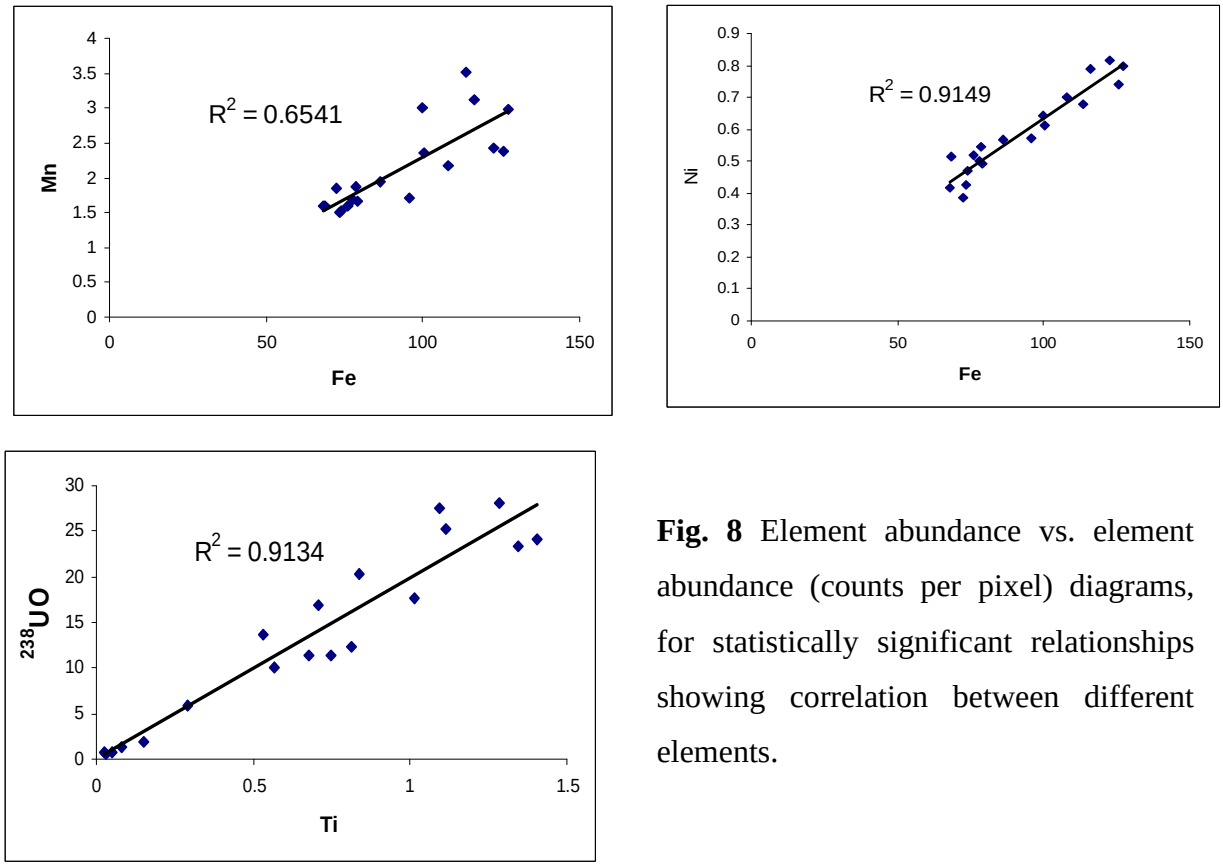

Fig. 8 Element abundance vs. element abundance (counts per pixel) diagrams, for statistically significant relationships showing correlation between different elements.

The element correlations in Fig 8 were significant at 95% confidence according to the critical value for 19 data points (Table S1, supporting information). The statistical analysis showed a correlation between U and Ti, and this may reflect the fact that the DU penetrators, and hence any residual material, contain 0.75 % Ti. There is a correlation between Fe, Mn, Ni, but Cr does not correlate with any element from the target material except Fe. However, there is a stronger correlation (R = 0.97, $p < 0.05$, significant relationship) between Cr and Fe in Cr-rich areas than in Fe-rich areas (R = 0.58, $p > 0.05$, non-significant relationship) (supporting information, Fig .S4), suggesting that Cr may have more than one physiochemical associations in this particle. Al, which correlates with background elements such as Ca and Mg in Particle A, does not correlate with any background element in this particle B. Al could be derived from composite armour (Chobham armour, which is composed of ceramic tiles encased within a metal matrix) or (less likely) the Al coating on the DU penetrator. Statistical analysis showed a relationship (R = 0.83, $p< 0.05$) between Al and Fe in Al, Fe and Cr areas (supporting information, Fig. S5), suggesting that Al derived from target material. A relationship (R = 0.83, $p < 0.05$)

between Al and Ti was also observed (supporting information, Fig. S6), suggesting that target material may be another source of Ti.

Isotopic composition of U

Particle B

Measurement using different ions

The $^{235}U/^{238}U$ atom ratio was also measured from the 125 x 125 μm area. The measurement was taken from a spot where the hydrocarbon interference was least, and gave an average ratio consistent with DU (Table 2).

Ion	Atom ratio 235/238
U^+	0.00237 ± 0.00059
UO^+	0.00283 ± 0.00024
UO_2^+	0.00240 ± 0.00021
Average	0.00255 ± 0.00025
Typical DU	0.002

Table 2. $^{235}U/^{238}U$ atom ratio measured from a spot on U ion images.

Determination of mean ratio

The mean atom ratio $^{235}U/^{238}U$ was measured from the same area (125 μm), by defining seven small areas of interest on UO_2^+ ion image (supporting information, Fig S3), and measuring the ratio in each area using the raw counts from $^{235}UO_2^+$ and $^{238}UO_2^+$ signals. The mean ratio was obtained by regressing $^{238}UO_2^+$ against $^{235}UO_2^+$ (Fig. 9).

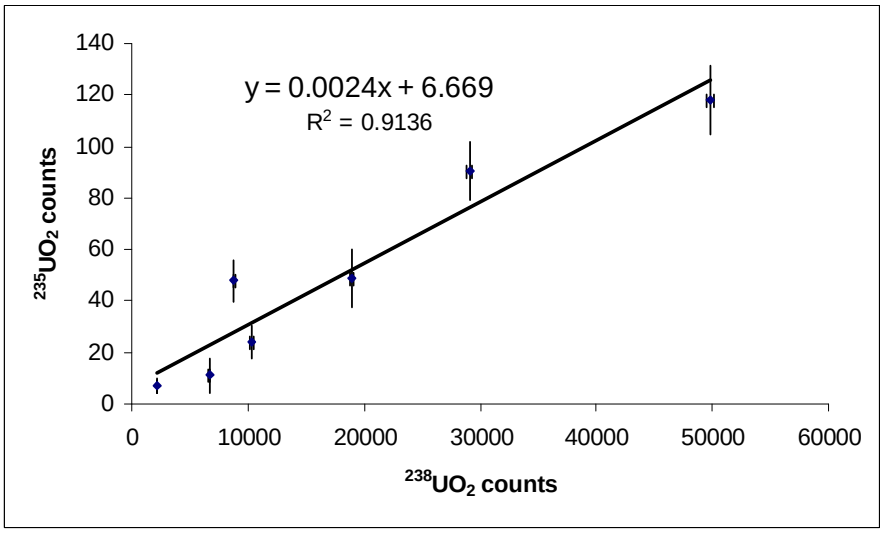

Fig. 9 Regression of $^{235}UO_2^+$ against $^{238}UO_2^+$ for seven data points collected from areas of interest on UO_2^+ image.

The value from regressing 7 data points according to the regression equation (Y= 0.0024X + 6.669), is $^{235}U/^{238}U$ = 0.0024±0.00032, which is consistent with DU ratio. The ratio obtained from a spot measurement is in agreement with the mean ratio and consistent with DU ratio as well.

Particle A

The isotopic composition of U was determined using the atom ratio $^{235}U/^{238}U$. The ratio was originally measured from spots across the 72 x 72 µm area of the particle section, but the hydrocarbons on the surface affected the ^{235}U signal. A better measurement was made by sputtering the primary ion beam continuously on a spot to minimize hydrocarbon interferences. The UO^+ or UO_2^+ secondary ions gave better count rates than U^+ signal, and they gave atom ratios of 0.0025±0.0003 and 0.0046±0.0005 respectively. The average ratio is 0.00355±0.00058 which is indicative of DU.

Summary and Conclusion

The results showed that SIMS is an imaging technique that exhibits better sensitivity than microscopic SEM-EDX, particularly for studying the spatial distribution of elements in solid materials which is important in investigating adsorption. By using quantitative analysis of secondary ion images, based on element correlations, it was possible to group elements derived from different origins. The elements Fe, Cr, Ni and Mn derive from target material, K, Ca, Na and Al derive from costal soil, and U and Ti from the DU projectile. Measuring the uranium atom ratio by SIMS showed that uranium was depleted, confirming the isotopic composition can reveal the history and origin of nuclear materials.

While SEM-EDX is useful in exploring homogeneity and in elemental mapping, its analytical capability is relatively limited. By utilizing the imaging capability, high spatial and mass resolution, and isotopic discrimination of TOF-SIMS, it is possible to obtain much more complementary detail through mapping major and trace elements within thin sections of DU particles, identifying elemental correlations, and measuring the isotopic composition of U.

Acknowledgment

We thank the UK Defence Science & Technology Laboratory for arranging access to the sampling sites, the Natural Environment Research Council and University of Aleppo, Syria for support. We would like to thank Dr Miranda Keith-Roach, University of Plymouth for samples.

References

1 A. Benninghoven, *Angew Chem Int Edit*,1994a, **10**, 1023-1043.

2 M. Betti, *Int J Mass Spectrom*, 2005, **2-3**, 169-182.

3 A. Benninghoven, *Surf Sci*, 1994b, **C**, 246-260.

4 J. Handley, *Anal Chem*, 2002, **11**, 335 A-341 A.

5 M. B. Robert, B. Paul, J. M. Steve, C. Clive, F. W. Kenneth, C. V. John, W. Nicholas, *Rapid Commun Mass Sp*, 1998, **18**, 1246-1252.

6 M. Betti, G. Tamborini, L. Koch, *Anal Chem*, 1999, **14**, 2616-2622.

7 G. Tamborini, M. Betti, *Mikrochim Acta*, 2000, **2-4**, 411-417.

8 G. Tamborini, *Microchim Acta* , 2004, **1-4**, 237-242.

9 Y. Ranebo, P. M. L. Hedberg, M. J. Whitehouse, K. Ingeneri, S. Littmann, S, *J Anal Atom Spectrom*, 2009, **3**, 277-287.

10 J. Jernstrom, M. Eriksson, R. Simon, G. Tamborini, O. Bildstein, R. C. Marquez, S. R. Kehl, T. F. Hamilton, Y. Ranebo, M. Betti, *Spectrochim Acta By*, 2006, **8**, 971-979.

11 S. Torok, J. Osan, L. Vincze, S. Kurunczi, G. Tamborini, M. Betti, Spectrochim Acta B, 2004, **5**, 689-699.

12 The Royal Society, *The health hazards of depleted uranium munitions*, report Part I, London, 2001

13 I. W. Oliver, M. C. Graham, A. B. MacKenzie, R. M Ellam, J. G Farmer, J Environ Monitor, 2007, **7**, 740-748.

14 M. Sajih, F. R Livens, R. Alvarez, M. Morgan, STOTEN, in press.

15 A. King, T. Henkel, D. Rost, I. C. Lyon, I, *Rapid Commun Mass Sp*, 2010, **1**, 15-20.

16 T. Stephan, *Planet Space Sci*, 2001, **9**, 859-906.

17 M. Edwards, A. Mathewson, *Int J Impact Eng*, 1997, **4**, 297-309.

18 M. Wolkenstein, H. Hutter, Ch. Mittermayr, W. Schiesser, and M. Grasserbauer, *Analytical Chemistry*, 1997, **69**, 777-782.

Supporting information

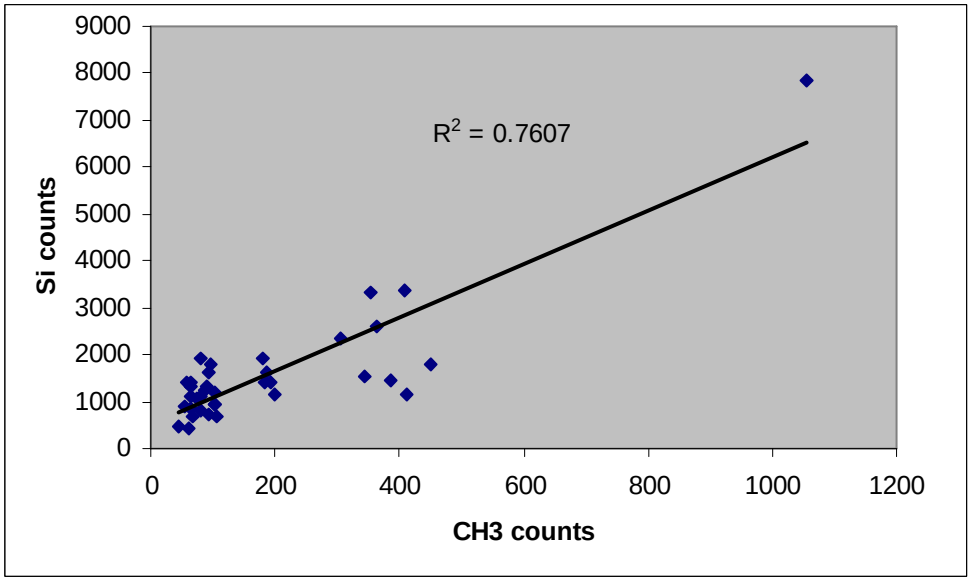

Fig. S1 Correlation plot shows the relationship between Si and CH_3. The 36 dots in the plot represent data collected from 36 areas (10 microns) covering almost the whole 64 x 64 area.

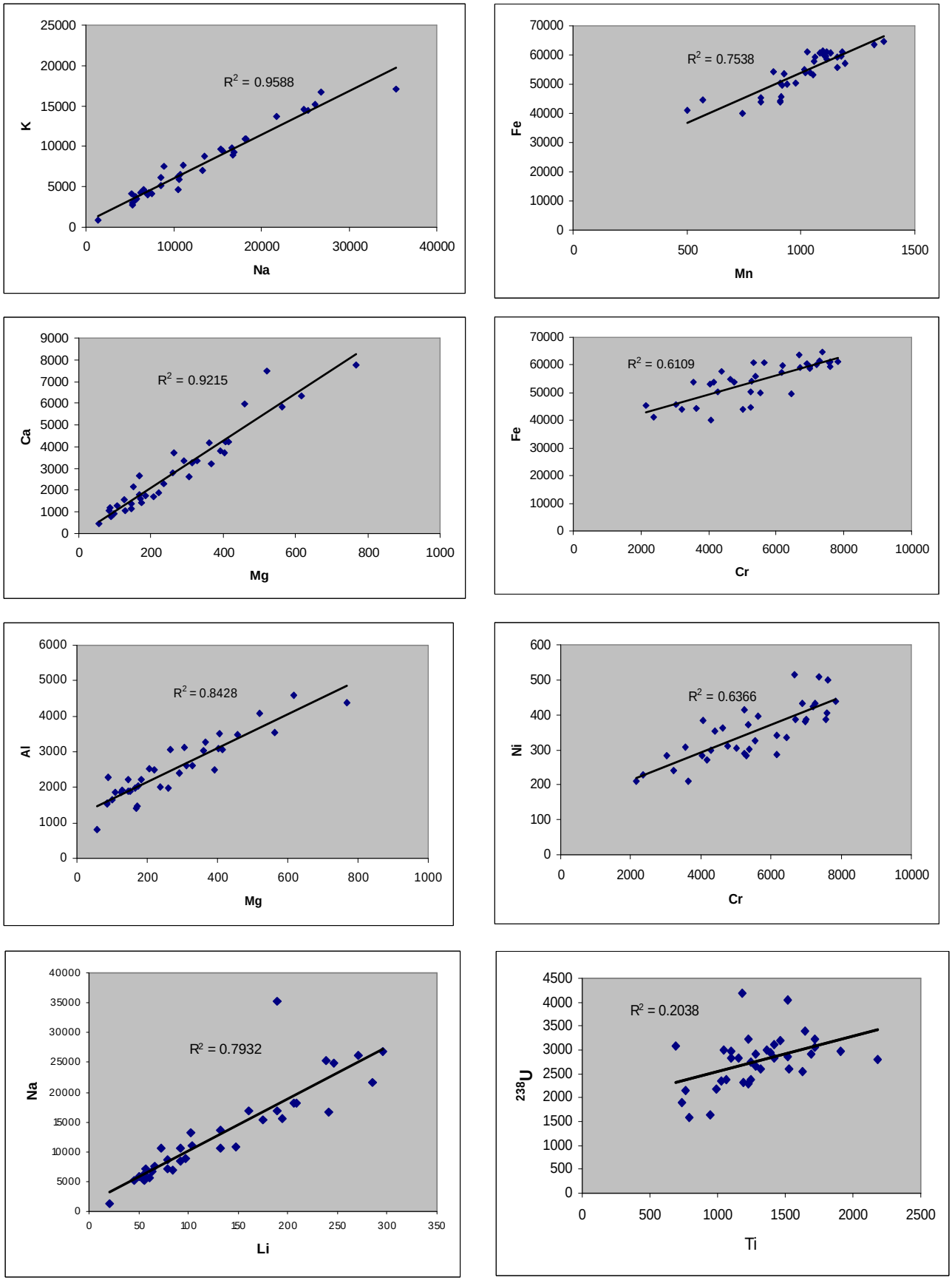

Fig. S2 Element abundance vs. element abundance (counts) plots, showing correlation between different elements.

Table S1. Critical Values of the Pearson Product-Moment Correlation Coefficient

df= n-2	Critical value (ρ= 0.05)	df=n-2	Critical value (*p*= 0.05)
1	0.997	19	0.433
2	0.950	20	0.423
3	0.878	21	0.413
4	0.811	22	0.404
5	0.754	23	0.396
6	0.707	24	0.388
7	0.666	25	0.381
8	0.632	26	0.374
9	0.602	27	0.367
10	0.576	28	0.361
11	0.553	29	0.355
12	0.532	30	0.349
13	0.514	35	0.325
14	0.497	40	0.304
15	0.482	45	0.288
16	0.468	50	0.273
17	0.456	60	0.250
18	0.444	70	0.232

df: degree of freedom , n: number of data points (sample size)

This table is used to decide whether there a significant relationship between two variables or there is not. For example, if the number of data points used to study the relationships between two variables is n = 17, df = 15. If the correlation coefficient is larger than the critical value 0.482, this means there is a significant relationship between the two variables.

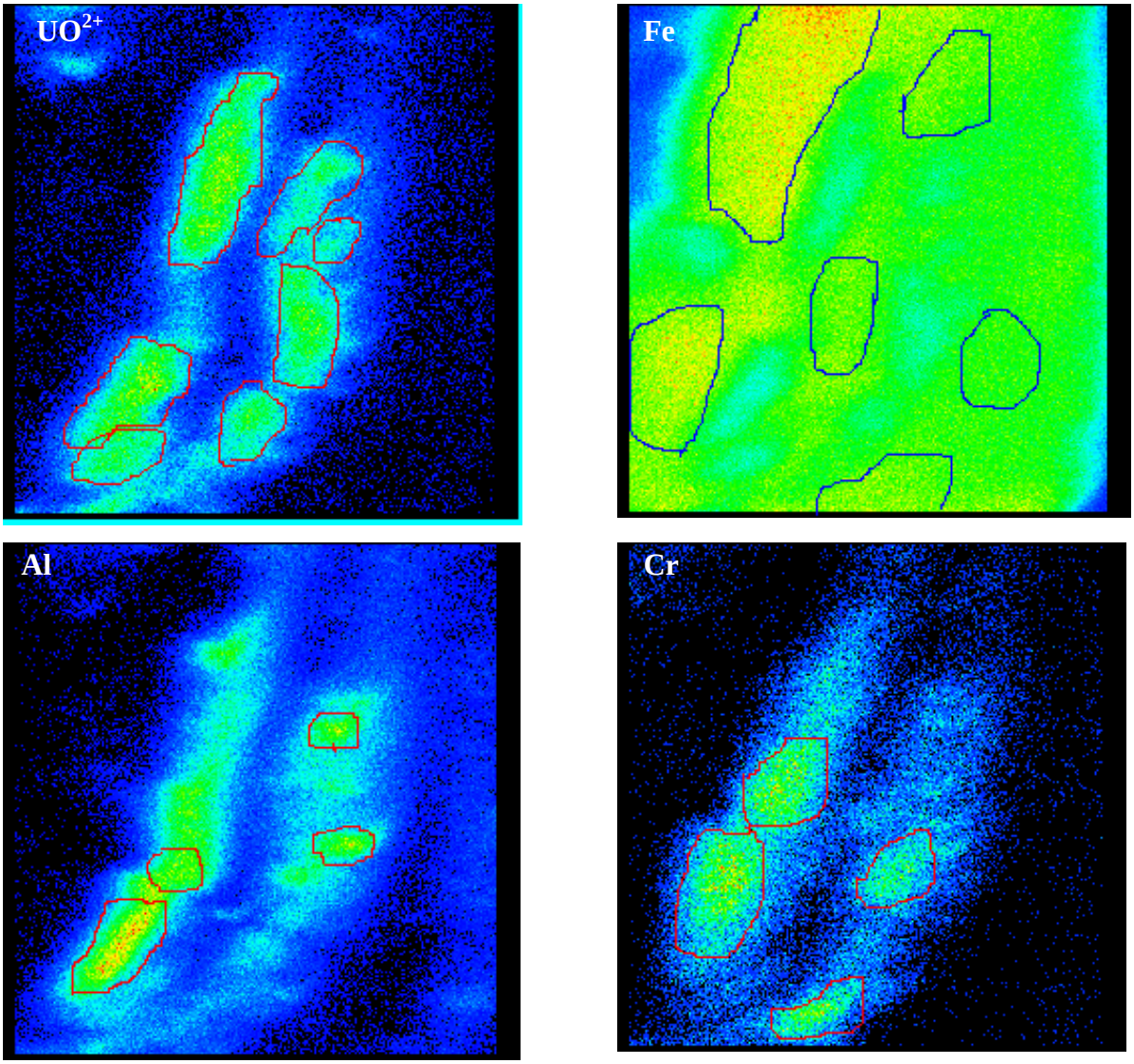

Fig. S3 Areas of interest used for quantitative analysis.

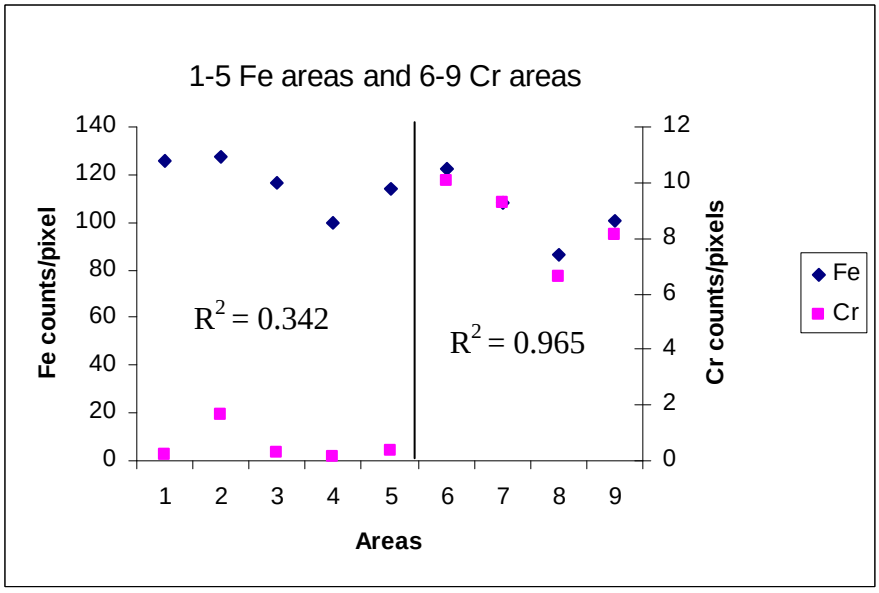

Fig. S4 Relationship between Fe and Cr showing stronger correlation in Cr areas than Fe areas.

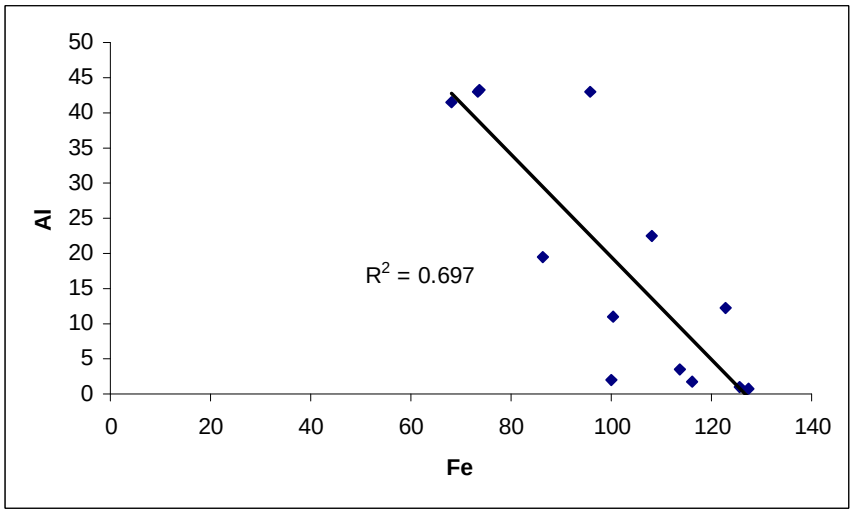

Fig.S5 Correlation between Fe and Al in Al, Fe and Cr areas

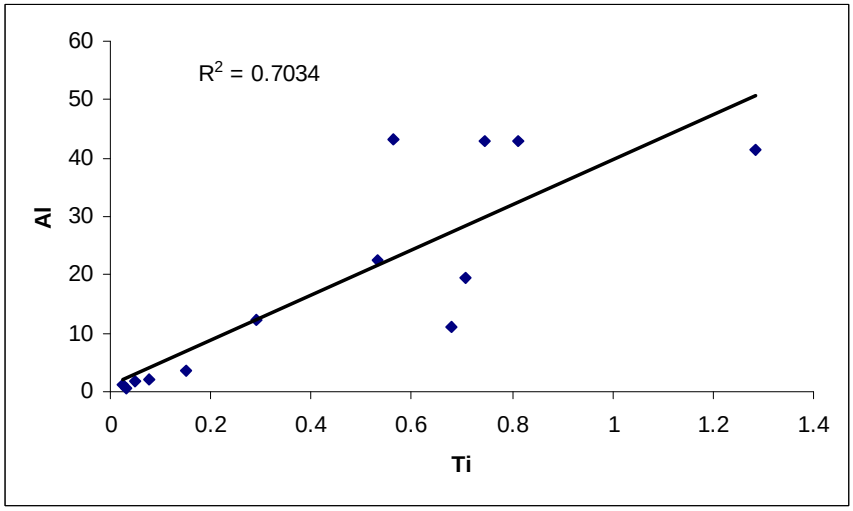

Fig. S6 Correlation between Ti and Al in Al, Fe and Cr areas

Chapter 5

Biogeochemical Controls on the Corrosion of Depleted Uranium Alloy in Subsurface Soils

The material in this chapter has been published in the journal Environmental Science and Technology.

***Environ. Sci. Technol.*, 2009, 43 (16), pp 6177–6182**
DOI: 10.1021/es901276e
Publication Date (Web): July 16, 2009

Candidate's contribution was particle isolation and analysis.

Soil from microcosms (field-moist and waterlogged) was screened using phosphor imaging analysis to isolate DU particles which were then analysed by SEM-EDX for size distribution, morphology and elemental composition. The field-moist soil contained sufficient quantities of DU particles which were analysed by X-ray powder diffraction (XRD) to determine the crystal structure of uranium.

Biogeochemical Controls on the Corrosion of Depleted Uranium Alloy in Subsurface Soils

Stephanie Handley-Sidhu[a], Paul J. Worsfold [a], Francis R. Livens[b,c], David J. Vaughan[b], Jonathan R. Lloyd[b], Christopher Boothman[b], Mustafa Sajih[c], Rebeca Alvarez[b,c] and Miranda J. Keith-Roach [a,*]

[a] Biogeochemistry and Environmental Analytical Chemistry Research Group, School of Earth, Ocean and Environmental Sciences, University of Plymouth, Drake Circus, Plymouth PL4 8AA, U.K.,

[b] Williamson Research Centre for Molecular Environmental Science, and School of Earth, Atmospheric and Environmental Sciences, University of Manchester, Manchester M13 9PL, U.K.

[c] Centre for Radiochemistry Research, School of Chemistry, University of Manchester, Manchester M13 9PL, U.K.

Abstract

Military activities have left a legacy of depleted uranium (DU) penetrator waste in the near-surface terrestrial environment. To understand the fate of this DU alloy, the mechanisms and controlling factors of corrosion need to be determined. In this study, field-moist and waterlogged microcosms were used to investigate the effect of redox conditions and soil water content on the corrosion and fate of DU in subsurface soil, and the impact of corroding DU on the soil microbial population. The mechanism of corrosion and the corrosion products formed were highly dependent on the water status of the soil. Under field-moist conditions, DU corroded at a rate of 0.49 ± 0.06 g cm^{-2} y^{-1} and the main U input to surrounding soil was large metaschoepite [$(UO_2)_8O_2(OH)_{12}\cdot(H_2O)_{10}$] particles. However, under waterlogged conditions the rate of corrosion was significantly slower at 0.01−0.02 g cm^{-2} y^{-1} and occurred with the release of dissolved species to the surrounding environment. Corrosion ceases under reducing conditions, thus redox conditions are important in determining the persistence of penetrators in the environment. Corroding DU alters the redox conditions in the surrounding environment and both mechanisms of corrosion impact the microbial community.

* Corresponding author e-mail: mkeith-roach@plymouth.ac.uk

Introduction

Depleted uranium (DU) penetrators were used extensively during the 1991 Gulf War, the 1999 Kosovo/Serbia conflicts, and the 2003 Iraq conflict (1). The 1991 Gulf War deposited approximately 321 tonnes of DU in the terrestrial environment (1), mainly consisting of whole penetrators and large fragments, since 70−90% of aircraft projectiles miss their targets (2). The depth that penetrators become embedded within the soil depends on the angle of impact and physical properties, with reported penetration depths of >2 m in denser clay soils (3) and 6−7 m in soft soils (4).

Moisture content, O_2 supply, pH, temperature, and microbial community influence soil corrosivity (5). Investigations into DU corrosion rates and products formed in soils have included in situ and laboratory studies. At two sites in an arid surface soil in the Mojave Desert, USA, U migration from corroding penetrators produced distinct layers (6, 7). The surface soil contained yellow-orange schoepite, whereas at 2−4 cm depth, yellow metaschoepite was observed, and below 4 cm, U was present as secondary U-silicate species (6, 7). At Kirkcudbright, UK, DU coupons were buried to 0.3 m depth in an organic, silty-clay soil and sampled over 4.4 years. Black and yellow corrosion products, characterized as uranium dioxide and schoepite, respectively, were observed on the DU coupons and in surrounding soil at the first sampling time (102 days), and corrosion rates over 4.4 years were 0.8−1.1 g cm^{-2} y^{-1} (8). In the laboratory, DU corrosion has been studied in two soils (sandy-loam and silty-loam) at 20 °C, with simulated rainfall (16 mm $week^{-1}$). Black and yellow corrosion products formed, and there was negligible difference in corrosion rates for the two soils (0.19 ± 0.03 g cm^{-2} y^{-1}) (9).

The diffusion rates of O_2 in soils range from 10^{-2} to 10^{-6} cm^2 s^{-1} for dry and water-saturated soils, respectively (10). Limited O_2 diffusion into waterlogged soils results in anaerobic conditions in which microorganisms utilize alternative terminal electron acceptors (TEAs) for organic matter oxidation. The relative energy yields govern TEA utilization, giving rise to the “redox cascade” of O_2, NO_3^-, Mn(IV), Fe(III), SO_4^{2-}, and CO_2 reduction. Corroding uranium is a strong reducing agent; this property together with hydrogen released during DU corrosion (11) may reduce TEA concentrations (12).

Investigations into DU corrosion have not explicitly considered the effect of soil water content and redox processes on corrosion, leaving a level of uncertainty when predicting the fate of DU penetrators in the wide-ranging environments found in test-fire and war zones. Microcosm experiments have therefore been carried out to investigate the corrosion of DU penetrator materials in field-moist and progressively anoxic waterlogged soils, to

test the hypothesis that the rate of DU corrosion and the nature of corrosion products formed are dependent on the water content and local redox processes.

Experimental Section

Sampling and Characterization

A soil (silty-loam) from North Wyke Research Station, Devon (Lat: 50.777451°N Long: 3.920402°W GB; 26.01.05) was sampled (10−40 cm depth), sieved (2 mm), stored (15 °C), and used within 6 months. Drain channel water collected at the same site was stored (4 °C) and used within 1 week. The full characterization protocols for soil and water subsamples have been described previously (12).

Microcosm Experiments

Experiments were designed to investigate DU corrosion under realistic subsurface soil environments. The variations in water and O_2 content generated three distinct subsurface environments, denoted as “field-moist”, “open waterlogged”, and “closed waterlogged”. DU from a penetrator (Dstl, Porton Down, UK) was cut into triangular “coupons” (triangular face of ca. 1.5 × 1.5 × 1.0 cm, thickness 0.5 cm; mass 5−10 g) by AWE (Aldermaston, UK). DU coupons were cleaned to remove cutting oil and surface contaminants (12). Microcosms consisting of 50 mL glass serum bottles and 15 g of soil were prepared on the same day. Waterlogged and field-moist conditions were simulated by adding 15 and 1 mL of drainage water, respectively. For the open systems (open waterlogged and field-moist), 15 microcosms containing a DU coupon were prepared, together with an equivalent number of controls without DU. A nylon mesh was tied around the neck of the open bottles to allow gas exchange. The microcosms were weighed monthly and water loss was compensated for by adding high purity water (MQ water, $\geq$18.2 MΩ cm^{-1}). For the closed waterlogged system, 30 microcosms containing a DU coupon were prepared, together with an equivalent number of controls. The microcosms were sealed with butyl stoppers and aluminum seals. A syringe needle was inserted through the stopper to prevent pressure build-up (none observed). All microcosms were incubated in the dark at 10 °C.

At each time-point of interest over 510 days, microcosms were opened for analysis (“sacrificed”) and characterized in triplicate, along with three controls. To preserve redox conditions, sacrifices and further manipulations were carried out within an anaerobic chamber (95% N_2, 5% H_2). The closed systems were swirled for 15 min (200 rpm) to homogenize the sample and then sacrificed. For the open systems, the microcosms were weighed and adjusted to contain 15 mL of water by addition of deoxygenated MQ water,

sealed, homogenized, and sacrificed. The addition of deoxygenated MQ water to the field-moist microcosms allowed the extraction of diluted pore-water. The entire contents of the microcosms were then filtered successively through nylon mesh (65 μm) and a disposable syringe filter (0.45 μm, mixed cellulose ester), and collected in polypropylene vials. The DU coupons, solution, and sediment were then prepared for further analysis as described below. All errors stated are one standard deviation of three replicate microcosms.

DU Coupon Analysis

The DU coupons were rinsed with MQ water to remove soil, air-dried, and stored in a desiccator (<1 month). For a visual record, coupons were photographed under a light microscope fitted with a digital camera. The corrosion products were removed as described previously (12) and reweighed to determine mass loss (%).

Geochemical Methods and Modeling

Apart from the adaptations stated here, all geochemical methods (pH, Eh, O_2 determination, redox indicator analysis; determination of colloidal and dissolved U in water) and modeling have been previously described (12). Acid-extractable Fe(II) was extracted from soils with 0.5 M HCl for 30 min (13) and determined spectrophotometrically (562 nm) using the ferrozine method (14). Accurately weighed subsamples of dried soil from the waterlogged microcosms on day 510 were refluxed with concentrated nitric acid for 8 h and analyzed for total U by inductively coupled plasma optical emission spectrometry (0.1 mg L^{-1} detection limit).

DU Distribution and Particle Analysis

Soil from day 337 of each series of microcosms was screened using phosphor imaging analysis. Representative dried soil (1 g) was thinly spread onto a grid plate and a phosphor screen was placed directly above it for 8 h. The image was used to identify areas of enhanced radioactivity, which were isolated and analyzed by environmental scanning electron microscopy energy-dispersive X-ray (ESEM-EDAX). The field-moist soil contained sufficient quantities of crystalline U mineral particles for analysis by X-ray diffraction (XRD).

Microbiological Methods

Field-moist and closed waterlogged samples and their controls were selected for microbial analysis to identify changes in the microbial community as a result of long-term (435 days) DU contamination. Ribosomal intergenic spacer analysis (RISA) was used to indentify

microbial community change. Further investigation by DNA sequencing of 16S rRNA gene clone libraries and phylogenetic analysis was also carried out. The methods used in this study have been described in detail previously (12).

Results and Discussion

Soil and Water Characterization

The soil had a moisture content of 22% (m/m), a particle size distribution of 54% sand, 41% silt, and 5% clay, organic carbon by mass of 12.0 ± 0.1%, CEC of 21.2 ± 0.4 meq/100 g, and an initial inorganic carbon content of 80 ± 1 mg kg^{-1}. Iron oxides comprised 6.0% (m/m) of the soil. The pH of the water prior to mixing with soil was 7.4, inorganic carbon content was 73 ± 2 mg L^{-1}, and anion concentrations (mg L^{-1}) were chloride 130 ± 2, nitrate 120 ± 2, and sulfate 10 ± 1.

Impact of DU on Redox Processes in Field-Moist Soil

In the field-moist microcosms pH (5.2−5.8) and Eh (500−600 mV) stayed constant over the 510 day experimental period. Changes in redox indicator (NO_3^-, Fe(II), SO_4^{2-}) concentrations over time are shown in Figure 1. In the control microcosms, redox indicators were not reduced over the experimental period, suggesting oxic conditions were maintained. This is consistent with the visible, air-filled macro-pores in the soil structure. However, in the DU-amended experiments, depletion of NO_3^- was observed from day 242 (510 ± 70 mg L^{-1}) to day 510 (17 ± 5 mg L^{-1}), with concurrent in-growth of Fe(II) into soils. Sulfate in the DU-amended and control microcosms remained fairly constant throughout the experiment, indicating that SO_4^{2-} reduction did not occur. This suggests that the presence of DU directly impacts soil redox processes, leading to reduction of TEAs.

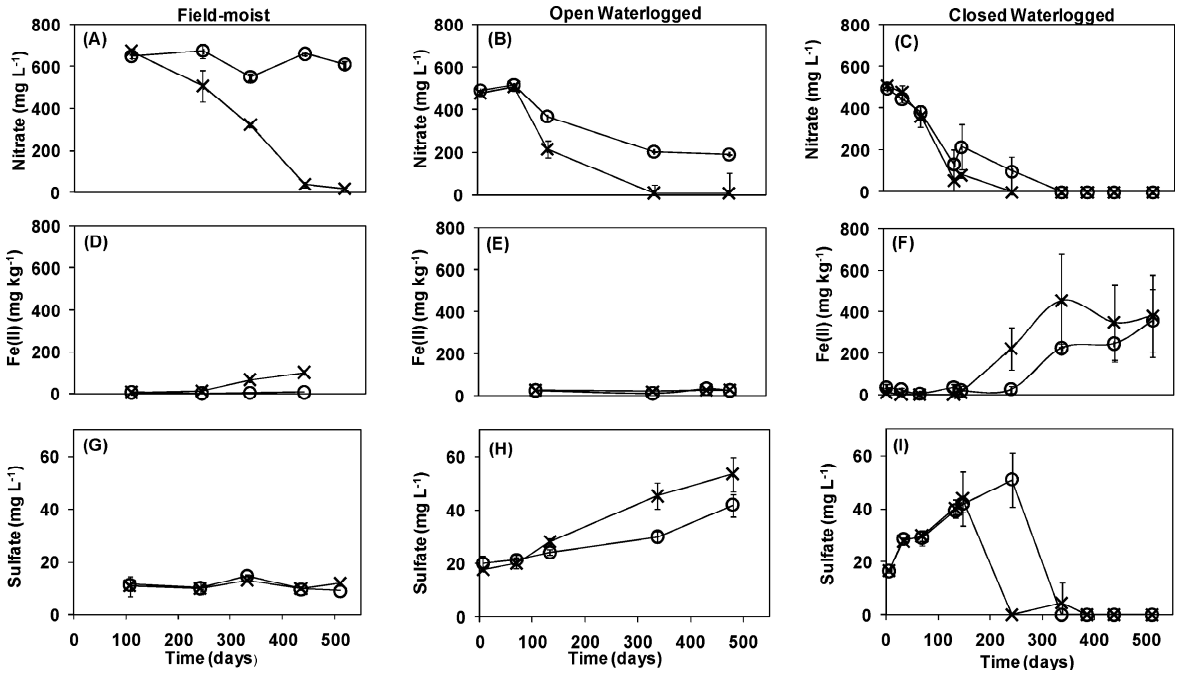

Figure 1. DU-amended (×) and control (o) redox indicator time series data for the subsurface field-moist (A,D,G), open waterlogged (B,E,H), and closed waterlogged (C,F,I) microcosms. Nitrate (A−C), acid extractable Fe(II) (D−F), and sulfate (G−I) concentrations are shown over time. Error bars ± 1 s.d. (n = 3).

Impact of DU on Redox Processes in Waterlogged Soil

Suboxic conditions developed in the open waterlogged microcosms and controls over time due to low diffusion rates of oxygen through waterlogged soil (10). Dissolved oxygen decreased from 84% initially to 35% by day 133. Eh decreased slightly from 610 to 570 mV and pH slightly increased over the duration of the experiment, from pH 5.0 to 5.2 in the controls, and from pH 4.9 to 5.5 in the DU-amended experiments. Nitrate reduction, indicated by the decrease in NO_3^- concentration, was observed in both the DU-amended experiments and controls after 69 days (Figure 1) although NO_3^- was more depleted in the DU-amended microcosms. Iron(III) reduction was not observed and SO_4^{2-} concentrations increased in both systems.

The closed waterlogged microcosms and controls became progressively anoxic, with Eh decreasing from 610 to −170 mV by day 510. Dissolved oxygen was depleted from 85% initially to 5% by day 34, and pH increased over the 510 days from 4.9 to 6.5. Differences in redox indicator concentrations were observed over time between control and DU-amended microcosms. Onset of NO_3^- reduction was observed on day 34, and was complete by day 242 and 337 in the DU-amended microcosms and controls, respectively. In-growth of Fe(II) into soils was observed by days 242 and 337 for the DU-amended microcosms and controls, respectively. Sulfate initially increased in both the DU-amended and control

microcosms. After this initial increase, SO_4^{2-} reduction was observed concurrently with Fe(III) reduction in the DU-amended and control microcosms between days 242 and 337, respectively. Thus, in both the waterlogged systems, the presence of DU increased the rate of progression through the redox cascade. An increased rate has also been observed in DU-amended estuarine sediment microcosms (12).

Corrosion of DU under Field-Moist Conditions

Representative DU coupons from the field-moist microcosms are shown in Figure 2 after 242 and 337 days incubation. DU coupons had visually corroded by day 242, via localized pitting and cracking of the metal surface and by day 337 the coupons were covered with protruding, predominately yellow corrosion products. Corrosion of DU, as indicated by % mass loss (Figure 3A), was not significant until day 242 (0.75 ± 0.20%; p = 0.0012), indicating a latent period prior to the onset of corrosion. After day 242, corrosion progressed linearly (r^2 = 0.99) with a mass loss of 21% by day 510. The latent period could reflect the presence of a protective oxide layer. For pure U, this protective oxide layer will thicken and eventually crack at 75 nm, accelerating corrosion (11). Depletion of NO_3^- and in-growth of Fe(II) occurred with the onset of DU corrosion. Corroding U is a strong reducing agent and generates H_2 (11), thus these redox indicators may be reduced biotically, through stimulation of H_2-reducing species, or abiotically (12). These induced changes in the redox processes did not influence the DU corrosion rate, which progressed linearly (R^2 = 0.99).

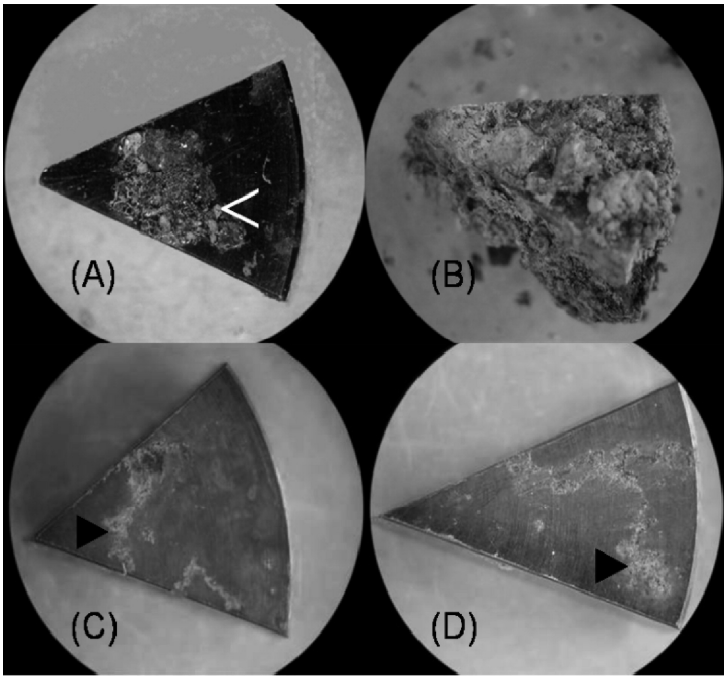

Figure 2. Black and white photographs showing DU coupons retrieved from the field-moist microcosm (A) after 242 days with a highlighted area (<) of pitting corrosion and a heavily corroded coupon (B) retrieved after 337 days. Also shown are DU coupons retrieved from the closed (C) and open waterlogged (D) microcosms after 337 days with highlighted areas (filled arrows) of pitting corrosion.

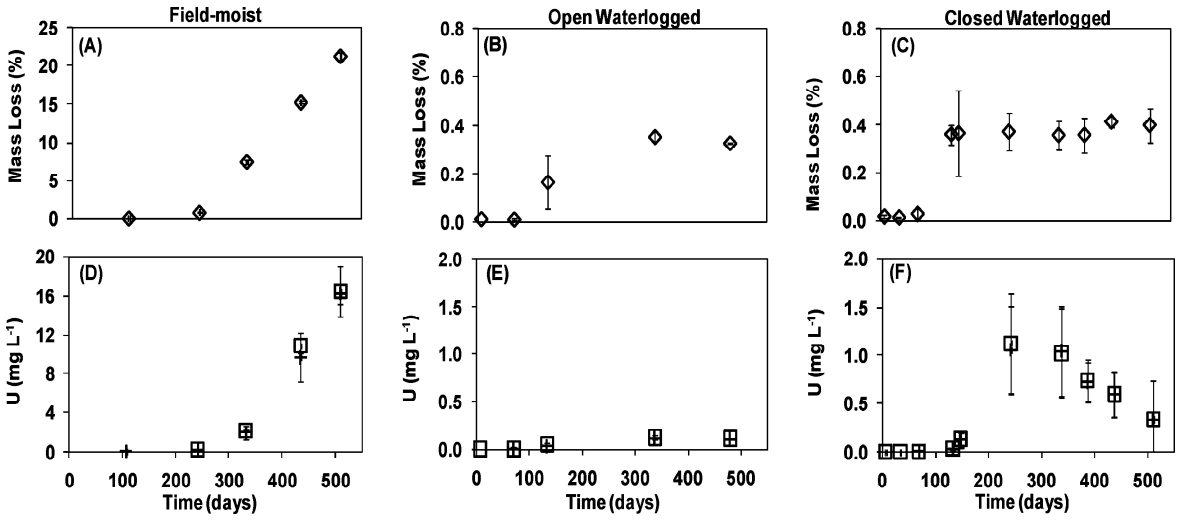

Figure 3. Time series for DU corrosion in the field-moist (A,D), open waterlogged (B,E), and closed waterlogged (C,F) microcosms. A−C show mass loss (%) of DU metal from the DU coupon (◊) and D−F show changes in uranium concentration in the <0.45 μm (+) and <10 kDa (□) fractions. Error bars ± 1 s.d. (*n* = 3).

Corrosion of DU under Progressively Reducing Waterlogged Conditions

Representative DU coupons retrieved from the open and closed waterlogged microcosms on day 337 both showed shallow pitting (Figure 2). DU corrosion, indicated by % mass loss (Figure 3), was not significant for the open (p = 0.59) and closed (p = 0.43) waterlogged microcosms until days 133 and 69, respectively, which corresponded with NO_3^--reducing conditions. Once NO_3^- reduction was complete (by days 337 and 242 for the open and closed waterlogged systems, respectively), % mass loss was similar (p = 0.84) at 0.36 ± 0.02% and 0.37 ± 0.08%, respectively. Concomitant DU corrosion and NO_3^- depletion suggests the two processes are related. In fact, NO_3^- reduction intermediates are reported to oxidize UO_2 to more mobile U(VI) species (15). For the remaining experimental period, no significant corrosion was observed in the open (p = 0.10) and closed (p = 0.99) waterlogged microcosms. Therefore, corrosion in the waterlogged systems occurred during NO_3^- reduction and ceased during Fe(III) and SO_4^{2-} reduction. Similar redox controls on DU corrosion have been observed in estuarine sediments, with corrosion ceasing during SO_4^{2-}-reducing conditions (12). In both studies the Eh/pH conditions were consistent with uraninite (UO_2) formation and subsequent passivation of the metal surface (16). This demonstrates that soil/sediment and water character do not appear to influence DU corrosion under anoxic conditions.

Rate of DU Corrosion as a Function of Redox Environment

The corrosion rates (g cm^{-2} y^{-1}) were calculated as described previously (12), but excluding the latent periods to increase accuracy and comparability. The time periods of corrosion used for calculations were: field-moist, days 242−510; open waterlogged, days 69−337; closed waterlogged, days 33−133. Experimental uncertainties on replicate microcosms for both time points were used to estimate total uncertainties. When calculating coupon surface area, the slightly curved side of the coupon was assumed to be straight, introducing a ± 2% uncertainty.

Corrosion was fastest in the field-moist microcosms (0.49 ± 0.06 g cm^{-2} y^{-1}), intermediate between reported rates in soils exposed to 16 mm $week^{-1}$ of simulated rainwater (0.19 ± 0.03 g cm^{-2} y^{-1}) (9) and the in situ rate at Kirkcudbright, UK (0.8−1.1 g cm^{-2} y^{-1}) (8). Corrosion rates in the open and closed waterlogged systems were 0.0092 ± 0.0005 and 0.020 ± 0.005 g cm^{-2} y^{-1}, respectively. This corrosion occurred only under NO_3^--reducing conditions and was at least an order of magnitude slower than that in field-moist soils. Corrosion rates in the waterlogged soils were also lower than observed in waterlogged marine sediments (0.056 ± 0.006 g cm^{-2} y^{-1}) (12) under suboxic conditions, highlighting the importance of chloride concentrations in DU corrosion (17, 18).

Total corrosion time for a 120 mm “Charm 3” penetrator was estimated using corrosion rate (g cm^{-2} y^{-1}), approximate mass (4500 g), and mean surface area during corrosion (i.e., 150 cm^2) (12). Under field-moist soil conditions, the total corrosion time would be 55−69 years. Under waterlogged soils, with NO_3^--reducing conditions, total corrosion times in open and closed systems would be 3100−3400 and 1200−1900 years, respectively.

Corrosion Products and their Solubility

DU coupons from the field-moist microcosms had loosely bound corrosion products. Phosphor imaging of the surrounding soil indicated a heterogeneous distribution of U with scattered intense radioactive hotspots (Figure S1, supporting information). These correlated with bright yellow corrosion products that were partially covered in soil. XRD analysis suggested the presence of metaschoepite or a similar phase, as previously reported (7). A representative ESEM image and EDAX spectrum of the selected particles are shown in Figure 4A-B. The image shows desiccation cracks, indicative of a partially dehydrated metaschoepite phase (7). The spectrum shows major U and O peaks and minor peaks from common matrix elements (Si, Fe, Mg, Al). In field-moist microcosms, dissolved U concentration correlated linearly with % mass loss (r^2 = 0.96) (Figure 3). By day 510, only 0.03% (16 ± 1 mg L^{-1}) of the corroded U was in solution, following a 15 min water extraction, which reinforces the dominance and low solubility of the particulate corrosion products observed. Colloidal U oxides were not important in this system, since the U concentrations in the <0.45 μm and <10 kDa fractions were not significantly different (p = 0.10). However, large particulate DU-oxides were observed and these would be naturally weathered in the environment.

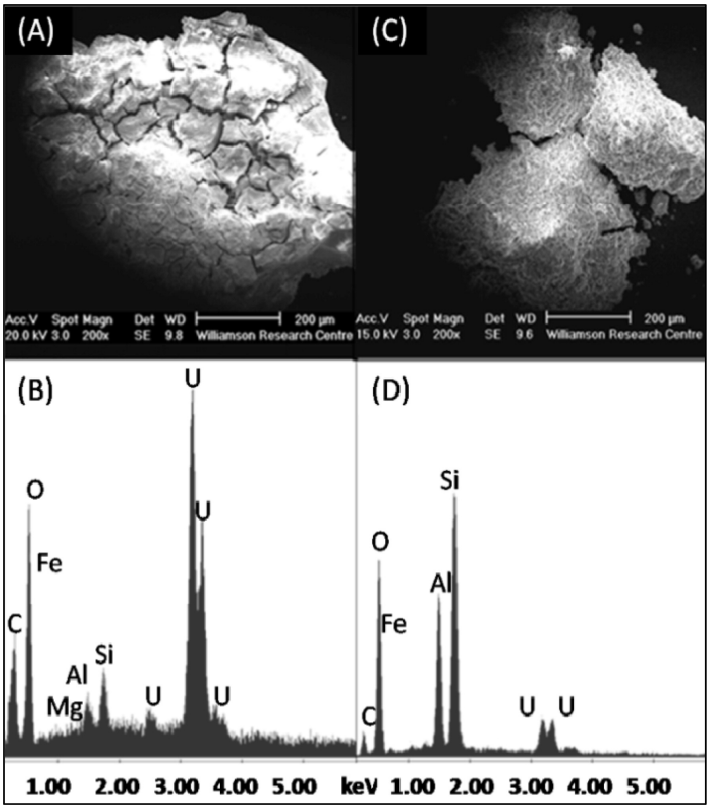

Figure 4. ESEM images (A,C) and EDAX spectra (B,D) of a corroded DU particle retrieved from field-moist microcosm (A,B) and a soil particle from a closed waterlogged microcosm (C,D).

DU coupons retrieved from the waterlogged soils had shallow pitting corrosion with no visible surface bound corrosion products. Phosphor imaging of the waterlogged systems indicated a dispersed, homogeneous distribution of U. A representative ESEM image and EDAX spectrum of selected soil particles are shown in Figure 4C,D. The spectrum shows minor U peaks and signals from Si, Fe, and Al. These results indicate that DU is present in the soil as sorbed species, rather than discrete corrosion products. Uranium concentrations in the <0.45 µm and <10 kDa fractions were not significantly different in the open (p = 0.13) and closed waterlogged (p = 0.11) microcosms, indicating that colloidal U oxides were not important (Figure 3). By day 337, 0.36% and 0.37% of the DU had corroded in the open and closed waterlogged microcosms, respectively. This corresponded with a dissolved U concentration in the open waterlogged system of 0.12 ± 0.01 mg L^{-1} (<0.01% of the corroded DU), with pH 5.7, Eh 600 mV, and NO_3^--reducing conditions. In the closed waterlogged systems, the dissolved U concentration was 1.02 ± 0.47 mg L^{-1} (<0.1% of the corroded DU), with pH 6.4, Eh −65 mV, and Fe(III)- and SO_4^{2-}-reducing conditions. Using the initial inorganic carbon concentrations, the geochemical model Hydra/Medusa (Puigdomenech, Royal Institute of Technology, Stockholm) suggests U will predominantly be in low solubility forms in both systems. In the open system, low solubility UO_2CO_3

would dominate, with some soluble species such as $UO_2(CO_3)_2^{2-}$ present. In contrast, reduced UO_2 species would dominate in the closed system, with minor amounts of soluble species such as $UO_2(CO_3)_2^{2-}$. Uranium soil extraction and water analyses show that by day 510, all corroded DU was associated with the soil (100 ± 4%) rather than the DU coupon and <0.1% U was in the solution phase. This provides further evidence that under waterlogged conditions, corrosion occurs by oxidation of DU metal to dissolved uranyl species, with subsequent dispersion into the environment. This corrosion mechanism has been proposed previously for DU in marine sediments (12), suggesting that water status is a major controlling factor.

Microbial Community Profile

The microbial community analysis using RISA of the field-moist and closed waterlogged soils on day 435 indicated DU had impacted the microbial community (Supporting Information (SI), Figure 1). Detailed phylogenetic analysis was conducted by PCR amplification, cloning and sequencing of fragments (approximately 1 kb) of the 16S rRNA genes within the bacterial community (SI Tables 1−4). The phylogenetic results obtained from DNA profiling are shown in Figure 5.

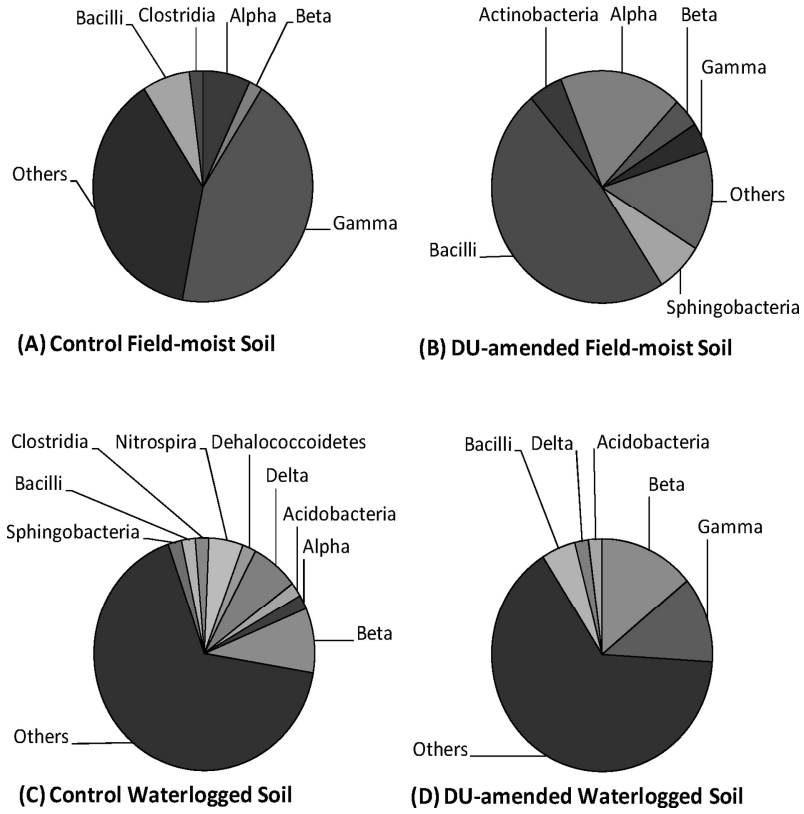

Figure 5. Phylogenetic affiliations of clones in field-moist (A,B) and the closed waterlogged (C,D) soils on day 435. Alpha, Beta, Delta, and Gamma represent proteobacterial divisions.

In the control field-moist soil, the clone library (55 clones analyzed, 15 RFLP types) was made up of a large number of novel, uncharacterized microorganisms, dominated by species of the Gammaproteobacteria genus *Rhodanobacter* (representing 38% and 44% of the 16S rRNA genes detected in the clone library, respectively). However, in the clone library from the field-moist DU-amended microcosm (55 clones analyzed, 20 RFLP types) the Gammaproteobacterial group was greatly reduced (consisting of 4% of the clones affiliated to *Rhodanobacter* species) while Gram-positive Bacilli, many of which can denitrify, dominated the clone library (48% of clones). The Bacilli phylogenetic class thrive in soil exposed to U_3O_8 (19) and at heavily contaminated U sites (20, 21). DU oxides (U_3O_8) have previously been shown to alter microbial community structures and reduce diversity (19), although reduced diversity was not shown in this system. The dominant organism detected in the DU impacted microbial community was closely related to *Sporosarcina Soli strain I80* (98% match over 925 bases), characterized as Bacilli phylogenetic class, aerobic, and NO_3^--reducing microorganisms.

In both the control and DU-amended waterlogged soils (Figure 5) the clone libraries were again dominated by a large number of novel uncharacterized microorganisms. In the DU-amended microcosm a loss in microbial diversity was suggested (24 compared to 31 RFLP types from 57 clones analyzed from each soil); with the phylogenetic classes Alphaproteobacteria, Clostridia, Dehalococcoidete, Nitrospiro, and Sphingobacteria not detected in the presence of DU. They were replaced by other organisms, including Gammaproteobacteria (12% of clone library), comprising mostly an organism related to *Aquicella siphonis,* previously isolated from water samples in central Portugal (22).

The different end-members identified in both the field-moist and waterlogged soils may arise from adaptation to the chemical environment associated with the DU, resistance to toxic soluble uranium and/or particulate corrosion products, or even direct use of the DU itself as an electron donor (23). In the system studied here the presence of metaschoepite corrosion product caused a marked shift in the microbial community composition, whereas the presence of dissolved U caused a marked decrease in microbial community diversity. A similar effect was reported in a waterlogged marine sediment system containing dissolved U (12).

DU Corrosion as a Function of Soil Conditions

This study shows that mechanisms of DU corrosion and the products formed in subsurface soils are controlled by redox processes and soil water content. In field-moist soil, the metaschoepite corrosion product observed is in agreement with other laboratory and in situ

studies (6-9). Under these conditions, DU corrodes at the fastest rate of 0.49 ± 0.06 g cm^{-2} y^{-1}, again broadly in agreement with literature data (8, 9), and is linear over time.

In waterlogged soils the mechanism of U release is the same as in waterlogged marine sediments (12), showing that water status and redox processes control UO_2 oxidation from the penetrator surface to mobile U(VI) species, and passivation of the metal surface as conditions become anoxic. DU corrosion has only been observed under NO_3^--reducing conditions in waterlogged soil and the corrosion rate correlated with the rate of NO_3^- reduction. Comparison of these rates (0.01−0.02 g cm^{-2} y^{-1}) with those in marine sediment (0.056 ± 0.006 g cm^{-2} y^{-1}) (12) highlights that the corrosion mechanism is controlled by water status and redox processes but the corrosion rate is influenced by the chloride concentration.

DU corrosion increased the rate of TEA utilization under all conditions investigated in this study and in a marine sediment (12). However, corroding DU impacts the microbial community in different ways under field-moist and waterlogged conditions, presumably due to the different corrosion products formed. The formation of predominantly metaschoepite corrosion products results in a shift in community structure, while the formation of predominantly soluble/ionic U species decreases diversity.

Acknowledgment

This research was funded by the Natural Environment Research Council (grant NE/C506799/1). We thank Dstl for supplying the DU penetrator, AWE for cutting this material, and North Wyke Research for soil and water samples.

References

1. Bleise, A.; Danesi, P. R.; Burkart, W. Properties, use and health effects of depleted uranium (DU): a general overview J. Environ. Radioact. 2003, 64, 93– 112

2. Mellini, M.; Riccobono, F. Chemical and mineralogical transformations caused by weathering in anti-tank DU penetrators (“the silver bullets”) discharged during the Kosovo war Chemosphere 2005, 60, 1246– 1252

3. Papastefanou, C. Depleted uranium in military conflicts and the impact on the environment Health. Phys. 2002, 83, 280– 282

4. UNEP. Depleted uranium in Kosovo, Post-conflict environmental assessment; United Nations Environment Programme: Geneva, 2001.

5. Mattsson, E. Basic Corrosion Technology for Scientists and Engineers; Ellis Horwood Limited: Chichester, 1989.

6. Johnson, W. H.; Buck, B. J.; Brogonia, H.; Brock, A. L. Variations in depleted uranium sorption and solubility with depth in arid soils Soil. Sediment Contam. 2004, 13, 533– 544

7. Buck, B. J.; Brock, A. L.; Johnson, W. H.; Ulery, A. L. Corrosion of depleted uranium in an arid environment: Soil-geomorphology, SEM/EDS, XRD, and electron microprobe analyses Soil. Sediment Contam. 2004, 13, 545– 561

8. Toque, C. C. L.; Baker, A. C. MOD DU program - The Corrosion of Depleted Uranium in the Kirkcudbright and Eskmeals Terrestrial Environments; Dstl report dstl/CR10978 V2.0; Alverstoke, 2006.

9. Schimmack, W.; Gerstmann, U.; Schultz, W.; Geipel, G. Long-term corrosion and leaching of depleted uranium (DU) in soil Radiat. Environ. Biophys. 2007, 46, 221– 227.

10. Smith, K. A. A model of the extent of anaerobic zones in aggregated soils, and its potential application to estimates of denitrification J. Soil. Sci. 1980, 31, 263– 277

11. Laue, C. A.; Gates-Anderson, D.; Fitch, T. E. Dissolution of metallic uranium and its alloys J. Radioanal. Nucl. Chem. 2004, 261, 709– 717

12. Handley-Sidhu, S.; Worsfold, P. J.; Boothman, C.; Lloyd, J. R.; Alvarez, R.; Livens, F.; Vaughan, D. J.; Keith-Roach, M. J. Corrosion and fate of depleted uranium penetrators under progressively anaerobic conditions in estuarine sediment Environ. Sci. Technol. 2009, 43, 350– 355

13. Lovley, D. R.; Phillips, E. J. P. Availability of ferric iron for microbial reduction in bottom sediments of the freshwater tidal Potomac River Appl. Environ. Microbiol. 1986, 52, 751– 757

14. Stookey, L. L. Ferrozine - a new spectrophotometric reagent for iron Anal. Chem. 1970, 42, 779– 781

15. Senko, J. M.; Istok, J. D.; Suflita, J. M.; Krumholz, L. R. In-situ evidence for uranium immobilization and remobilization Environ. Sci. Technol. 2002, 367, 1491– 1496

16. Pourbaix, M.Corrosion. In Atlas of Electrochemical Equilibria in Aqueous Solution; Pourbaix, M., Ed.; Pergamon Press: Oxford, 1966.

17. Trzaskoma, P. P. Corrosion rates and electrochemical studies of depleted uranium alloy tungsten fiber metal matrix composite J. Electrochem. Soc. 1982, 192, 1398– 1402

18. McIntyre, J. F.; Lefeave, E. P.; Musselman, K. A. Galvanic corrosion behaviour of depleted uranium in synthetic seawater coupled to aluminium, magnesium, and mild steel Corros. Sci. 1988, 44, 502– 510

19. Ringelberg, D.; Reynolds, C.; Karr, L. Microbial community composition near depleted uranium impact points Soil. Sediment Contam. 2004, 13, 563– 577

20. Pollmann, K.; Raff, J.; Merroun, M.; Fahmy, K.; Selenska-Pobell, S. Metal binding by bacteria from uranium mining waste piles and its technological applications Biotechnol. Adv. 2006, 24, 58– 68

21. Selenska-Pobell, S.; Panak, P.; Miteva, V.; Boudakov, I.; Bernhard, G.; Nitsche, H. Selective accumulation of heavy metals by three indigenous Bacillus strains, *B-*

cereus, *B-megaterium* and *B-sphaericus*, from drain waters of a uranium waste pile FEMS. Microbiol. Ecol. 1999, 29, 59– 67

22**.** Santos, P.; Pinhal, I.; Rainey, F.; Empadinhas, N.; Costa, J.; Fields, B.; Benson, R.; Ver¦ssimo, A.; da Costa, M. S. Gamma-proteobacteria *Aquicella lusitana* gen. nov., sp. nov., and *Aquicella siphonis* sp. nov. infect protozoa and require activated charcoal for growth in laboratory media Appl. Environ. Microbiol. 2003, 69, 6533–6540

23**.** Lovley, D. R.; Phillips, E. J. P.; Gorby, Y. A.; Landa, E. R. Microbial reduction of uranium Nature 1991, 350, 413– 41

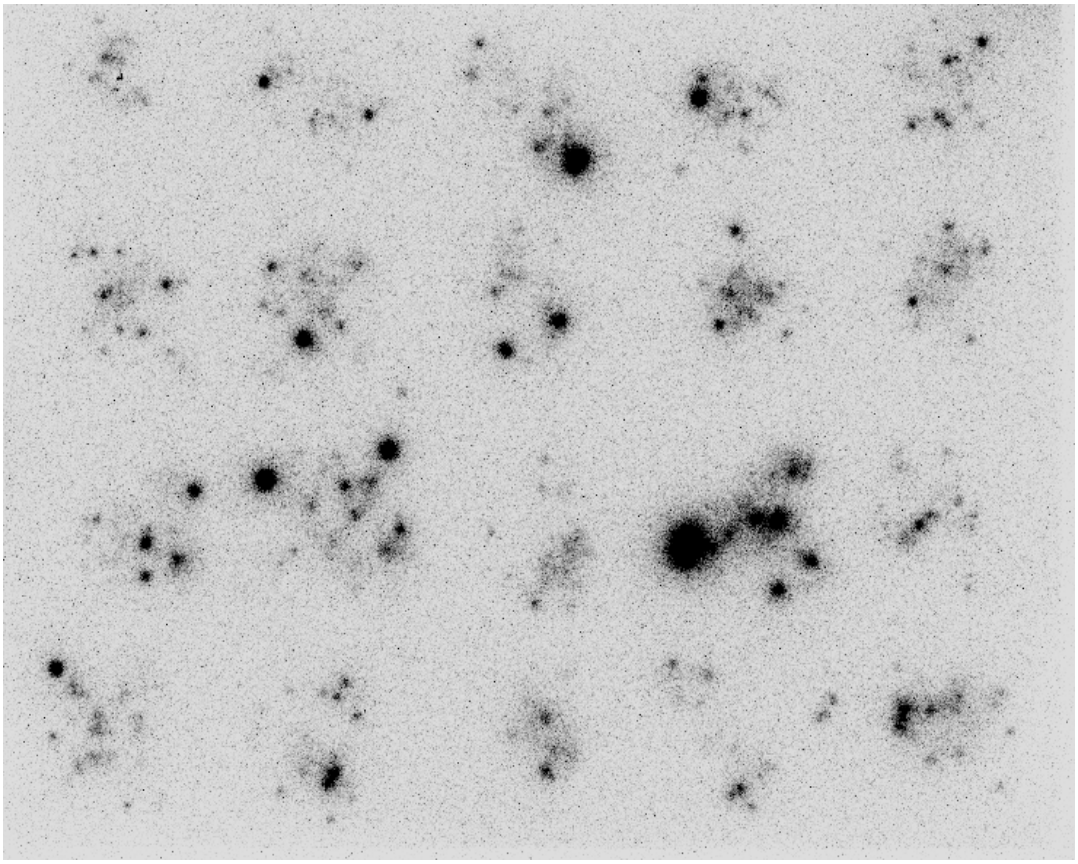

Figure S1. A representative phosphor image of field-moist soil showing the distribution of DU particles (black spots) in the sample.

RISA profiles and tables containing the clone library DNA sequencing results. This material is available free of charge via the Internet at http://pubs.acs.org.

Chapter 6

Summary, Conclusions and Suggestions for Future Work

Summary and Conclusions

The importance of radioactive particles as a source of radionuclides released into the environment has been known since the start of nuclear weapons tests, when micrometer particles were observed at the test sites. Since that time concern about the significance of environmental radioactive particles which can be released from different sources (e.g. nuclear accidents, nuclear fuel cycle, and the use of depleted uranium munitions) has increased. Characterisation of environmental radioactive particles helps in understanding their behaviour and fate in the environment as well as the environmental impact of these particles.

In this study, radioactive particles from two sources were identified and characterised using a wide range of microanalytical, analytical and radiometric techniques to obtain information on the particles.

Depleted uranium particles produced from testing of DU projectiles against hard targets and corrosion of unfired DU metal buried in soil, were characterised in terms of size and shape, surface elemental composition, elemental and isotopic compositions and crystalline structure of uranium forms. Three classes of particles were identified:

a) DU aerosols and fragments produced from firing impact. The particles are typically 1-20µm diameter, composed mainly of uranium.
b) Firing impact particles (fragments and molten particles), typically 200-500µm, composed of a mixture of uranium (as UO_2 and U_3O_8) and iron from target material. SIMS analysis showed that they were composed of U and Ti derived from the DU projectile, Fe, Cr, Mn and Ni derived from target materials and Al, K, Mg, Ca, Na, Si as background elements.
c) Sand grains up to 500µm, coated with corroding uranium in the form of metaschoepite. Microcosm experiments on corrosion of DU metal under field-moist conditions showed that corrosion rate is dependent on the water status and redox conditions, and the main input to the surrounding soil was metaschoepite particles. Precipitation of metaschoepite on surrounding sand grains is believed to be the mechanism limiting uranium mobility.

It was possible to identify and quantify DU contamination in particulate environmental samples by utilising the different isotopic signatures of natural and depleted uranium. The isotopic ratio $^{234}U/^{238}U$ was measured with higher precision using alpha spectrometry, whereas the isotopic ratio $^{235}U/^{238}U$ was measured with higher precision using ICP-MS.

The results demonstrated the diversity of particles which can be formed through the use of DU munitions and the potential for these to persist in the environment. The small size of firing impact particles (particles of a size that may be respired) found in this study and in post-conflict environments may favour resuspension of these particles after deposition. This is especially true in arid environments (e.g. Iraq and Kuwait), where soil erosion by wind will redisperse DU aerosols particles in the conflict area and may redistribute them. The presence of uranium in firing impact particles in the non-leachable oxidation state (IV) reflects the potential for these particles to survive in the environment for many years, whereas the presence of uranium in corrosion particles in the soluble oxidation state (VI) suggests the potential dissolution of uranium as mobile UO_2^{2+}.

Nuclear fuel particles released from Sellafield effluent discharges and retained in intertidal salt mash sediments, were isolated using autoradiography and heavy liquid density separation and characterised in terms of morphology, surface elemental composition, radionuclide composition and isotopic composition of uranium and plutonium. The particles were typically 1-20 µm size, composed mainly of uranium, although alpha spectrometry showed that the particles have been irradiated, and transuranium radionuclides (Pu, Am and Cm) can be identified in them. The isotopic composition of Pu, represented by the activity ratio $^{238}Pu/^{239+240}Pu$, was consistent with that from Sellafield discharges and the isotopic composition of U, represented by the atom ratio $^{235}U/^{238}U$ showed that uranium was depleted, suggesting that U was derived from the reprocessing of spent fuel at Sellafield.

The results demonstrated conclusively the persistence for some decades of irradiated nuclear fuel particles in the marine and estuarine environments, which suggests that uranium is present in the low solubility oxidation state IV. This is consistent with studies of DU firing impact particles which were found to survive in the environment for many years, and with the observation of Handley et al (2009) that DU weathering ceases under anaerobic conditions.

The work in this thesis demonstrated that a variety of analytical techniques can be successfully applied to the study of environmental radioactive particles. Autoradiography and density separation were useful to find and isolate individual particles in soil samples. SEM-EDX provided information on size, morphology and surface composition of particles, while XRD was used to assist in determining the crystal structure of uranium phases. ICP-AES quantified stable elements, SIMS revealed the internal chemistry and ICP-MS and alpha spectrometry assessed DU contamination in particulate environmental samples.

The information obtained on radioactive particles in this thesis made it possible to assess the origin, fate, and environmental behaviour and impact of actinide-containing particles in the environment.

Suggestions for future work

In order to gain better understanding of the environmental behaviour of radioactive particles, more information on their physicochemical characteristics should be obtained. Other analytical techniques, such as transmission electron microscopy (TEM), could provide information on particle phases and homogeneity, structural composition and oxidation states of uranium. An attempt was made to analyse nuclear fuel particles using TEM, but the difficulty in separating these tiny particles (1-20 µm) from the clay sediment and the scarce of particles in the sample, led to the situation where the particle is being lost or placed on the TEM grid in a way (embedded in matrix) which was not suitable for analysis. A similar problem was faced when analysing the particles with SIMS, where the particle was not exposed enough for analysis as it was embedded in the resin. Ultrasonic dispersion to break up the matrix, could help in further attempts to isolate individual particles. The first class of DU particles (1-20 µm) could be analysed by TEM, as they are easy to separate from sand and more abundant.

In this study, nuclear fuel particles from the middle section of sediment core sample (reflects 1970s discharges) were investigated. It would be interesting to characterise particles from the bottom and top sections, which reflect discharges before and after the 1970s.

The information obtained on DU particles in this study can be used to inform assessments of battlefield environments. It would be interesting to analyze DU samples from post-conflict environments (e.g. the Gulf War area) using the same characterization techniques applied in this study and compare the results with that from Eskmeals firing test range.

It would be useful to investigate radioactive particles from other sources (e.g. Chernobyl) to assess the environmental behaviour of radioactive particles from different nuclear sources.

Appendix

Experimental Techniques

A) Particle separation

Environmental radioactive particles are generally embedded in a bulk matrix, therefore, it is necessary to isolate them and perform specific single grain analysis. Ionising radiation emitted by radioactive particles can be detected by radiation-sensitive sensors, so they can be localized in the soil samples as "hot spots" using direct imaging techniques. Actinide-containing particles are dense particles; therefore they can be separated from soil matrix by density separation.

1. Autoradiography

Autoradiography provides a map of the distribution of radioactive particles in a sample. The map of the radioactivity emitted by a sample is obtained by placing a sample in contact with a storage phosphor screen that is sensitive to various forms of radiation (mainly beta and gamma), alpha radiation can be differentiated from other radiations as a function of phosphor screen thickness (Cheng et al., 1996). After exposing the screen over a sufficient length of time (the longer exposure the time, the better the image resolution), the screen can then be read by scanning with laser light. The resulting image can be used to map out the distribution of radioactive particles and then locate them quite precisely based on the obtained image.

Storage phosphor screens are typically coated with a lanthanide complex, such as BaFBr:Eu^{2+}. Incident radiation excites an electron from the Eu^{2+} ion's valence band into the conduction band. This effectively frees the electron from the original ion and transfers it to the BaFBr complex, causing an oxidation of Eu^{2+} to Eu^{3+}. The excited BaFBr complex absorbs strongly at ~600nm, and irradiation with laser light (λ = 633 nm) returns the electron to the Eu^{3+} ion, causing reduction back to an excited state of Eu^{2+}*. This decays to ground state Eu^{2+} by releasing a photon of wavelength 390 nm (in the near UV part of the spectrum). The photostimulable luminescence (PSL) is measured and stored digitally in relation to the position of a scanning laser beam. Once the whole plate has been scanned, the distribution of radioactive particles is displayed on screen as an image (Johnston et al., 1990). This technique can also be used to estimate the particle activity which is proportional to PSL signal and exposure time (Koarashi et al., 2007).

An example of an autoradiograph of a soil sample containing radioactive particles is shown below (Figure 1).

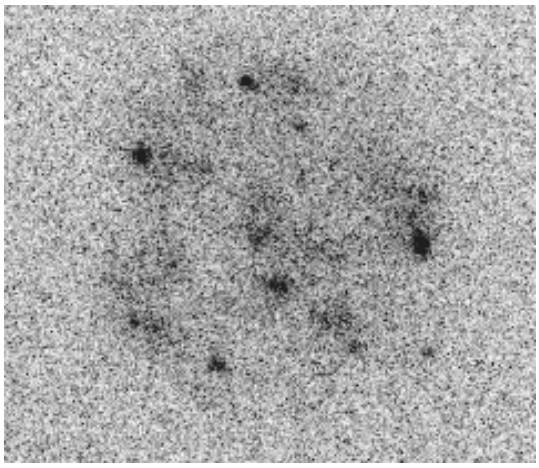

Figure 1. Autoradiograph of a sample showing hot spots. Black spots represent depleted radioactive particles particles.

2. Heavy liquid density separation

Heavy liquids are dense fluids or solutions used to separate materials of different density through their buoyancy. In the mineral industry, heavy liquids are commonly used in the laboratory to separate the light minerals such as quartz and clay from the heavy minerals. Because heavy minerals have a high density (~ 5-10 g/cm^3) higher than that of bulk soil (~ 2.5 g/cm^3), separation in a heavy liquid provides a suitable method of preconcentration. The heavy liquid density used for this type of separation is about 2.85 g/ml.

All organic heavy liquids have problems with toxicity; and have therefore been substituted with low-toxic tungsten based heavy liquids such as LST fast float lithium hetropolytungstate, density 2.83 g/cm^3, which was used in this study to separate uranium oxide particles from soil.

Uranium oxide particles with a density of about 10 g/cm^3 are much denser than soil matrix, therefore they can be separated using LST. The separation of these particles from soil presents problems due to their fine particle size and adhesive nature of clay soil which causes flocculation.

Approximately 1g of dry clay sediment was hand ground using a pestle and mortar to a powder of < 200 µm. The material is transferred into a separating funnel and the heavy liquid is added. The funnel is then shaken to disperse the particles and left to permit light particles to float and heavy particles to sink (Figure 2). The heavier particles are transferred

into a 10 ml vial, then washed with deionized water, filtered and left to dry for further analysis.

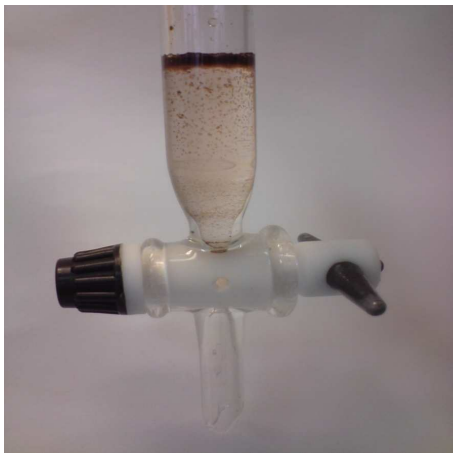

Figure 2. Heavy liquid density separation with heavy particles in the bottom and soil matrix floating on top.

The small size of the desired particles and the adhesive nature of the clay soil make density separation difficult.

B) Electron microscopy and X-ray analysis

When the environmental impact of radioactive particles is assessed, information is needed on particle size distribution, morphology and crystal structure, and oxidation states of uranium which influence particle weathering and subsequent mobility and solubility of uranium, when in contact with soil-water system (Salbu et al., 1998). Electron microscopy is used to obtain information on particle size, morphology and elemental composition, and X-ray diffraction to determine the crystal structure.

1. Scanning electron microscopy equipped with energy dispersive X-ray analysis (SEM-EDX)

Electron microscopy is a technique that is used to gain information about the physical nature and chemical composition of the surface of solid materials. A variety of signals is produced when an electron beam interacts with a solid sample (Figure 3). Three signals are measured in SEM, providing different information about the sample.

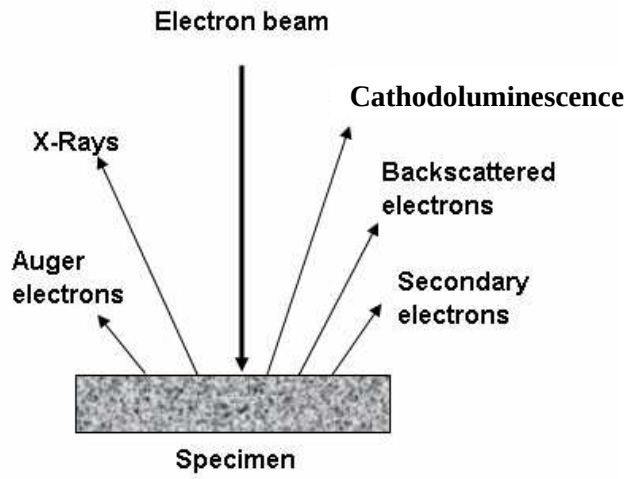

Figure 3. The different signals produced by interaction of electron beam with solid sample.

1) Secondary electrons (SE): low energy electrons (~ 50 eV) generated by inelastic collisions of primary electron with atoms within the sample. They provide information on the morphology and surface topography of the sample.
2) Backscattered electrons (BSE): high energy electrons from the electron beam, deflected as a result of Coulombic interaction with the nucleus. The production of backscattered electrons is dependant on atomic number of elements in the sample. High atomic number elements (strong scatterers) appear as bright areas in BSE images.
3) X-Ray emission: characteristic X-ray is specific for an element in the sample and X-ray spectrum provides compositional information of the sample.

A scanning electron microscope (FEI XL30 ESEM) equipped with energy dispersive X-ray analysis (SEM-EDX), was used to obtain information on size, morphology and composition of particles. The samples were prepared by fixing the particles (dense particles separated by heavy liquid or soil particles which had been shown by autoradiography to contain radioactive particles) on sticky carbon pads stuck on aluminium stubs (12 mm dia) suitable for SEM analysis. SEM was used in backscattered mode to search for high atomic number elements (uranium) as bright spots. When a uranium particle is identified, the BSE and SE images are collected and the qualitative elemental composition is determined by acquiring EDX spectra of spots or areas on particle surface. Detection limits for EDX analysis are variable but typically 0.2 -0.5%.

2. X-ray diffraction (XRD)

XRD is a technique that can be used to reveal the atomic structure of a crystalline solid. When a crystal is bombarded with X-rays of a fixed wavelength (similar to the spacing between crystal lattice planes) and at certain incident angles, intense reflected X-rays are produced when the wavelengths of the scattered X-rays interfere constructively. In order for the waves to interfere constructively, the differences in the travel path must be equal to integer multiples of the wavelength. When this constructive interference occurs, a diffracted beam of X-rays will leave the crystal at an angle equal to that of the incident beam. The process is described by Bragg's Law: $n\lambda = 2d\sin\theta$

Where n (an integer) is the order of diffraction, λ is the wavelength of the incident X-rays, d is the spacing of the crystal and θ is the angle of incidence. Figure 4 illustrates the parameters in the Bragg's law equation.

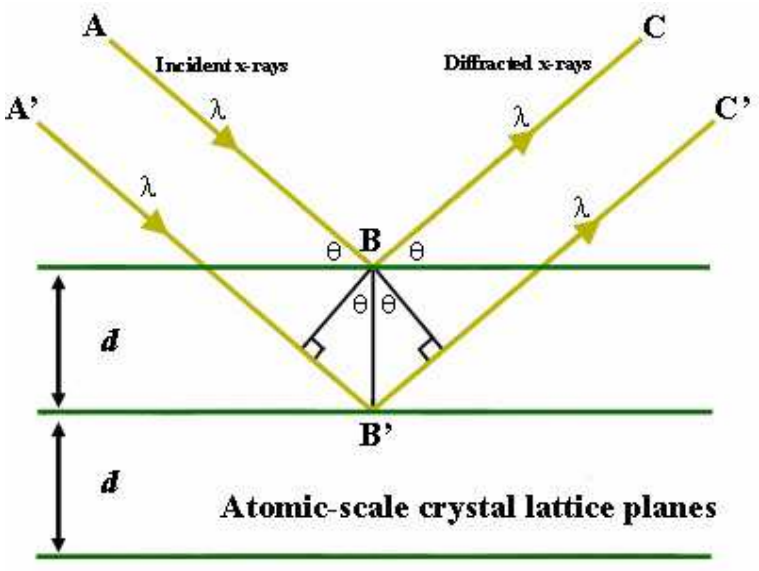

Figure 4. Bragg's Law diffraction. The arrows are the incident and diffracted X-rays, the horizontal lines are lattice planes, d is the lattice spacing and θ is the diffraction angle.

An X-ray diffractometer (Xcalibur-2 with Sapphire-3 CCD detector, MoKα radiation λ = 0.071 nm, beam size approximately 300 µm) was used to identify the crystal structure of uranium phases in the particles. Powder diffraction patterns were collected from single particles by mounting the particle on the tip of a thin glass fibre and X-rays are directed onto all sample orientations (0^o, 90^o, 180^o, 270^o). The diffracted X-rays are collected by the CCD detector (at 2θ from 0^o to 35^o) to produce a diffraction pattern which is then matched with a reference pattern.

C) Atomic and mass spectrometric techniques

The capability of determining elemental and isotopic composition of materials at the trace and ultra trace level is the main feature of atomic and mass spectrometry. The measurement of isotopic ratios of radionuclides (e.g. U and Pu) released into the environment is essential to identify their origin and monitor contamination. Elemental composition analysis of environmental radioactive particles is required qualitatively and quantitatively to understand the chemical weathering of these particles in the environment.

1. Inductively coupled plasmas-atomic emission spectroscopy/mass spectrometry (ICP-AES/MS)

ICP-AES utilizes a plasma (~ 10000 K) as atomization and excitation source. The ICP source consists of a torch that contains a plasma stream of an inert gas (usually argon) that is maintained via an induction radio-frequency coil, which is wrapped around the ICP torch. The sample is introduced into the flowing gas stream and the resultant plasma passes through the region surrounded by the induction coil in the form of a spray. The steps involved in the analysis of a liquid sample by ICP-AES are explained in Figure 5.

A VG Horizon ICP-AES was used to measure the concentrations of U and a range of stable elements (Fe, Ti, W, Cr, and B) in solutions of dissolved DU particles. The precision of ICP-AES measurements was verified by analysing standards (0.01, 0.05, 0.1 and 1 mg/l) of each element before and at the end of the measurements, and all elements were recovered within ± 4%. Detection limits of the elements analysed are shown in Table 2.

1- Sample preparation includes treatment with acids, heating or microwave digestion.

2- Nebulization: liquid converted to aerosols.

3- Desolvation/volatization: water is driven off, and remaining liquid and solid converted to gases.

4- Atomization: gas phase bonds are broken by plasma temperature and only atoms are present.

5- Excitation/ emission: atoms gain energy from collisions and emit light of a characteristic wavelength.

6- Separation/ detection: A grating disperses the light that is quantitatively measured.

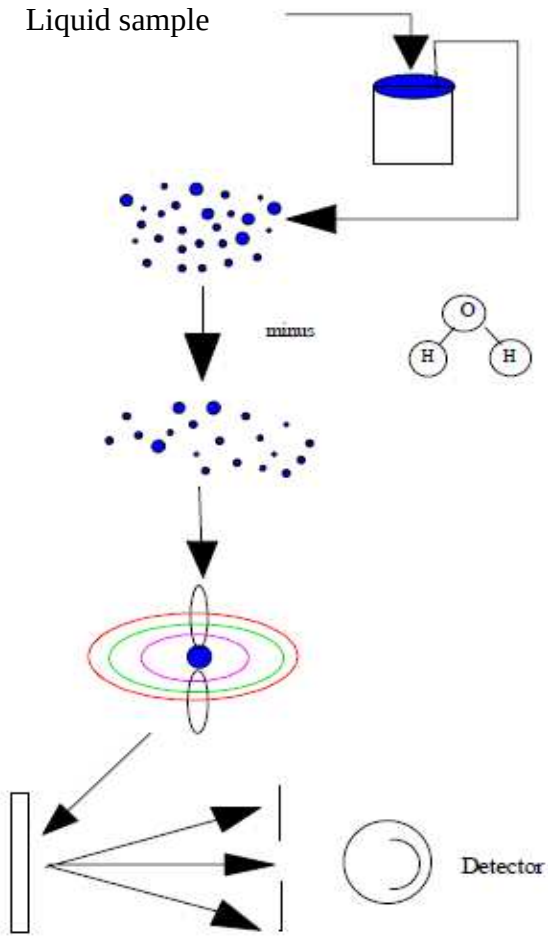

Figure 5. Steps involved in the analysis of a liquid sample by ICP-AES (Manning and Grow, 1997).

In mass spectrometry, an ICP source is used again as an ionization source. However, in contrast to ICP-AES, the plasma is used to ionize the sample and the ions are separated and measured by a mass spectrometer according to their mass to charge ratios. A Quadrupole mass analyser is used to separate different ions and electron multiplier detector to measure them. ICP-MS (Plasma Quad PQII) manufactured by VG elemental (Winsford, Cheshire, UK), was used in standard conditions (Table 1) to determine the isotopic composition of U. The analytical quality of ICP-MS was checked by analysing uranium calibration standards (10 ppb, 50ppb, and 100ppb, dilutions of a certified Johnson Matthey uranium solution 1000 ± 3 ppm) before and after running the samples. The mean error of the measurements was 0.91% and 4.59% for the measured atom ratios $^{235}U/^{238}U$ and $^{234}U/^{238}U$ respectively. Detection limits of the elements analysed are shown in Table 2.

Table 1. Parameters of ICP-MS

Incited power/W	1350
Reflected power/W	< 0.1
Coolant gas flow/ 1 min^{-1}	13.5
Auxiliary gas flow/ 1 min^{-1}	1.0
Nebuliser gas flow rate /min^{-1}	0.82
Impact bead spray chamber temperature /°C	10
Total acquisition time/s	37, repeated 3 times for each sample
Detection mode	Pulse counting

Table 2. Detection limits for the elements analysed by ICP-MS and ICP-AES

Element	Detection limit (ppb) ICP-AES	Detection limit (ppb) ICP-MS
U	15	0.0005
Fe	2	0.002
Ti	0.4	0.001
W	8	0.001
Cr	2	0.0005
B	0.8	0.05

2. Secondary Ion Mass Spectrometry (SIMS)

Secondary ion mass spectrometry is an analytical technique that can be used to characterise the surface and near surface (~ 30 μm) region of solid samples. The technique uses an energetic primary ion beam (e.g. O_2^+, Cs^+, Au^+, 1-30 keV), which hits the surface of the sample, an energy transfer occurs between the ions from the beam and the atoms of the first few monolayers of the sample. Cascades of collisions then happen in the solid and many species (e.g. single and multiple charged ions, clusters of several atoms and neutrals) are formed by the interaction of the beam with the sample (Figure 6), but the positive and negative ions are the species of interest for SIMS. The sputtered secondary ions provide information about the elemental, isotopic and molecular composition of the material, and they are detected by a mass spectrometer.

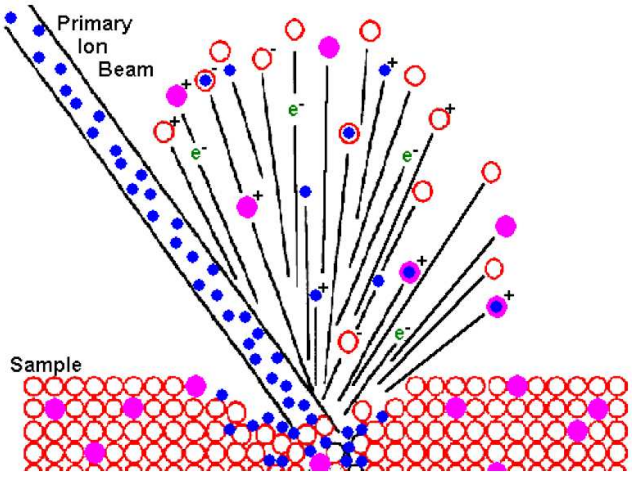

Figure 6. Ion beam sputtering. (Source: http://www.cea.com/cai/simstheo/caistheo.htm)

Depending on the analytical application, different kind of m/z analysers can be applied to perform the mass separation. In the first generation of SIMS, magnetic sector analysers were used. Later on, double-focusing, quadrupole and time-of-flight (TOF) analysers have been applied. TOF analysers are used with secondary ion beams that are generated in short pulses. Ions are accelerated into a drift tube in which the ions are separated according to the time taken to traverse the drift space. When ions have the same energy, heavier ions take longer to reach the detector than do lighter ones.

The detection of the secondary ions can be done either by counting the ions (electron multiplier or Faraday cup) or using ion sensitive imaging detectors (microchannel plate/ Fluorescent screen or resistive anode encoder). Ion imaging shows secondary ion intensities as a function of location on sample surface. Image dimensions vary from 1 μm to 500 μm.

D) Radiometric techniques

As radionuclides emit various types of radiation (alpha, beta and gamma) which can be detected by radiation sensitive detectors, radiometric methods such as alpha or gamma spectrometry and liquid scintillation counting can be applied to identify radioisotopes and measure their activity. The shorter the half-life of radionuclide, the higher the specific activity, therefore, radiometric methods are more sensitive for short-lived radionuclides, whereas mass spectrometric techniques are more sensitive for long-lived radionuclides. Alpha spectrometry can be used to determine the radionuclide and isotopic composition which is useful to identify the origin of radionuclides and the nature of the nuclear fuel.

Alpha and Gamma spectrometry

Sources emitting alpha particles and/or gamma rays can be counted using alpha or gamma spectrometer which is based on a semiconductor detector made of Ge or Si. A band structure exists in the semiconductor crystal, with a band gap of about 1.1 eV for Si and 0.66 eV for Ge. The passage of ionizing radiation injects enough energy into the system to raise electrons from the valence band to the conduction band, creating electron-hole pairs (Figure 7). The hole and the electron can migrate through the crystal in response to an electric field applied on the semiconductor, producing an electrical signal which is amplified and transported to the ancillary counting equipment.

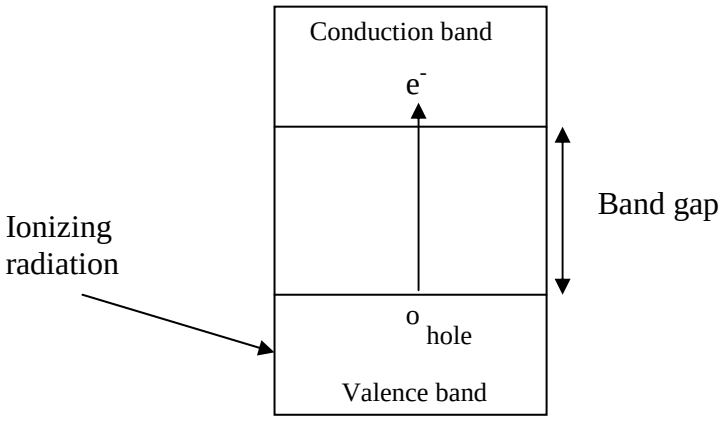

Figure 7. Band structure of a semiconductor detector

The signal is converted to a digital form, and then stored in the memory of a multichannel analyser (MCA) to give a sample spectrum. The number of electron-hole pairs created is proportional to the energy dissipated in the detector crystal by ionizing radiation (Ehmann and Vance, 1991).

Alpha spectrometry was used to identify radionuclide composition of nuclear fuel particles and measure the activity ratios $^{234}U/^{238}U$ and $^{238}Pu/^{239+240}Pu$. Alpha sources were prepared after radiochemical separation and counted using a PIPS type Si detector (Canberra, Belgium, model A 450 – 18 AM), counting efficiency 20-25%. Counting time was variable depending on sample activity. Detection limit is about 0.5 m Bq.

References

Cheng, Y. T., T. Soodprasert, et al. (1996). Radioactivity measurements using storage phosphor technology. Applied Radiation and Isotopes **47**(9-10): 1023-1031.

Ehmann, D W. Vance, D E (1991). Rdaiochemistry and Nuclear Methods of Analysis. Book.

Johnston, R F. Pickett, S C. Barker, D L (1990). Autoradiography using storage phosphor technology. Electrophoresis **5**, 355-360.

Koarashi, J., F. Saito, et al. (2007). A new digital autoradiographical method for identification of Pu particles using an imaging plate. Applied Radiation and Isotopes **65**(4): 413-418.

Manning, T J., Grow, W (1997). Inductively Coupled Plasma-Atomic Emission Spectrometry. The Chemical Educator **2**, 1-19.

Salbu, B., T. Krekling, et al. (1998). Characterisation of radioactive particles in the environment. Analyst **123**(5): 843-849.